



January 2015

# Local Buckling Restraining Behavior Of Concrete-Filled Steel Tubular Columns Under Seismic Loads

Fokruddin Ahmad

Follow this and additional works at: <https://commons.und.edu/theses>

---

## Recommended Citation

Ahmad, Fokruddin, "Local Buckling Restraining Behavior Of Concrete-Filled Steel Tubular Columns Under Seismic Loads" (2015). *Theses and Dissertations*. 1859.  
<https://commons.und.edu/theses/1859>

This Thesis is brought to you for free and open access by the Theses, Dissertations, and Senior Projects at UND Scholarly Commons. It has been accepted for inclusion in Theses and Dissertations by an authorized administrator of UND Scholarly Commons. For more information, please contact [zeinebyousif@library.und.edu](mailto:zeinebyousif@library.und.edu).

LOCAL BUCKLING RESTRAINING BEHAVIOR OF CONCRETE-FILLED STEEL  
TUBULAR COLUMNS UNDER SEISMIC LOADS

by

Fokruddin Ahmad  
Bachelor of Science, Bangladesh University of Engineering and Technology, 2012

A Thesis

Submitted to the Graduate Faculty

of the

University of North Dakota

In partial fulfillment of the requirements

for the degree of

Master of Science

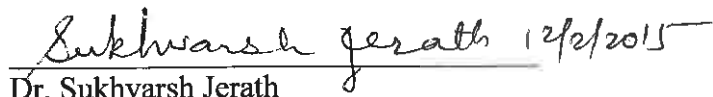
Grand Forks, North Dakota

December  
2015

This thesis, submitted by Fokruddin Ahmad in partial fulfillment of the requirements for the Degree of Master of Science from the University of North Dakota, has been read by the Faculty Advisory Committee under whom the work has been done and is hereby approved.



Dr. Iraj H.P. Mamaghani (Chairperson)

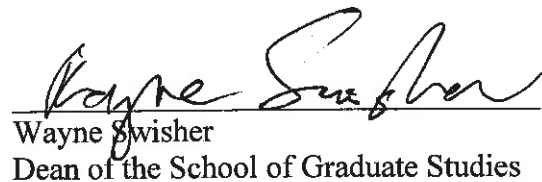


Dr. Sukhvarsh Jerath



Dr. Surojit Gupta

This thesis is being submitted by the appointed advisory committee as having met all of the requirements of the School of Graduate Studies at the University of North Dakota and is hereby approved.



Wayne Swisher  
Dean of the School of Graduate Studies

December 2, 2015  
Date

## PERMISSION

Title           Local Buckling Restraining Behavior of Concrete-Filled Steel Tubular  
                  Columns under Seismic Loads

Department   Civil Engineering

Degree        Master of Science

In presenting this thesis in partial fulfillment of the requirements for a graduate degree from the University of North Dakota, I agree that the library of this University shall make it freely available for inspection. I further agree that permission for extensive copying for scholarly purposes may be granted by the professor who supervised my thesis work or, in his absence, by the Chairperson of the department or the dean of the School of Graduate Studies. It is understood that any copying or publication or other use of this thesis or part thereof for financial gain shall not be allowed without my written permission. It is also understood that due recognition shall be given to me and to the University of North Dakota in any scholarly use which may be made of any material in my thesis.

Fokruddin Ahmad  
5/28/2015

## TABLE OF CONTENT

LIST OF FIGURES .....	vi
LIST OF TABLES .....	x
ACKNOWLEDGEMENTS .....	xi
ABSTRACT .....	xii
CHAPTER	
I.    INTRODUCTION.....	1
II.   LITERATURE REVIEW .....	4
2.1 Background.....	4
2.2 Material Properties and Constitutive models.....	6
2.3 Finite element modeling .....	20
2.4 Interface Modeling.....	24
III.  HOLLOW STEEL COLUMN.....	26
3.1 Introduction.....	26
3.2 Specimen.....	28
3.3 Material Modeling .....	29
3.4 Finite element modeling .....	30
3.5 Result .....	34
3.6 Conclusion .....	51
IV.  CONCRETE FILLED STEEL COLUMN .....	54
4.1 Introduction.....	54

4.2 Specimen.....	55
4.3 Material Modeling .....	58
4.5 Result .....	67
4.6 Conclusion .....	95
V. CONCLUSION.....	97
REFERENCE.....	103

## LIST OF FIGURES

Figure	Page
1. Confined stress-strain diagram used by Susantha <i>et al.</i> (2001).....	7
2. Stress-strain diagram of confined concrete used by Hu <i>et al.</i> (2005).....	9
3. Lateral confining pressure on concrete calculated by Hu <i>et al.</i> (2005) .....	11
4. $k_3$ as a function of $F/F_u$ as calculated by Hu <i>et al.</i> (2005).....	12
5. $k_4$ as a function of $F/F_u$ as calculated by Hu <i>et al.</i> (2005).....	13
6. Stress-strain diagram of confined concrete by Mander, Priestley <i>et al.</i> 1988.....	14
7. $k_3$ as a function of $D_t$ as calculated by Hu <i>et al.</i> (2003).....	16
8. Lateral confining pressure on concrete calculated by Hu <i>et al.</i> (2003) .....	16
9. Stress-strain diagram of steel proposed by Tao <i>et al.</i> (2013) .....	18
10. Effect of boundary condition experimented by Tao <i>et al.</i> (2013).....	20
11. Damage parameter for concrete in ABAQUS .....	22
12. Elements used in analysis .....	24
13. Detailing of the cross section of specimen. ....	28
14. Stress strain behavior of used material .....	30
15. Boundary condition and meshing of the specimen .....	31
16. Meshing of No. 2 specimen .....	31
17. Meshing of KD-3 specimen .....	32
18. Loading pattern on the specimens.....	33
19. Material behavior for isotropic hardening .....	34
20. Expansion of yield surface for isotropic hardening .....	35

21. Material behavior for kinematic hardening.....	35
22. Translation of yield surface, kinematic hardening.....	36
23. Comparison of hysteresis diagram for specimen No.6 .....	37
24. Comparison of hysteresis diagram for specimen No.8 .....	38
25. Comparison of hysteresis diagram for specimen KC-1 .....	39
26. Comparison of hysteresis diagram for specimen No.2 .....	40
27. Comparison of hysteresis diagram for specimen KD-3 .....	41
28. Buckling behavior of No.6 specemen at 10 $\delta y$ using Isotropic Hardening .....	42
29. Buckling behavior of No.6 specemen at 10 $\delta y$ uding Kinematic Hardeing .....	42
30. Buckling behavior of No.8 specemen at 9 $\delta y$ using Isotropic Hardening rule .....	43
31. Buckling behavior of No.8 specemen at 9 $\delta y$ using Kinematic Hardening.....	43
32. Buckling behavior of KC-1 specemen at 9 $\delta y$ using Isotropic Hardening .....	44
33. Buckling behavior of KC-1 specemen at 9 $\delta y$ using Kinematic Hardening.....	44
34. Buckling behavior of No.2 specemen at 7 $\delta y$ using Isotropic Hardening .....	45
35. Buckling behavior of No.2 specemen at 7 $\delta y$ Kinematic Hardening .....	45
36. Buckling behavior of KD-3 specemen at 11 $\delta y$ using Isotropic Hardening.....	46
37. Buckling behavior of KD-3 specemen at 11 $\delta y$ Kinematic Hardening rule .....	46
38. Comparison between envelop curve for specimen No.6 .....	47
39. Comparison between envelop curve for specimen No.8 .....	48
40. Comparison between envelop curve for specimen KC-1 .....	49
41. Comparison between envelop curve for specimen No.2 .....	50
42. Comparison between envelop curve for specimen KD-3 .....	51
43. Pinching behavior of Concrete Filled Tube .....	55
44. Dimension detailing of the Specimen .....	56
45. Boundary and loading condition of the specimen.....	57



46. Stress-Strain diagram of steel SS400.....	59
47. Stress-Plastic Strain of Steel SS400.....	60
48. Compressive Stress-Strain of Concrete .....	61
49. Compressive Plastic Stress-Strain curve of Concrete.....	62
50. Compressive damage of Concrete .....	62
51. Tensile stress- crack opening of Concrete .....	63
52. Tension Damage of Concrete.....	63
53. Meshing of the specimen .....	65
54. Crack behavior of the CFT .....	66
55. Loading condition of specimen.....	67
56. Comparison between Experimental and Analytical data .....	68
57. Details of No.16 hollow specimen.....	70
58. Details of No.16 specimen with 30% concrete fill .....	71
59. Details of No.16 specimen with 50% concrete fill .....	72
60. Details of No.16 specimen with 53% concrete fill .....	74
61. Details of No.16 specimen with 67% concrete fill .....	75
62. Buckling height for different concrete fill height .....	77
63. Improvement in buckling pattern for different concrete height.....	78
64. Improvement in hysteresis diagram for different height of concrete.....	79
65. Details of No.30 hollow specimen.....	81
66. Details of No.30 specimen with 30% concrete fill .....	82
67. Details of No.30 specimen with 50% concrete fill .....	83
68. Details of No.30 specimen with 53% concrete fill .....	85
69. Details of No.30 specimen with 67% concrete fill .....	86
70. Buckling position in column, specimen No.30.....	88

71. Improvement in buckling pattern for different concrete height.....	89
72. Improvement in hysteresis diagram for different height of concrete.....	90
73. Effect of diaphragm in concrete filled tubular structure, No.16.....	91
74. Effect of diaphragm in concrete filled tubular structure, No.30.....	92
75. Comparison between hysteresis diagram of hollow steel columns .....	94
76. Comparison of hysteresis diagram for different axial load.....	95

## LIST OF TABLES

Table	Page
1. Geometric properties of test specimens under unidirectional loading.....	29
2. Material properties of test specimens under unidirectional loading. ....	29
3. Loading of test specimen under unidirectional loading.....	32
4. Geometric and Material Properties of Specimens .....	56
5. Height of concrete in Concrete Filled Tube.....	57
6. Parameters for steel.....	59
7. ABAQUS material parameter for Concrete .....	64

## **ACKNOWLEDGEMENTS**

I wish to express my sincere appreciation and gratitude to the University of North Dakota and especially the Civil Engineering Department for their continued support and guidance throughout my graduate academic career. My academic success is a direct impact of the Civil Engineering Department at the University of North Dakota. I would specifically like to thank my graduate advisor, Dr. Iraj Mamaghani, for his supervision and direction throughout the years. My sincere thanks are also extended to my committee members, Dr. Sukhvarsh Jerath and Dr. Surojit Gupta, for their valuable support and advice to complete this thesis. The leadership and knowledge provided has made a graduate degree a reality for me.

## **ABSTRACT**

Extensive investigations have verified that frame systems consist of concrete-filled steel tubular (CFST) columns have more benefits than ordinary reinforced concrete and steel systems. The CFST column increases earthquake resistant capabilities due to the concrete filling inside the steel tubes and are ideal for buildings subjected to large compressive stress. The use of CFST columns is drawing attention due to their strength and quake-proof advantages. Local buckling of the steel tube is delayed by the restraint of the concrete, and the strength of concrete is increased by the confining effect of the steel tube.

This thesis deals with the local buckling restraining behavior of thin-walled CFST columns under seismic loads by conducting a bidirectional cyclic loading numerical analysis. The CFST columns are modeled and analyzed, by the commercial computer program ABAQUS, to calculate the responses of the CFST columns under bidirectional cyclic load. The obtained results from analysis indicate that the buckling deformation should be slowed for the reduction in compressive force on buckled part due to shifting of compressive force from steel tube to the in-filled concrete. In addition, under a cyclic load applied after the occurrence of local buckling, the opening and closing of major horizontal cracks and dilation occur in the in-filled concrete. As a result, a predominant tensile axial force will act repeatedly on the buckled part of the outer steel tube. This tensile force restrains or restores the local buckling deformations by stretching them. The magnitude of

the tensile force could be enhanced by installing diaphragms on the steel tube at the upper surface of the in-filled concrete. The ratio between the residual sway displacement  $\delta_r$  and the maximum response sway displacement  $\delta_m$ , defined as  $\delta_r/\delta_m$  for partially CFST columns, is smaller than that for hollow columns because of the enhanced strength and ductility of CFST columns. An extensive study will be carried out to derive seismic design equations for Concrete Filled Steel Tubular Columns.

# CHAPTER I

## INTRODUCTION

With the technological advancement, structural engineers are always trying to push the limit of accuracy and predictability, which seemed impossible before. One of the great challenges in structural engineering is to design infrastructures which can withstand all kinds of extreme load even seismic load which is highly unpredictable in nature. Recent advancement in structural material, member fabrication method, material modeling, and computer technology provides the tools to improve the design standard and increase the accuracy in predicting. The use of thin-walled steel tubular columns in highway bridge systems as bridge piers is increasing in Japan and other countries (Mamaghani *et al.*, 2010). These steel bridge piers are light, ductile, and can be built in limited spaces which made these advantageous, especially in highly populated urban areas, over other types of reinforced concrete bridge piers (Goto *et al.*, 2006). Recent research shows the ductile behavior of steel tubular column under seismic loading (Mamaghani *et al.*, 2014a, 2014b, 2015a, 2015b, 2015c).

However, after the Kobe earthquake (Japan, 1995) a lesson was learnt about the stability and ductility of thin-walled hollow tubular steel columns which motivated researchers to do more research on concrete-filled tubular columns. During the earthquake, most of the hollow steel bridge piers failed except some of the partially concrete-filled piers. In Japan, prior to the Kobe earthquake, concrete was poured in hollow steel piers to

prevent the column from indenting due to accidental car crashes, not for structural load-transfer mechanism purposes.

The concrete-filled steel tubular (CFST) columns have evolved an alternative to the conventional hollow steel and reinforced concrete (RC) columns in recent years. Its usage as a structural member in transferring load from super structure is increasing as the in-filled concrete increases the strength and ductility of columns without increasing the given amount of steel. Research shows, by using concrete-filled steel columns, 60% of structural steel can be saved for a given load (Zhong, 1988). Because of its high strength, stability, ductility and better seismic resistance, found by most of the researchers, CFST is more advantageous than ordinary RC columns, and is even more advantageous than the hollow steel column (Patil, 2012). The main reason for its high-strength and ductility lies in the composite in-filled concrete-steel interaction. The concrete is confined by outer steel which acts like longitudinal and transverse reinforcement. Moreover due to the confinement, the inner concrete core experiences tri-axial compression which restrained the formation of tension crack in concrete. Conversely, the outer steel shell is strengthened by the inner core which delays the inward local buckling and causes the outward buckling of steel member (A. Z. Y. H. Fam, 2000). Therefore the outer thin-walled steel can reach to the yield stress before local buckling occurs (Lu and Kennedy, 1994). Hence strength and stability of the CFST column is increased by 50% just because of introducing concrete (A. Fam *et al.*, 2004; A. Z. Fam and Rizkalla, 2002). In addition strength deterioration in CFST is not severe compared to hollow steel columns because the spalling of concrete is restrained by outer steel (Patil, 2012). CFST shows enhanced ductility and delayed buckling under seismic load (Mamaghani *et al.*, 2015d). On the other hand, CFST has higher fire resistance



compared to hollow steel column, especially when the concrete core is designed to sustain the dead and live load (Kodur, 1997), as concrete has a larger thermal resistance than air which is entrapped in hollow columns. Besides, due to the steel confinement the use of formwork can be discarded. The potential economic advantages are more apparent for tall buildings or heavy superstructures where the axial load is higher. Because of the lower poisson's ratio of the core concrete at the initial stages which impairs the advantageous composite interaction by weakening the steel-concrete bonding, the outer steel has no confining effect on the concrete core (Furlong, 1967). However, with the increase of strain, the lateral expansion of the concrete core become larger than the outer steel tube expansion (Patil, 2012).

This manuscript provides an insight about the local buckling behavior of concrete-filled tubular columns. Chapter 2 discusses the previous work of researchers regarding the strength and stability of hollow thin-walled steel tubular columns and concrete-filled thin-walled steel tubular columns. This chapter will also give the idea about the constitutive material property and FEM modeling of CFST columns. Chapter 3 provides a comparison between the experimental result and FEM analysis for stability and buckling behavior of hollow thin-walled steel columns subjected to multi-axial loading. Restrained buckling behavior of CFST columns and a comparison between hollow steel columns and CFST columns is explained in Chapter 4. Chapter 5 presents the suggested design equation for CFST columns. Chapter 6 gives conclusions and discusses the scope of future research.

## CHAPTER II

### LITERATURE REVIEW

#### 2.1 Background

Due to the increasing popularity of CFST columns throughout the world for its excellent seismic resistance, extensive experimental and analytical studies have been conducted to understand the composite behavior of CFST columns since early 1960's. These studies were carried out to understand the confined concrete material behavior and composite concrete-steel interaction by applying compressive axial loads by early investigators (Chen and Chen, 1973; Furlong, 1967; Gardner and Jacobson, 1967; Ghosh, 1977; Knowles and Park, 1969; Zhong, 1988) and very recently (Ellobody *et al.*, 2006; Patil, 2012; Susantha *et al.*, 2001, 2002; Tao *et al.*, 2009; Tao *et al.*, 2013; Thai *et al.*, 2014). To understand the seismic property, in recent decades the researchers are investigating the cyclic behavior of CFST columns by applying lateral cyclic load in the presence of axial load (A. Fam *et al.*, 2004; Ge and Usami, 1996; Gourley *et al.*, 2008; Hu *et al.*, 2005; Mamaghani and Packer, 2002; Nie *et al.*, 2013; Usami and Ge, 1994) and torsion (Han *et al.*, 2007; Nie *et al.*, 2012, 2013). Using these studies many countries, such as Australia, China, Japan, USA and European countries are developing their design code, design philosophies and analysis criteria for CFST columns (Brian Uy *et al.*, 2008).

The development in finite element technique has provided with a new dimension for modeling of CFST columns. Nowadays, using commercially available modern softwares, such as ABAQUS and ANSYS, allows us to model the composite interaction between concrete core and outer steel as well as other different factors such as residual stress, initial imperfection and, different boundary condition in a highly precise manner. Expensive experimental studies are giving place to new analytical simulations and hence are enabling researchers to carry on extensive studies to investigate the behavior of CFST columns more accurately.

To understand the behavior of CFST columns, researchers are investigating the influencing factors on strength and ductility. B Uy (2001), Gho and Liu (2004), Sakino *et al.* (2004) and, Patton and Singh (2014) investigated the effect of the constituent material property, such as concrete compressive strength, concrete tensile strength and, steel yield strength, on the ultimate strength of CFT column. The influence of the confining pressure of concrete, which is determined by the shape of the tube, on the overall behavior of CFT column was discussed by Susantha *et al.* (2001) and, Hu *et al.* (2003). The effects of the geometric properties of the outer steel tubes such as diameter-thickness ratio, spacing of the diaphragms and spacing of the longitudinal stiffeners were investigated by Schneider (1998), Huang *et al.* (2002), Giakoumelis and Lam (2004), Sakino *et al.* (2004) and, Tao *et al.* (2009). The effects of some other important parameters such as column slenderness ratio and height of the concrete infills on the ductility and stability of CFST are discussed by Mamaghani and Packer (2002). The effect of initial imperfections, residual stress and different steel grades, which affects the thermal stress, is also considered by Tao *et al.* (2009), Brian Uy *et al.* (2011) and, Thai *et al.* (2014).

The magnitude of compressive axial load considerably affects the overall seismic behavior of CFST columns. An extensive experimental were carried out to understand the behavior of CFST columns under low axial load and cyclic lateral load. The seismic response of CFST columns subjected to higher axial load is important because during severe earthquakes such as Kobe Earthquake, the column of structures such as the bridge piers, suspension bridge tower, arch ribs etc. are subjected to higher axial load. But the cyclic behavior and seismic performance of CFST columns under high axial load is known a little.

## **2.2 Material Properties and Constitutive models**

### **2.2.1 Concrete modeling**

In a CFST column under axial loading and lateral displacement, the confined concrete core expands. This expansion is restrained by the outer steel tube which exerts tri-axial stress on concrete core while the steel tube itself is in bi-axial stress state. It is important to consider this confined pressure as this pressure increases the strength, ductility and enhance the behavior of concrete core. There are many models to describe the behavior of this composite confined concrete such as Mander *et al.* (1988), Sakino and Sun (1994), Susantha *et al.* (2001), Hu *et al.* (2005) etc. There are some models for high strength concrete material (Thai *et al.*, 2014) and pure torsion (Han *et al.*, 2007). It is worthy to mention that one model is not a corrected or updated version of another model, each of the existing model has its own advantages and limitations.

Confined concrete model of Susantha *et al.* (2001) is based on the steel thickness, circumferential stress of steel and concrete material property.

$$f_c = f'_{cc} \frac{x^r}{r - 1 + x^r} \quad (1)$$

$$x = \frac{\epsilon}{\epsilon_{cc}} \quad (2)$$

$$r = \frac{E_c}{(E_c - f'_{cc}/\epsilon_{cc})} \quad (3)$$

$$\epsilon_{cc} = \epsilon_c \left[ 1 + 5 \left( \frac{f'_{cc}}{f'_c} \right) \right] \quad (4)$$

Where,  $f_c$  and  $\epsilon$  denote the longitudinal compressive stress and strain;  $E_c$  is the tangent modulus of elasticity for concrete. This equation can describe the post peak behavior of the concrete.

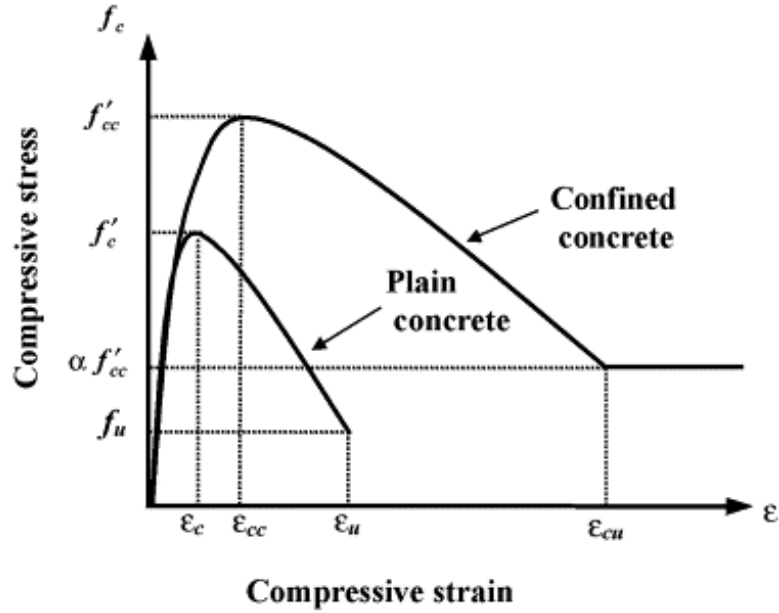


Figure 1: Confined stress-strain diagram used by Susantha *et al.* (2001)

For CFST columns, in triaxial stress state the peak stress of the confined concrete can be defined as the equation below.

$$f'_{cc} = f'_c + m f_{rp} \quad (5)$$

Here,  $f_{rp}$  is the maximum radial pressure on concrete and  $m$  is an empirical coefficient whose value is taken 4.0 by Susantha *et al.* (2001). For circular section,

$$f_{rp} = \frac{2t}{D - 2t} f_{sr} \quad (6)$$

Here,  $f_{sr}$ ,  $t$  and  $D$  denote the circumferential stress in steel, thickness and the outer diameter of the steel column section.

Mamaghani (2005) developed a new confined concrete model under cyclic loading that has a better prediction of confined concrete behavior than Susantha *et al.* (2001) model. Confined concrete strength is not only a function of geometry properties such as plate width-to-thickness ratio,  $R$ , and column's slenderness ratio,  $\lambda$ , but also a function of other material properties, which Sakino and Sun (1994) model take into consideration. According to them:

$$f'_{cc} = \gamma_u f'_c + 4.1 f_{rp} \quad (7)$$

Here,  $\gamma_u$  is the shape factor and other terms are defined previously. The shape factor is a function of the diameter of the steel column and defined as the equation below.

$$\gamma_u = 1.67 D^{-0.112} \quad (D \text{ in } mm) \quad (8)$$

$$f_{rp} = -0.19 \frac{2t}{D - 2t} f_y \quad (9)$$

Here,  $D$  is the diameter of the tube and  $t$  is the thickness of the tube. To describe the post buckling behavior of the confined concrete, which is expressed by  $r$  and is a function of  $D$ ,  $t$ ,  $\gamma_u$  and concrete strength parameter, another control parameter  $K$  is used where,

$$K = \frac{f'_{cc}}{\gamma_u f'_c} \quad (10)$$

$$r = -0.0152 \ln \left( \frac{D}{t} \frac{f'_{cc}{}^5}{f_y \sqrt{\varepsilon'_{cc}}} \right) + 0.6647; \text{ For } K > 1.5 \quad (11)$$

$$r = 2 \times 10^{-12} \left( \frac{D}{t} \frac{f'_{cc}{}^2}{f_y \sqrt{\varepsilon'_{cc}}} \right)^2 - 10^{-6} \left( \frac{D}{t} \frac{f'_{cc}{}^2}{f_y \sqrt{\varepsilon'_{cc}}} \right) + 1.202; \text{ For } K \leq 1.5 \quad (12)$$

Sakino and Sun (1994) model is good enough to predict the strength of column under compressive axial load. But applying higher bending moment or lateral displacement may cause the tension crack in concrete core, which is not considered in this model. Hu *et al.* (2005) assume a strength factor ( $k_4$ ), where  $k_4 \leq 1$ , in the original equation to consider the tensile stress. The stress-strain diagram of confined concrete used by Hu *et al.* (2005) is depicted in Figure 2. According to their model:

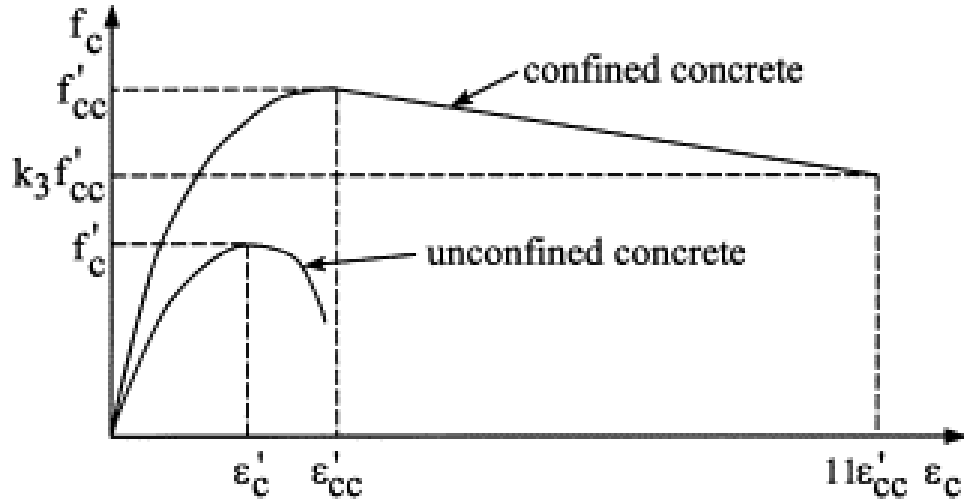


Figure 2: Stress-strain diagram of confined concrete used by Hu *et al.* (2005)

In this figure:

$$f'_{cc} = k_4 f'_c + k_1 f_{rp} \quad (13)$$

$$\varepsilon'_{cc} = \varepsilon'_c \left[ 1 + k_2 \left( \frac{f_1}{f'_c} \right) \right] \quad (14)$$

Here,  $k_1, k_2, k_4$  are the constants and can be obtained from the experimental result. On the basis of Richart *et al.* (1928) works, the constant  $k_1$  and  $k_2$  are set 4.1 and 20.5 and the value of  $k_4$  is kept  $\leq 1$  by Hu *et al.* (2005).  $\varepsilon'_c$  is taken 0.002 in their confined concrete model.

When  $\varepsilon_c \leq \varepsilon'_{cc}$

$$f_c = \frac{E_c \varepsilon_c}{1 + (R + R_E - 2) \left(\frac{\varepsilon_c}{\varepsilon'_{cc}}\right) - (2R - 1) \left(\frac{\varepsilon_c}{\varepsilon'_{cc}}\right)^2 + R \left(\frac{\varepsilon_c}{\varepsilon'_{cc}}\right)^3} \quad (15)$$

When  $\varepsilon_c > \varepsilon'_{cc}$

$$f_c = k_3 \varepsilon_c \quad (16)$$

and

$$\varepsilon_u = 11 \varepsilon'_{cc} \quad (17)$$

The lateral confining pressure on concrete calculated by Hu *et al.* (2005) is depicted in Figure 3. Here, lateral confining force on the concrete is defined by the following equations.

$$\begin{aligned} f_{rp}/f_y &= 0; & 0 \leq F/F_u \leq 0.23 \\ f_{rp}/f_y &= -0.00859 + 0.0373 \left(\frac{F}{F_u}\right); & 0.23 \leq \frac{F}{F_u} \leq 0.56 \\ f_{rp}/f_y &= 0.0104 + 0.00333 \left(\frac{F}{F_u}\right); & 0.56 \leq F/F_u \leq 0.74 \end{aligned} \quad (18)$$



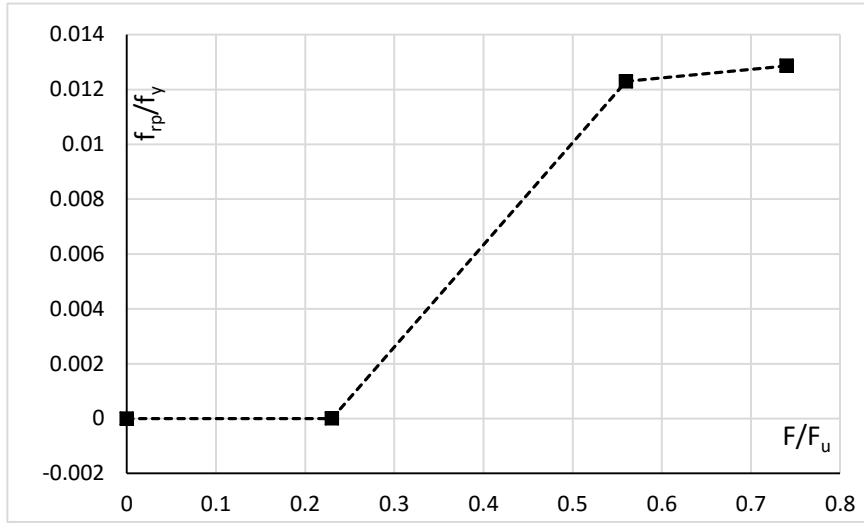


Figure 3: Lateral confining pressure on concrete calculated by Hu *et al.* (2005)

Where,  $F$  is the applied vertical load on CFST column and  $F_u$  is the axial ultimate strength of the column. The degrading slope of the confined concrete stress-strain diagram  $k_3$  is expressed as a function of  $F/F_u$ .

$$k_3 = 1 - 0.304 \left( \frac{F}{F_u} \right); 0 \leq F/F_u \leq 0.23$$

$$k_3 = 1.195 - 1.152 \left( \frac{F}{F_u} \right); 0.23 \leq \frac{F}{F_u} \leq 0.56 \quad (19)$$

$$k_3 = 0.55; 0.56 \leq F/F_u \leq 0.74$$

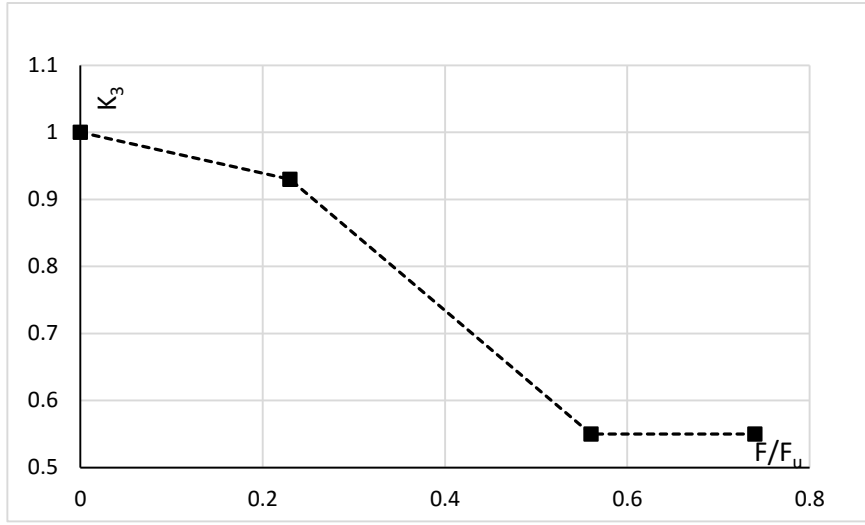


Figure 4:  $k_3$  as a function of  $\frac{F}{F_u}$  as calculated by Hu *et al.* (2005)

Figure 4 illustrates  $k_3$  as a function of  $\frac{F}{F_u}$  as calculated by Hu *et al.* (2005). Figure 5 illustrates  $k_4$  as a function of  $\frac{F}{F_u}$  as calculated by Hu *et al.* (2005). For the value of  $k_4$ , a constant for tension crack adjustment, which is less than equal to 1 the equations are:

$$k_4 = 0.7 + 1.304 \left( \frac{F}{F_u} \right); \quad 0 \leq F/F_u \leq 0.23$$

$$k_4 = 1; \quad 0.23 \leq F/F_u$$
(20)

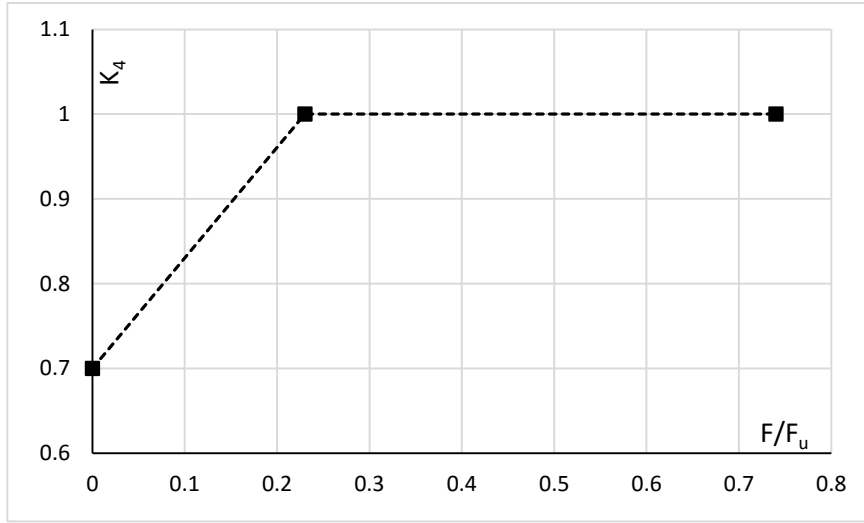


Figure 5:  $k_4$  as a function of  $\frac{F}{F_u}$  as calculated by Hu *et al.* (2005)

Concrete is a composite anisotropic material and its behavior in compression and tension is considerably different. So, to model the confined concrete in the column under bending moment or cyclic lateral load, the constitutive material model for concrete should have different sets of criteria for tensile and compressive response. Patton and Singh (2014) use the original Mander's model (Mander *et al.*, 1988) for confined concrete. Where the confined pressure is calculated from the values measured by Hu *et al.* (2003).

$$f'_{cc} = f'_c + k_1 f_{rp}$$

$$\varepsilon'_{cc} = \varepsilon'_c \left[ 1 + k_2 \left( \frac{f_1}{f'_c} \right) \right] \quad (21)$$

Here,  $k_1$  and  $k_2$  are taken 4.1 and 20.5 respectively. The constitutive equations are assumed below.

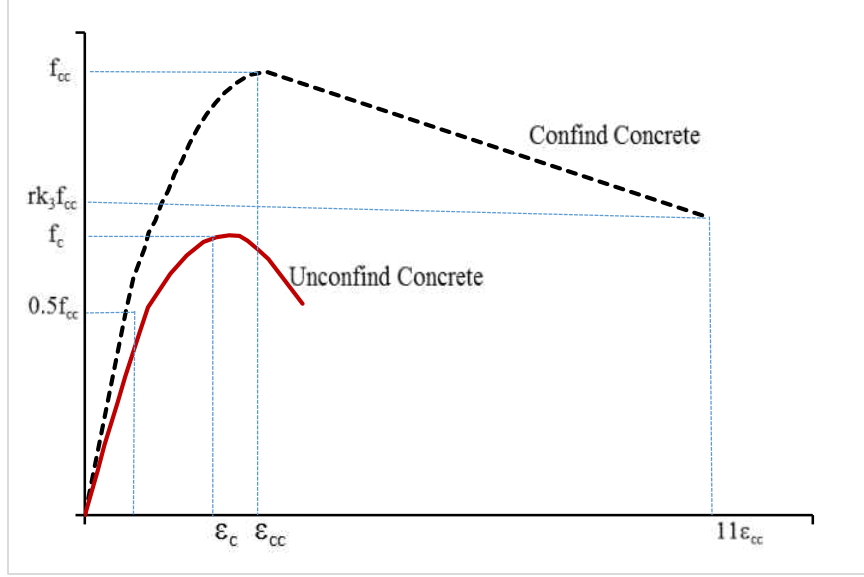


Figure 6: Stress-strain diagram of confined concrete by Mander, Priestley et al. 1988

Figure 6 illustrates the stress-strain diagram of confined concrete by Mander, Priestley et al. (1988).

When  $\varepsilon_c \leq 0.5f'_{cc}$ ; this part is assumed straight line as within proportional limit.

$$f_c = E_c \varepsilon_c \quad (22)$$

Here,

$$E_c = 4700 \sqrt{f'_{cc}} \quad (23)$$

When  $0.5f'_{cc} \leq \varepsilon_c \leq f'_{cc}$

$$f_c = \frac{E_c \varepsilon_c}{1 + (R + R_E - 2) \left(\frac{\varepsilon_c}{\varepsilon'_{cc}}\right) - (2R - 1) \left(\frac{\varepsilon_c}{\varepsilon'_{cc}}\right)^2 + R \left(\frac{\varepsilon_c}{\varepsilon'_{cc}}\right)^3} \quad (24)$$

Where:

$$R_E = \frac{E_c \varepsilon'_{cc}}{f'_{cc}} \quad (25)$$

$$R = \frac{R_E(R_\sigma - 1)}{(R_\varepsilon - 1)^2} - \frac{1}{R_\varepsilon} \quad (26)$$

The constants  $R_\sigma$  and  $R_\varepsilon$  are assumed 4.0 by Hu *et al.* (2003).

When  $\varepsilon_c > f'_{cc}$

$$f_c = k_3 \varepsilon_c \quad (27)$$

and

$$\varepsilon_u = 11 \varepsilon'_{cc} \quad (28)$$

Here,  $k_3$  is the softening factor and is a function of the geometric parameter ( $D/t$ ).

According to Hu *et al.* (2003):

$$k_3 = 1; 21.7 \leq \left(\frac{D}{t}\right) \leq 40$$
$$k_3 = 0.0000339 \left(\frac{D}{t}\right) * 2 - 0.010085 \left(\frac{D}{t}\right) + 1.3491; 40 \leq \left(\frac{D}{t}\right) \leq 150 \quad (29)$$

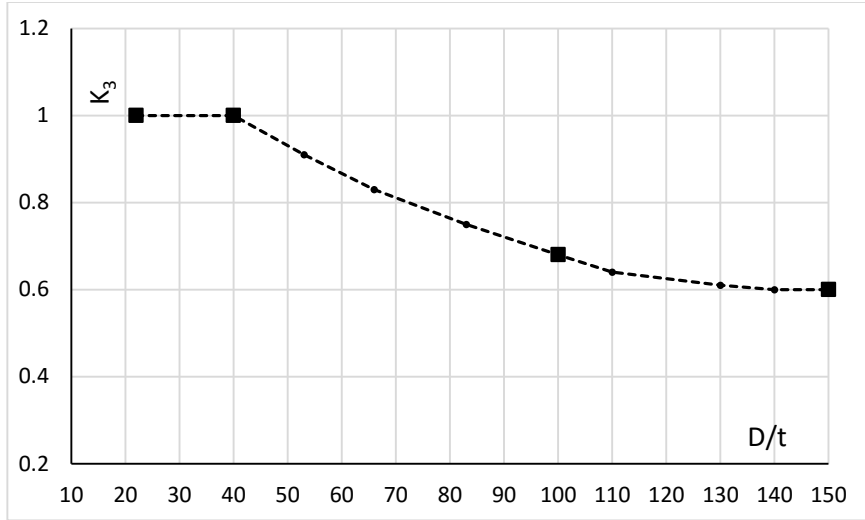


Figure 7:  $k_3$  as a function of  $\frac{D}{t}$  as calculated by Hu *et al.* (2003)

Properties on confined concrete depends on the confining pressure of the concrete. For the case of Circular Concrete Filled Tube, the confined pressure is a function of diameter and thickness of the steel tube. Figure 7 illustrates the lateral confining pressure on concrete calculated by Hu *et al.* (2003). According to Hu *et al.* (2003) confining pressure on the concrete is calculated from the given equations.

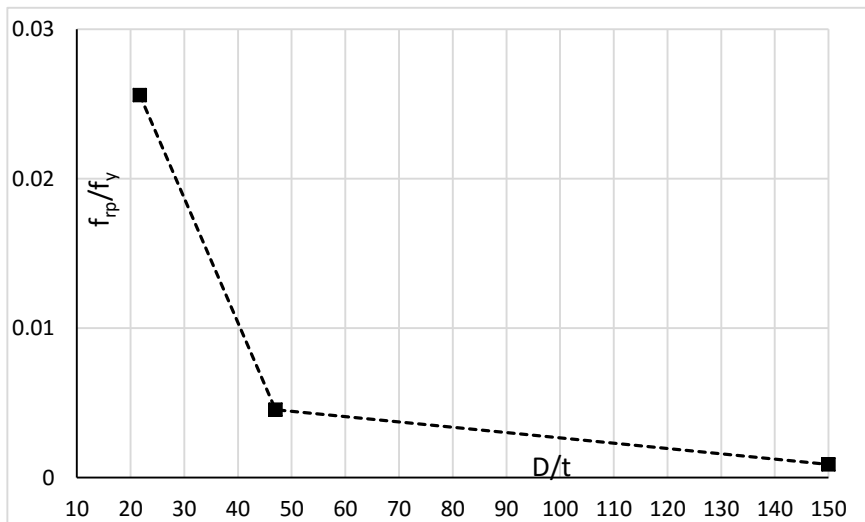


Figure 8: Lateral confining pressure on concrete calculated by Hu *et al.* (2003)

In this figure:

$$f_{rp}/f_y = 0.043646 - 0.000832 \left(\frac{D}{t}\right); \quad 21.7 \leq \left(\frac{D}{t}\right) \leq 47$$

$$f_{rp}/f_y = 0.006241 - 0.0000357 \left(\frac{D}{t}\right); \quad 47 \leq \left(\frac{D}{t}\right) \leq 150$$
(30)

For the tensile behavior, which is characterized by the fracture energy balance approach (Hillerborg *et al.*, 1976) and fracture energy,  $G_f$  is calculated from the equation given by Bažant and Becq-Giraudon (2002).

$$G_f = (0.0469d_{max}^2 - 0.5d_{max} + 26) \left(\frac{f'_c}{10}\right)^{0.7}$$
(31)

Here,  $f'_c$  is in MPa and  $d_{max}$  is the aggregate size (in mm). When there no data is available,  $d_{max}$  could be taken as 20 mm.

Another approach to define the damage is to use “damage parameter”  $d_c$  and  $d_t$  Goto *et al.* (2010). To calculate the damage parameter the following equations are used.

Compressive damage parameter,  $d_c$ :

$$d_c = \frac{k_{ci}\varepsilon_c}{\left[1 + \left(\varepsilon_c/\varepsilon_o\right)^n\right]^n}; \quad \varepsilon_c \leq 0.0184$$

$$d_c = 0.3485; \quad \varepsilon_c > 0.0184$$
(32)

Here,  $k_{ci} = 155$ ,  $\varepsilon_o = 0.0035$ ,  $n = 1.08$

Tension damage parameter,  $d_t$ :

$$d_t = \frac{1.24k_t}{\sigma_{to}} u^{cr} \quad (33)$$

Here,  $k_t, \sigma_{to}, u^{cr}$  depends on the concrete material property.

### 2.2.2 Steel Modeling

To model the steel material in CFST, different stress-strain data such as elastic-perfectly plastic (Schneider, 1998), elastic-plastic with linear hardening (Guo *et al.*, 2007) and, elastic-plastic with multi-linear hardening (Han *et al.*, 2007) was used by different investigators. Within the general strain of interest, normally  $\leq 5\%$ , steel doesn't show significant hardening. Tao *et al.* (2013) shows structural response, axial load- axial strain, is almost independent of used stress-strain model such as linear hardening, multi-linear hardening and, elastic-perfectly plastic model. Figure 9 illustrates the stress-strain diagram of steel proposed by Tao *et al.* (2013). Tao *et al.* (2013) used elastic-plastic model with linear hardening where the hardening modulus  $E_p$  is 0.5% of steel elastic modulus  $E_s$ .

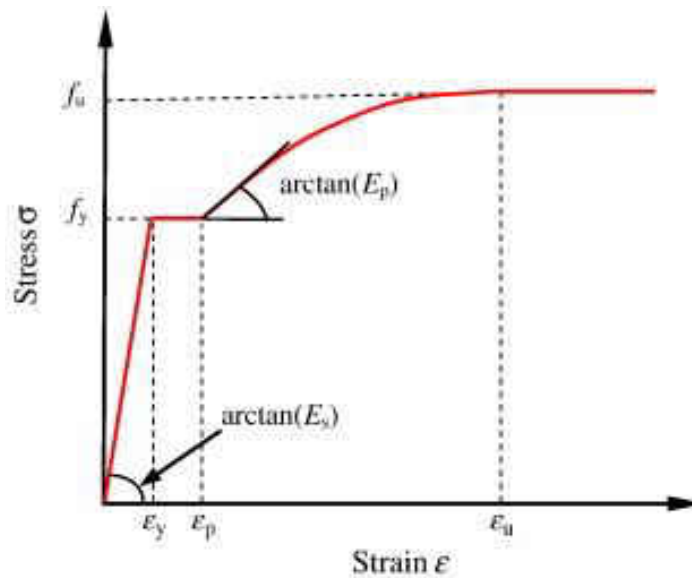


Figure 9: Stress-strain diagram of steel proposed by Tao *et al.* (2013)



In the case of rectangular CFST columns, due to easier local buckling and less effective steel confinement leads them to use elastic-perfectly plastic model.

$$\sigma = \begin{cases} E_s \varepsilon & 0 \leq \varepsilon \leq \varepsilon_y \\ f_y & \varepsilon_y \leq \varepsilon \leq \varepsilon_p \\ f_u - (f_u - f_y) \left( \frac{\varepsilon_u - \varepsilon}{\varepsilon_u - \varepsilon_p} \right)^p & \varepsilon_p \leq \varepsilon \leq \varepsilon_u \\ f_u & \varepsilon \geq \varepsilon_u \end{cases} \quad (34)$$

Here,  $f_u$  is the ultimate strength,  $\varepsilon_y$ ,  $\varepsilon_p$ ,  $\varepsilon_u$  are the yield strain, onset hardening strain and ultimate strain respectively.  $p$  is the strain-hardening exponent, which is expressed by:

$$p = E_p \left( \frac{\varepsilon_u - \varepsilon}{\varepsilon_u - \varepsilon_p} \right) \quad (35)$$

$E_p$  is the modulus at the onset of hardening,  $\varepsilon_p$  and  $\varepsilon_u$  are determined by the following equations.

$$\varepsilon_p = \begin{cases} 15\varepsilon_y & f_y \leq 300 \text{ MPa} \\ [15 - 0.018(f_y - 300)] \varepsilon_y & 300 < f_y \leq 800 \text{ MPa} \end{cases} \quad (36)$$

$$\varepsilon_u = \begin{cases} 100\varepsilon_y & f_y \leq 300 \text{ MPa} \\ [100 - 0.15(f_y - 300)] \varepsilon_y & 300 < f_y \leq 800 \text{ MPa} \end{cases} \quad (37)$$

This following equation could be used to calculate  $f_u$ , if the value is not given to make sure the continuity of the stress strain diagram. This equation is proposed by Nie *et al.* (2013).

$$f_u = \begin{cases} [1.6 - 2 \times 10^{-3}(f_y - 200)] f_y & 200 < f_y \leq 400 \text{ MPa} \\ [1.2 - 3.75 \times 10^{-4}(f_y - 400)] f_y & 400 < f_y \leq 800 \text{ MPa} \end{cases} \quad (38)$$

## 2.3 Finite element modeling

### 2.3.1 Geometry

Lot of experiments have been carried out ranging from short columns to long columns to predict the strength of circular or rectangular CFST columns. Most of the analytical or experimental studies include the end rigid plate in order to distribute axial load uniformly over the cross-section. However, Liew *et al.* (2011) didn't use any end plate in their experiment. In their analytical analysis, Tao *et al.* (2013) fixed all the degrees of freedom except displacement at end surface of the specimen to represent the Liew *et al.* (2011) model. They showed that, in the case of circular CFST columns almost the same result is obtained irrespective of end plate (Tao *et al.*, 2013). However, in the case of rectangular CFST columns there is an effect of end plate on buckling behavior.

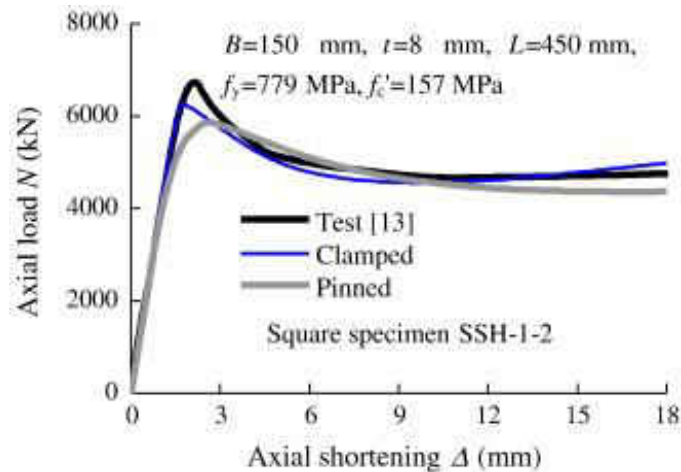


Figure 10: Effect of boundary condition experimented by Tao *et al.* (2013)

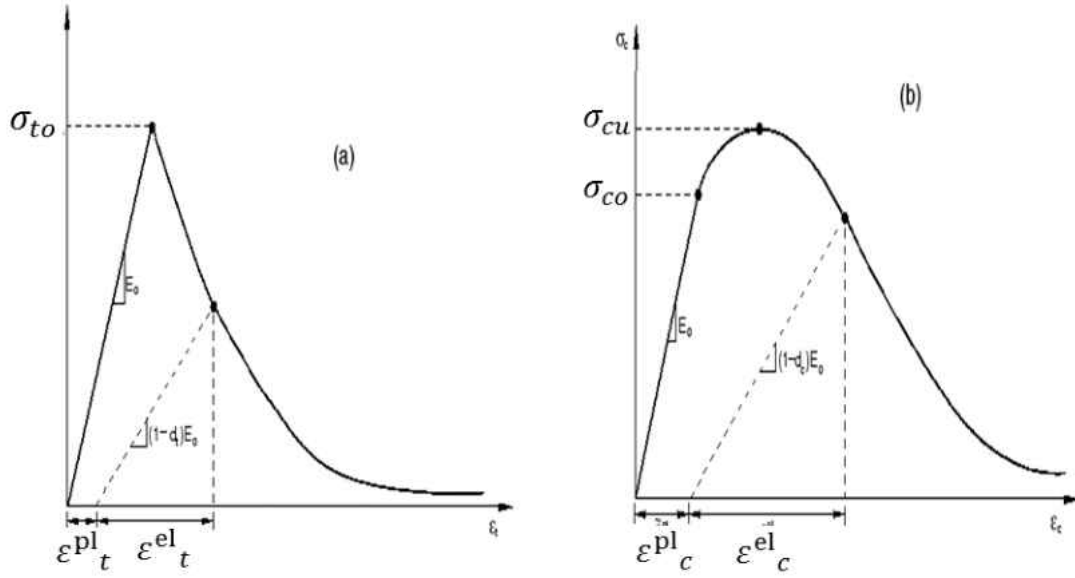
### 2.3.2 Material and Geometric Initial Imperfection

In the case of hollow steel columns, initial imperfection and residual stress has an effect on the behavior of thin walled steel member. But in CFST the effect of residual stress is minimized by introducing concrete in the hollow section and hence in modeling this

effect can be ignored (Tao *et al.*, 2011). Using the model from Tomii *et al.* (1977), Tao *et al.* (2013) showed the effect of  $L/D$  on initial imperfection by comparing axial load-axial strain graph. They showed that, even though the effect of initial imperfection increases when  $L/D < 2$  and  $L/D > 5$ , the effect is almost negligible when  $2 \leq L/D \leq 5$ .

### **2.3.3 Material property**

To model the concrete property in ABAQUS, damaged plasticity model was used by most of the investigators (Hu *et al.*, 2003; Patton and Singh, 2014; Tao *et al.*, 2013; Thai *et al.*, 2014). Though for axial compressive force there is no formation of tension cracks, the non-linearity of concrete was modelled as plastic material without considering damage variables by most of the researchers such as Tao *et al.* (2013), Patton and Singh (2014). In this manuscript, due to applying lateral displacement, concrete stiffness softening as a result of crack formation is considered. Damage variables for both tension damage and compression damage is calculated as discussed in ABAQUS theory manual (23.6.3) and Jankowiak and Lodygowski (2005). Figure 11 illustrates the damage parameters for concrete embedded in the ABAQUS software that is used in this study.



(a) Tension damage parameter

(b) Compression damage parameter

Figure 11: Damage parameter for concrete in ABAQUS

An important parameter of damaged plasticity model is  $K_c$ , the ratio of the second stress invariant of tensile meridian to the same of compressive meridian, defines the yield surface. The effect of  $K_c$  on the CFST column behavior is shown by Tao *et al.* (2013).  $K_c$  is a function of concrete strength,  $f'_c$ , and calculated by the experimental equation given by Yu *et al.* (2010a).

$$K_c = \frac{5.5}{5 + 2f'_c{}^{0.075}} \quad (39)$$

Generally the value of  $K_c$  ranges from 0.715 to 0.703 depending on the concrete compressive strength.

The behavior of CFST column is also influenced by another important parameter known as dilation angle  $\Psi$ , which define the plastic flow potential. The effect of  $\Psi$  in CFST strength prediction is discussed by Tao *et al.* (2013). According to Yu *et al.* (2010b)  $\Psi$  is a

function of steel confining stress and concrete plastic deformation and is calculated by given regression equation.

$$\Psi = \begin{cases} 56.3(1 - \zeta_c); & \zeta_c \leq 0.5 \\ 6.672e^{\frac{7.4}{4.64 + \zeta_c}}; & \zeta_c > 0.5 \end{cases} \quad (40)$$

Where, the confinement factor  $\zeta_c$  is defined as:

$$\zeta_c = \frac{A_s f_y}{A_c f'_c} \quad (41)$$

Here,  $A_s$  and  $A_c$  are the cross sectional area of the steel tube and concrete.

Other important factor to define damaged plasticity model is concrete elasticity modulus,  $E_c$ , which is calculated from the equation recommended by ACI-318. The ratio of equibiaxial concrete strength to axial compressive concrete strength,  $\frac{f_{bo}}{f'_c}$ , is calculated by the empirical equation given by (Papanikolaou and Kappos (2007)).

$$\frac{f_{bo}}{f'_c} = 1.5(f'_c)^{-0.075} \quad (42)$$

### 2.3.5 Element

Most of the researchers used 3D solid element to model concrete and 2D shell element to model steel. For circular concrete section to have a good mesh agreement 6 node wedge shape 3D element, C3D6, is used while rest of it is 8 node C3D8 element. For steel, a uniform plane stress shell element S4 is used. Even though almost all of the recent researcher use C3D8 and S4 elements, some early investigation were carried out (Susantha *et al.*, 2001) using a combined complex interface between shear flexible beam-column

element B21 using Timoshenko beam theory. In this study the adopted finite elements in analysis are illustrated in Figure 12.

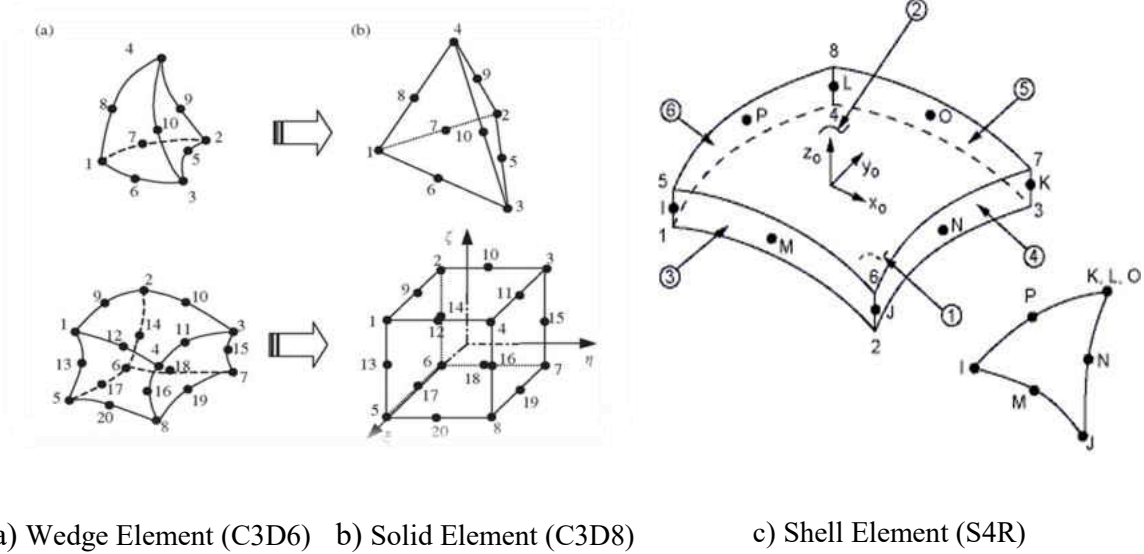


Figure 12: Elements used in analysis

## 2.4 Interface Modeling

### 2.4.1 Interface between Concrete

Even though, when structure is under cyclic load, using Damage Plasticity Model gives more numerical stability compared to other concrete modeling but it has some drawback. Damage Plasticity Model assumes isotropic plasticity, so there is a strength enhancement of concrete due to steel confinement in compression side and tension side as well. Therefore this model fails to predict the behavior of crack more specifically opening and closing of cracks. To fix this problem, a discrete crack is inserted horizontally at the place where maximum tension occurred in the preliminary analysis. To model this discrete

crack, hard contact surface (ABAQUS 2013) is used between the facing concrete surfaces as normal behavior and penalty frictional surface (ABAQUS 2013) as tangential behavior.

#### **2.4.2 Interface between Steel and Concrete**

To simulate the contact between steel and concrete hard contact model is used. Hard contact model allows separation after contact and it calculates the over closure pressure on concrete from the penetration resisting force. Penalty frictional surface model is used as tangential behavior between the steel-concrete interfaces. The frictional force at the interface is expressed by the Coulomb friction model. The resulting shear force at the interface is calculated by:

$$\tau_{\Sigma} = \sqrt{\tau_1^2 + \tau_2^2} \quad (43)$$

Where,  $\tau_{\Sigma}$  is total shear stress acting on the plane;  $\tau_1$  and  $\tau_2$  are the orthogonal stress. The maximum shear stress  $\tau_{cr}$  is proportional to the contact pressure  $p$ , and expressed as,  $\tau_{cr} = \mu p$ . If  $\tau_{\Sigma} \geq \tau_{cr}$  then sliding will occur.

## CHAPTER III

### HOLLOW STEEL COLUMN

#### 3.1 Introduction

Frequent use of thin-walled steel columns as piers in urban areas for elevated highways in Japan draw the attention of the researcher. As to ensure the safety of the structure during earthquakes the seismic behavior of thin-walled piers should be predicted accurately. This is done by applying cyclic load on the structure and comparing its hysteresis behavior. It is well-established that the major influencing factors affecting seismic behavior of the thin-walled member are cyclic material plasticity and the local buckling behavior of the plates (Goto *et al.*, 1998). There are many reliable finite element material models to describe the plasticity of steel. The main focus of the first portion of this chapter is to show the differences in inelastic cyclic behavior due to different hardening rules, namely Isotropic hardening and Kinematic hardening.

As mentioned earlier, cyclic behavior of thin-walled members depend on the local buckling which is a key factor of stiffness degradation. The earthquake waves consist of 3D components, especially two horizontal components of the earthquake create torque which has a highly deteriorating effect on ultimate strength (Goto *et al.*, 2006). Hence the simulating input cyclic data should be multidirectional in order to predict the seismic behavior more accurately.



While designing the thin-walled member, the most important parameters which are considered for design and ductility evaluation are the width-to-thickness ratio parameter,  $R_f$ , radius-to-thickness ratio,  $R_t$ , and the slenderness ratio parameter,  $\lambda$ . The equations given by Mamaghani and Packer (2002) are given below:

$$R_f = \frac{b}{t} \frac{1}{n\pi} \sqrt{3(1 - \nu^2)} \frac{\sigma_y}{E} \quad (\text{For box section}) \quad (44)$$

$$R_t = \frac{r}{t} \sqrt{3(1 - \nu^2)} \frac{\sigma_y}{E} \quad (\text{For circular section}) \quad (45)$$

$$\lambda = \frac{2h}{r_g} \frac{1}{\pi} \sqrt{\frac{\sigma_y}{E}} \quad (46)$$

Where,  $b$  = flange width;  $t$  = plate thickness;  $\sigma_y$  = yield stress;  $E$  = Young's modulus;  $\nu$  = Poison's ratio;  $n$  = number of subpanels;  $r$  = outer radius of the circular section;  $h$  = column height;  $r_g$  = radius of gyration of the cross section.

The hysteresis diagram is normalized by using yield strength,  $H_{y0}$  and the yield deformation,  $\delta_{y0}$ . The equations for  $H_{y0}$  and  $\delta_{y0}$  are given below:

$$H_{y0} = \frac{M_y}{h} \quad (47)$$

$$\delta_{y0} = \frac{H_{y0} h^3}{3EI} \quad (48)$$

Where,  $M_y$  = yield moment and  $I$  = moment of inertia of the cross section. Under the case of combined effect of multidirectional loading and axial compression, yield strength and yield deformation reduced to  $H_y$  and  $\delta_y$ . The following equations are used to define these two parameters.

$$\frac{P}{P_u} + \frac{0.85H_y h}{M_y \left(1 - \frac{P}{P_E}\right)} = 1 \quad (49)$$

$$\frac{P}{P_u} + \frac{H_y h}{M_y} = 1 \quad (50)$$

Here,  $P$  = the axial load;  $P_y$  = the yield load;  $P_u$  = the ultimate load; and  $P_E$  = the Euler load.

### 3.2 Specimen

The model used in the cyclic loading test at the Public Work Research Institute of Japan (Nishikawa *et al.*, 1996) was scaled down to 1/3 of the original one. The details of the specimens are given in Table: 1.

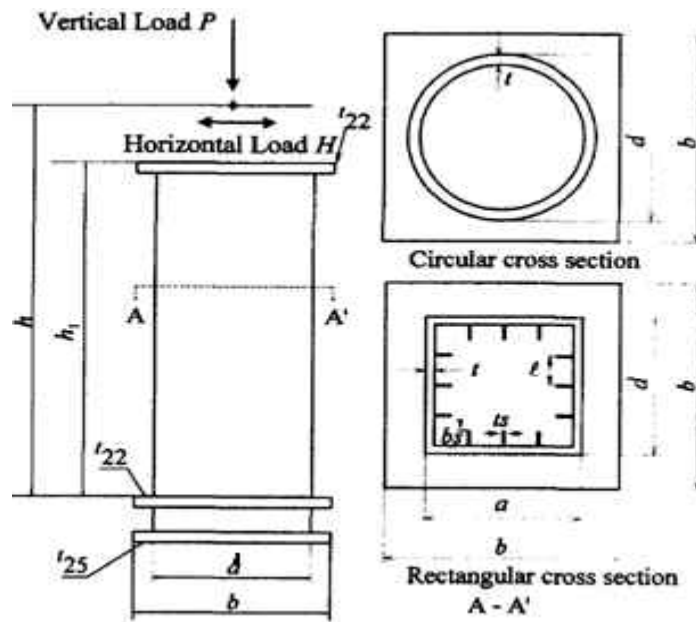


Figure 13: Detailing of the cross section of specimen (Nishikawa *et al.*, 1996).

Table 1: Geometric properties of test specimens (Nishikawa *et al.*, 1996).

Specimen	No.6	No.8	KC-1	No.2	KD-3
$h$ (mm)	3403	3403	3303	3403	3303
$h_1$ (mm)	3173	3173	3173	3173	3173
$d$ (mm)	900	900	600	900	750
$b$ (mm)	1300	1300	1300	1300	1300
$t$ (mm)	16	9	20	9	12
$b_s$ (mm)	-	-	-	80	90
$t_s$ (mm)	-	-	-	6	9
$(n_s+1) \times l$	-	-	-	4 x 225	3 x 246
$A$ (m <sup>2</sup> )	0.04435	0.025192	0.036442	0.032076	0.035424
$R_t$	0.076	0.115	0.031	-	-
$R_f$	-	-	-	0.56	0.46
$\lambda$	0.30	0.26	0.37	0.26	0.30

### 3.3 Material Modeling

In the experiment SS400 steel, which is comparable to A36, is used for fabricating the specimen. The detailed steel property is given in Table 2 and stress-stain curve is shown in Figure 18. For comparison, both multi-linear isotropic hardening and multi-linear kinematic hardening is taken into consideration for simulation to find out the better hardening rule in predicting seismic behavior more accurately.

Table 2: Material properties of test specimens (Nishikawa *et al.*, 1996).

Specimen	Material	$E$ (GPa)	$\nu$	$\sigma_y$ (MPa)	$\sigma_u$ (MPa)	$\epsilon_y$	$\epsilon_{yp}^0$
No. 6	SM490	206.0	0.3	344.3	610.0	0.0017	0.0133
No. 8	SS400	206.0	0.3	289.6	495.0	0.0014	0.0183
KC-1	SS400	206.0	0.3	269.1	464.4	0.0013	0.0170
No. 2	SM490	206.0	0.3	378.6	630.0	0.0018	0.0165
KD-3	SM490	206.0	0.3	363.7	607.0	0.0018	0.0159

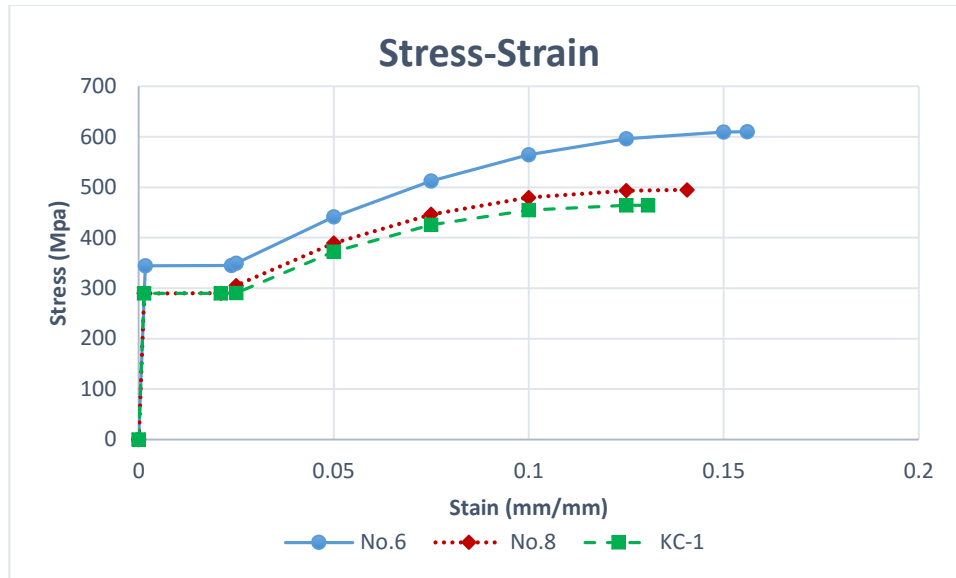
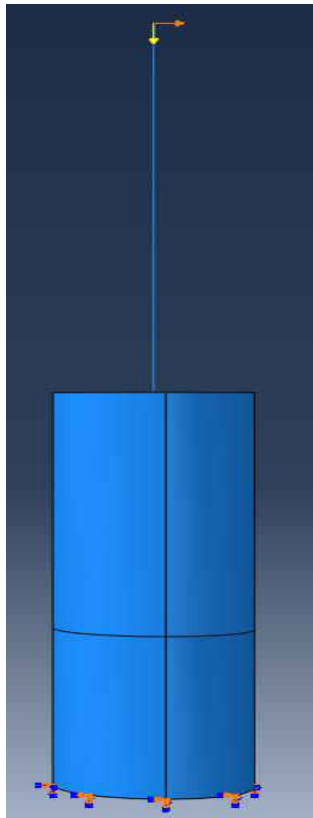


Figure 14: Stress strain behavior of used material (Nishikawa *et al.*, 1996)

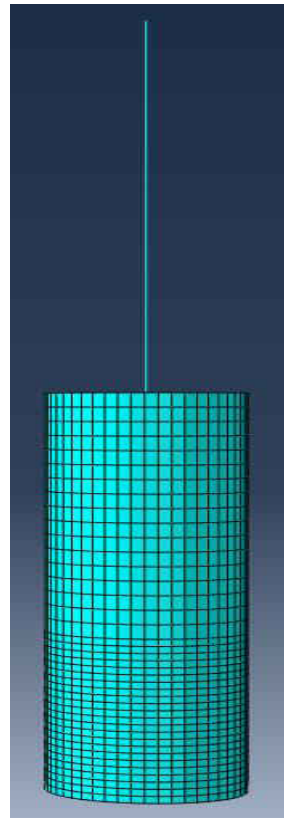
### 3.4 Finite element modeling

#### 3.4.1 Mesh and Element

To reduce the simulation clock time the model is simplified to the combination of beam and shell element. The bottom half of the column is modeled as shell element (S4R) and the upper half of the column is modeled as beam element (B31). To facilitate the understanding of buckling shape, denser mesh is used at the bottom 60% of the column. After analysis for mesh sensitivity, in the lower denser part the mesh size is B/15 while for the rest of the shell element the mesh size is B/10 and for the beam element the mesh size is B/8. Figure shows the loading and the meshing of the specimen.



a) Loading of the specimen



b) Meshing of the Specimen

Figure 15: Boundary condition and meshing of the specimen

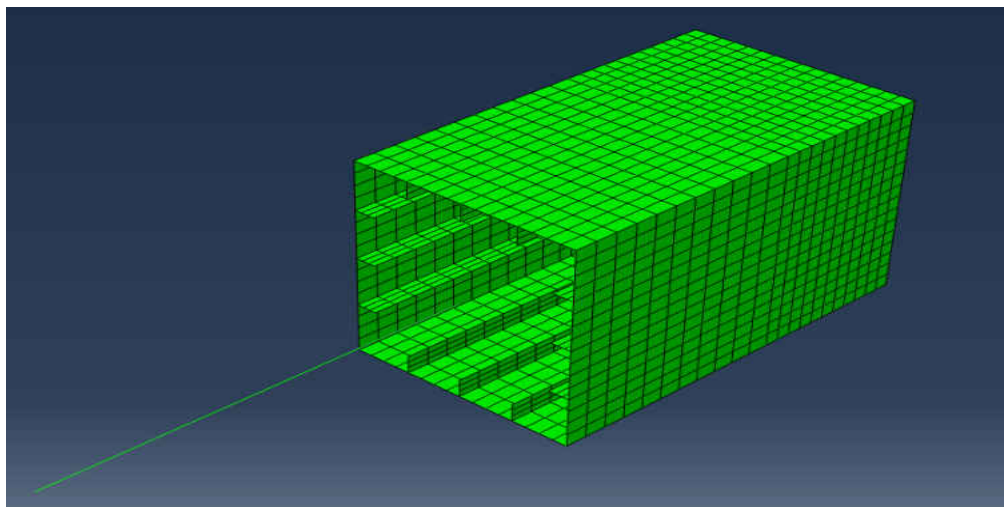


Figure 16: Meshing of No. 2 specimen

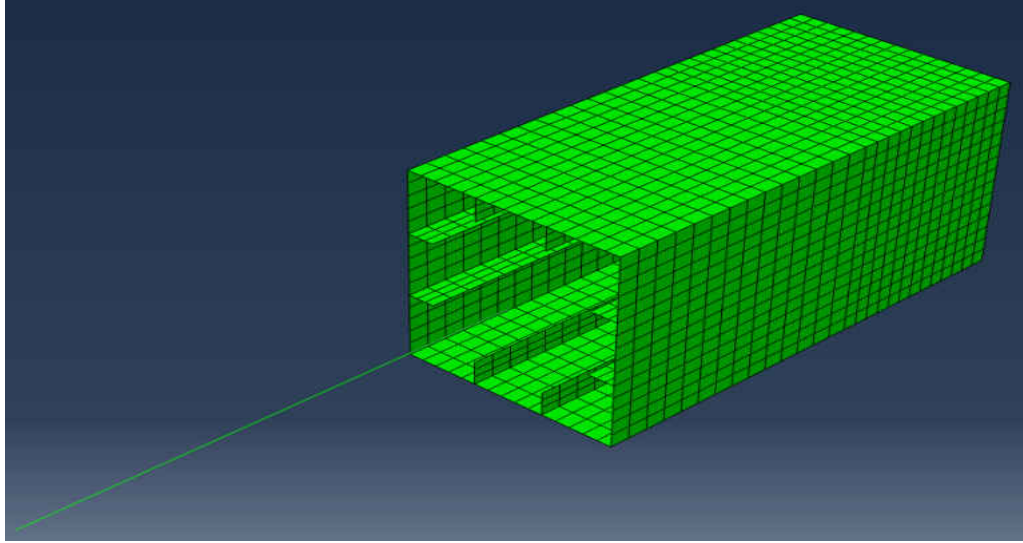


Figure 17: Meshing of KD-3 specimen

### 3.4.2 Loading Program

For loading, unidirectional loading along X direction is used. The amplitude of the load is an integer multiplication of yield displacement  $\delta_y$ . An axial load  $P$  is applied at the top of the column.  $\delta_y$  is calculated from the given equation.

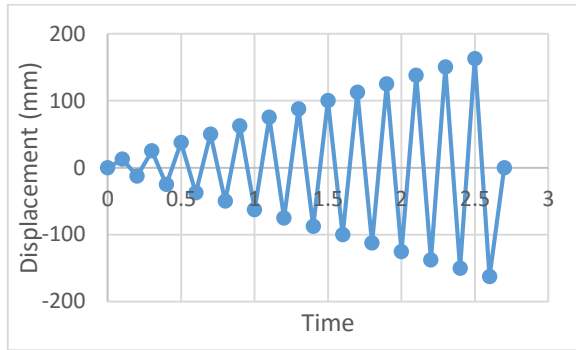
$$\delta_y = \frac{H_y h^3}{3EI} \quad (51)$$

Here,  $H_y = (\sigma_y - P/A)z/h$  and represents the horizontal force,  $A$  = the cross-sectional area,  $h$  = the column height,  $EI$  = the bending rigidity, and  $z$  = the plastic modulus of section. The loading parameters for each specimen is given in Table: 3

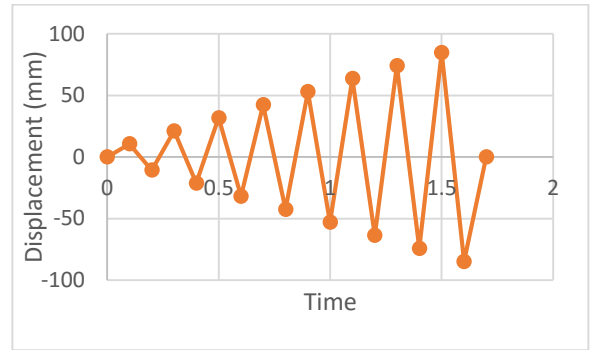
Table 3: Loading of test specimens (Nishikawa *et al.*, 1996).

<i>Specimen</i>	$\alpha$	$P_y$ (KN)	$P$ (KN)	$H_y$ (KN)	$\delta_y$ (mm)
<b>No. 6</b>	0.138	15299.0	2111.0	848.6	12.5
<b>No. 8</b>	0.124	7295.6	9046.5	414.9	10.6
<b>KC-1</b>	0.091	9806.5	8923.9	378.6	14.4
<b>No. 2</b>	0.122	12143.9	1481.5	1039	13.8
<b>KD-3</b>	0.117	12883.7	1507.3	931.5	15.1

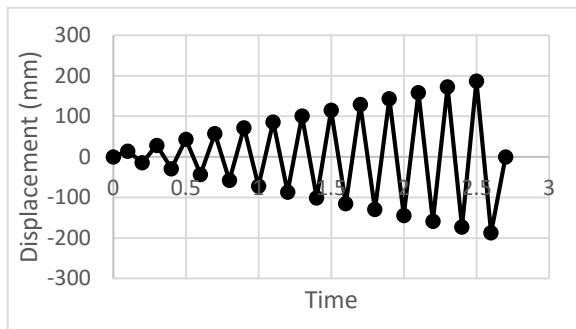
Loading pattern on the specimens are given in the figures. Though it's a static analysis so time has no physical interpretation.



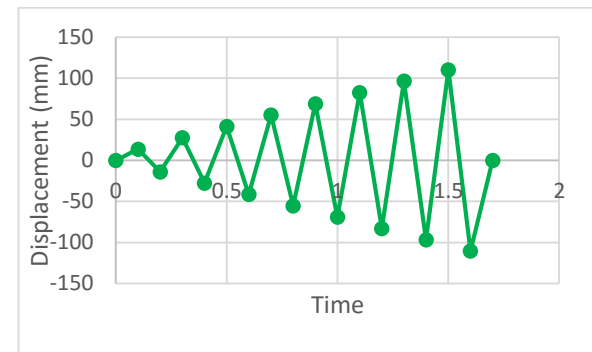
a) No.6



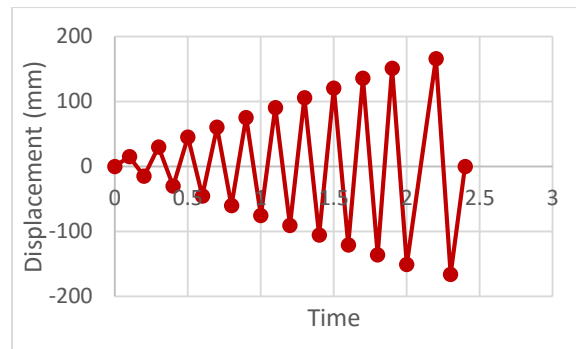
b) No.8



c) KC-1



d) No.2



e) KD-3

Figure 18: Loading pattern on the specimens

### 3.5 Result

#### 3.5.1 Material Behavior

Figure 23 shows the material behavior for isotropic hardening. This figure shows that yield surface is increasing radius in both direction until it touches ultimate stress or bounding surface. Once it touches bounding surface then it becomes constant. Increasing bounding surface is more obvious from Figure 24. After yielding, yield surface is increasing in both direction and it is symmetric about X-axis.

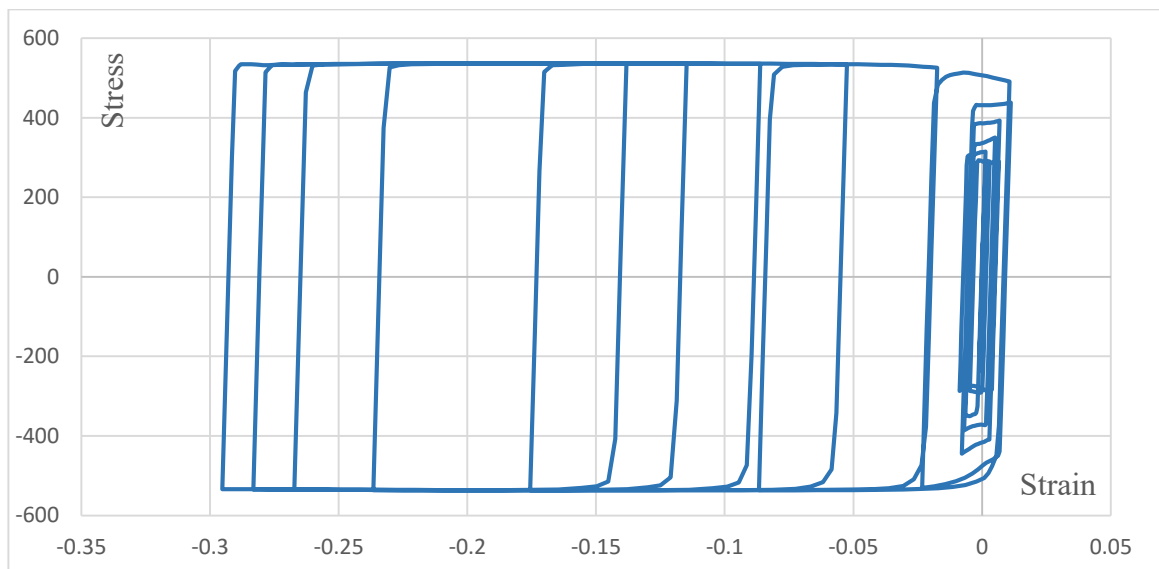


Figure 19: Material behavior for isotropic hardening



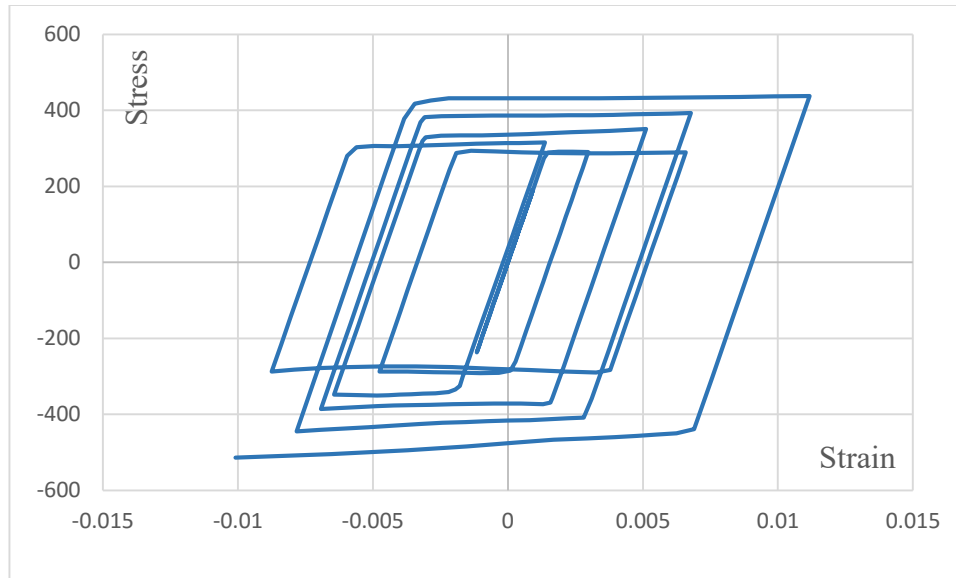


Figure 20: Expansion of yield surface for isotropic hardening

The following figures show the kinematic behavior of material. Figure 25 proves Bauschinger effect, translation of yield surface without changing radius. Figure 26 shows, after yielding, the radius of yield surface is constant due to yield plateau. Then the yield surface starts to translate, moving without changing the radius of yield surface.

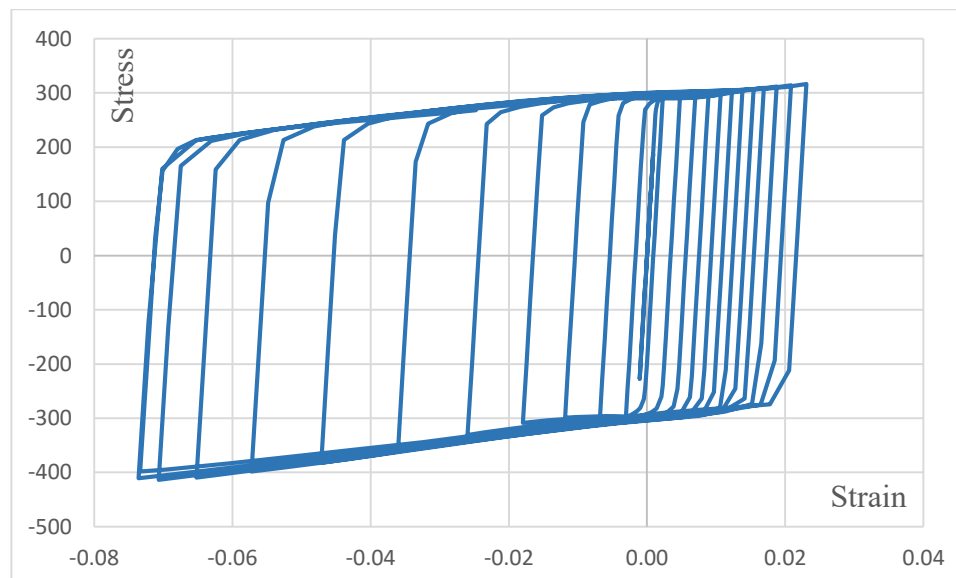


Figure 21: Material behavior for kinematic hardening

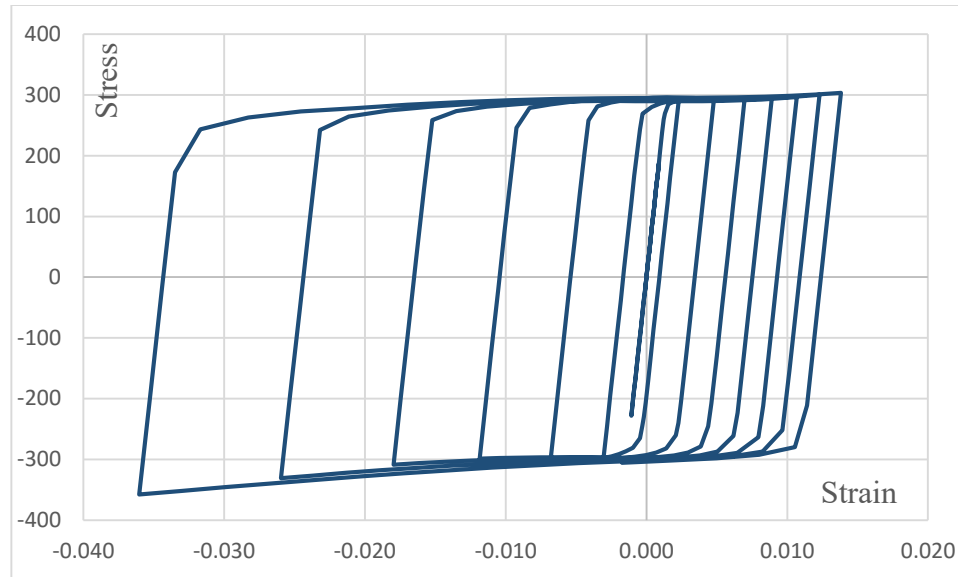
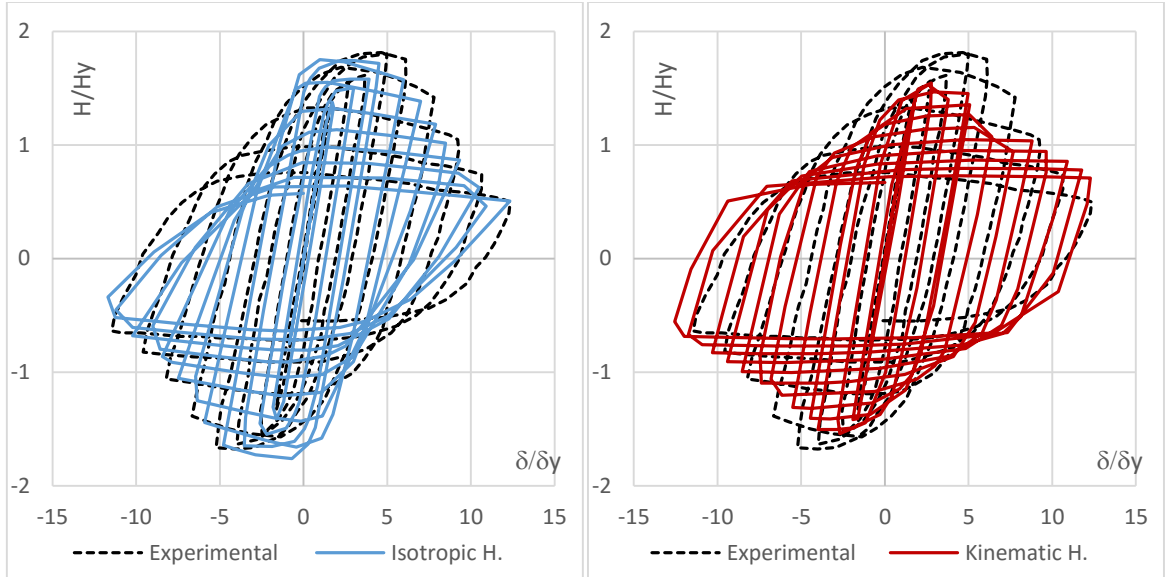


Figure 22: Translation of yield surface, kinematic hardening

### 3.5.2 Structural Behavior

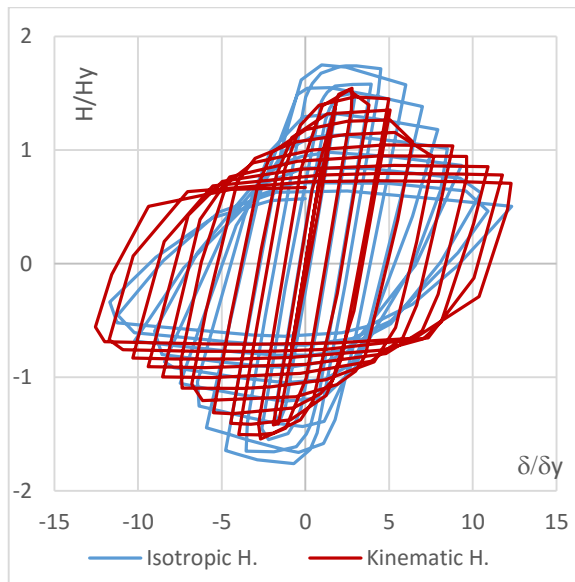
All the above mentioned models are analyzed by commercially available software ABAQUS. Then the horizontal load  $H$  and the horizontal displacement  $\delta$  were normalized by yield horizontal force  $H_y$  and yield displacement  $\delta_y$ . The hysteresis diagrams, buckling patterns, and envelop curves are compared with the experimental results carried by Public Works Research Institute of Japan.

Figure 23 shows a comparison between hysteresis diagrams using different hardening rules of specimen No.6. This diagram shows a clear difference between kinematic hardening rule and isotropic hardening rule. Isotropic hardening overestimate the maximum load carrying capacity and underestimate the deterioration of post buckling envelop curve.



a) Isotropic Hardening & Experimental

b) Kinematic Hardening & Experimental

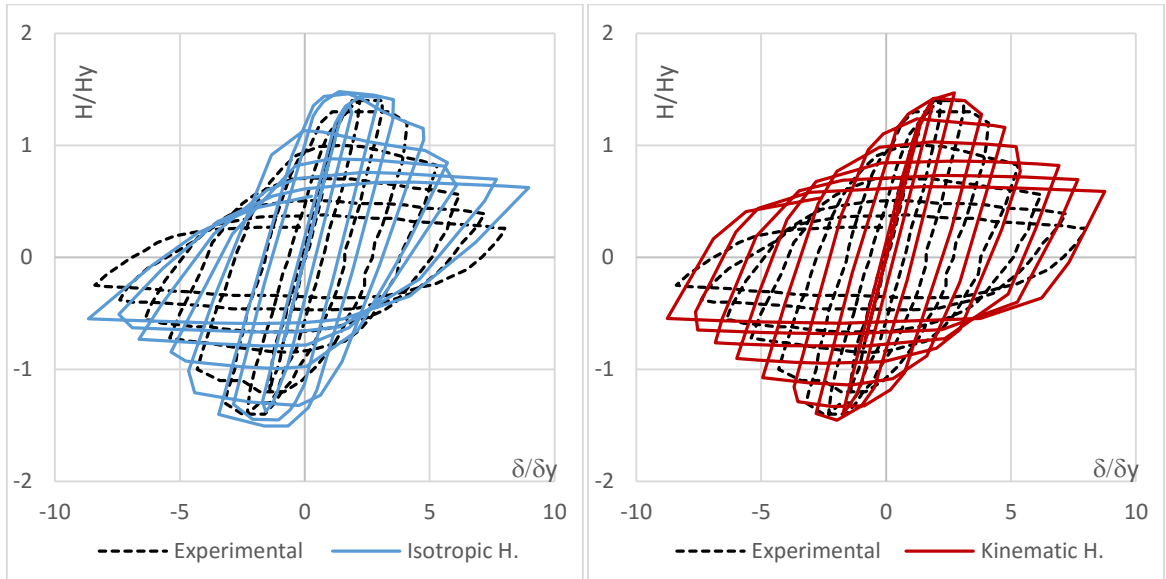


c) Isotropic Hardening & Kinematic Hardening

Figure 23: Comparison of hysteresis diagram for specimen No.6

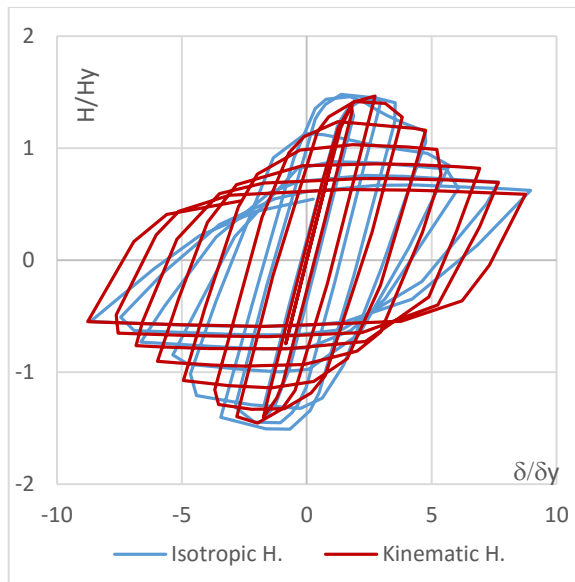
Figure 24 shows the comparison of specimen No.8. Hysteresis diagram comparison shows even though the peak normalized horizontal force value is same for both isotropic hardening and kinematic hardening but there is a subtle difference in hysteresis envelop curve which is inflected in the buckling behavior. Even though Initial stiffness, shape of the hysteresis

diagram and the value of the peak normalized horizontal force closely matches with the experimental values in initial cycles but both types of hardening overestimate peak buckling strength of the specimen.



a) Isotropic Hardening & Experimental

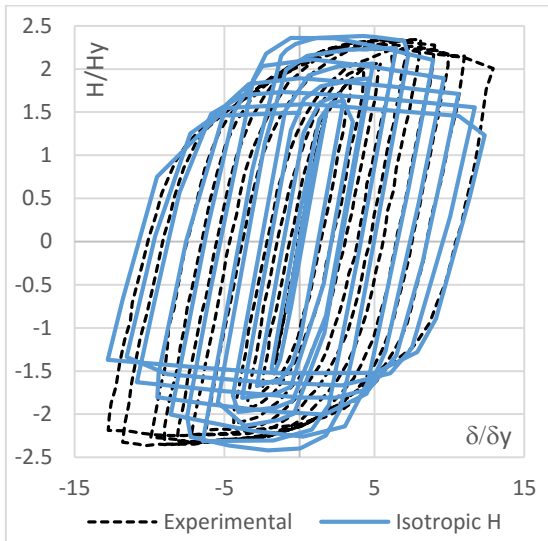
b) Kinematic Hardening & Experimental



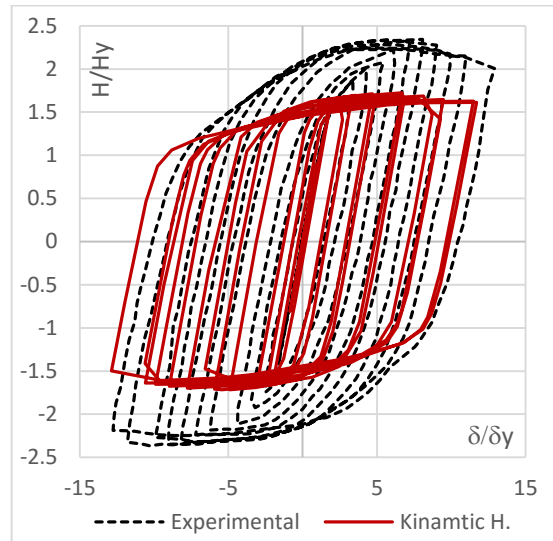
c) Isotropic Hardening & Kinematic Hardening

Figure 24: Comparison of hysteresis diagram for specimen No.8

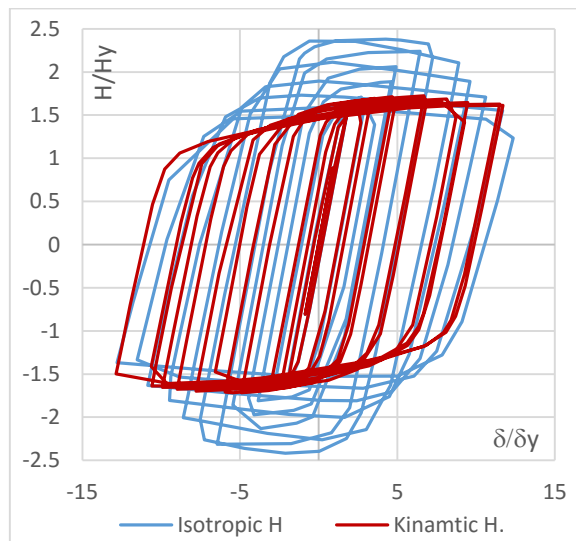
From the analysis of specimen KC-1, in Figure 25, difference between kinematic hardening rule and isotropic hardening rule is noticeable. Influence of hardening rule in material behavior is more apparent in the shape of normalized hysteresis diagram. For isotropic hardening material is getting stronger in both direction while for kinematic hardening when material is getting stronger in one direction become weaker in another direction.



a) Isotropic Hardening & Experimental

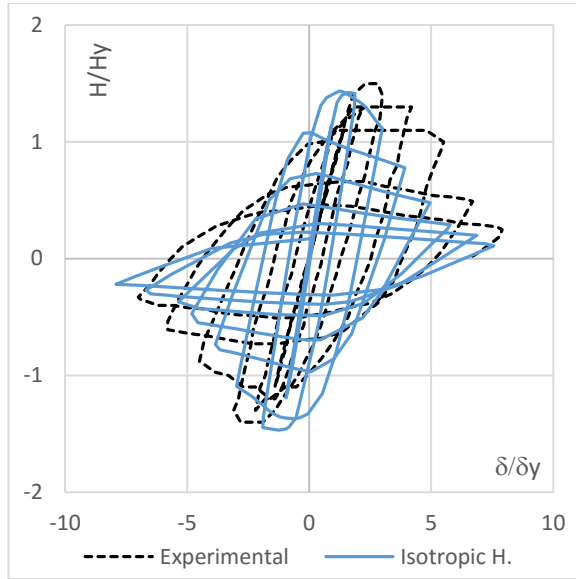


b) Kinematic Hardening & Experimental

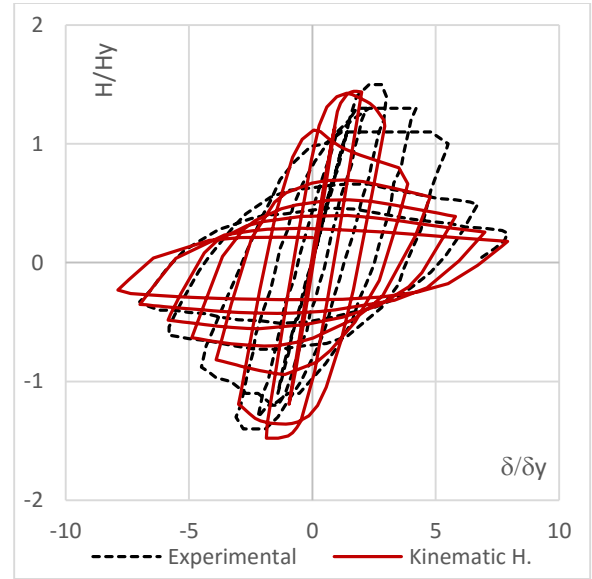


c) Isotropic Hardening & Kinematic Hardening

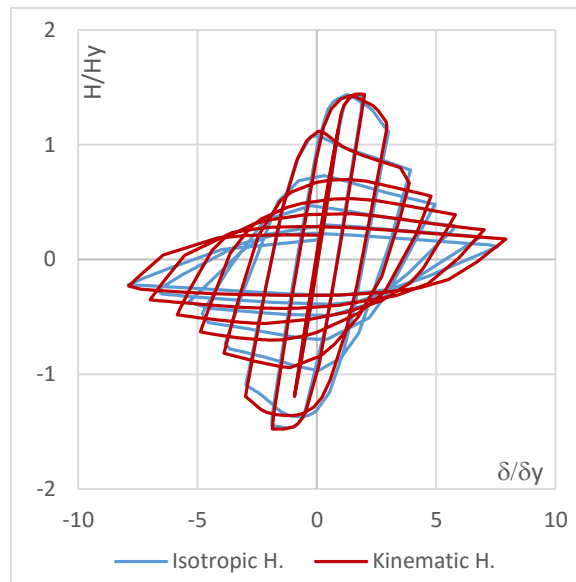
Figure 25: Comparison of hysteresis diagram for specimen KC-1



a) Isotropic Hardening & Experimental



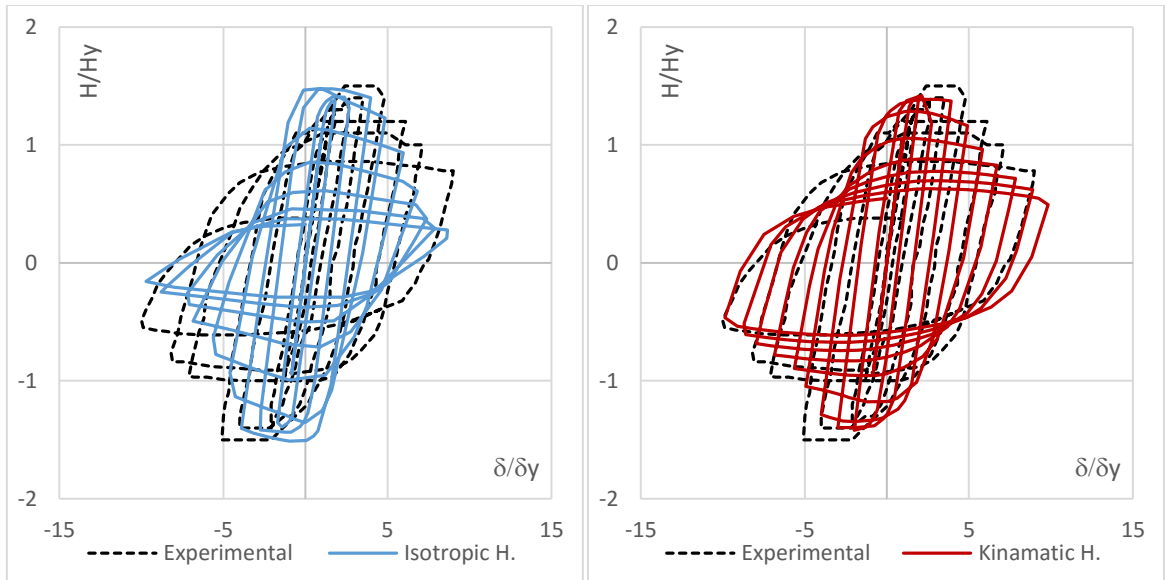
b) Kinematic Hardening & Experimental



c) Isotropic Hardening & Kinematic Hardening

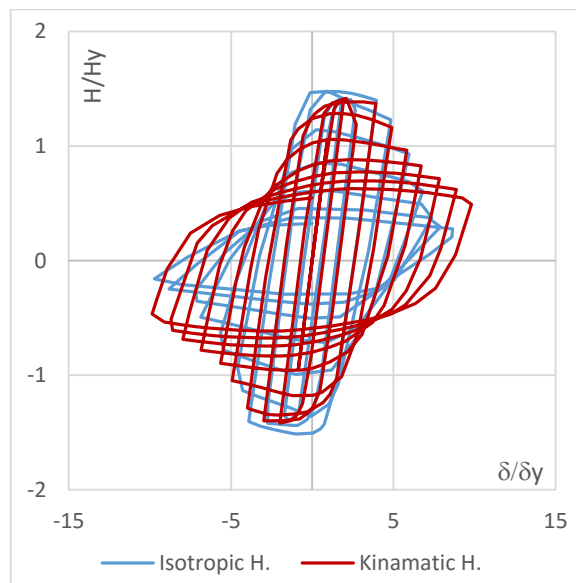
Figure 26: Comparison of hysteresis diagram for specimen No.2

In Figure 27, for the specimen KD-3, behavior of column matches more with experimental result for kinematic hardening. Eventhough in experiment peak normalized horizontal force is slightly greater then the value obtained from kinemetic hardening but the post buckling behavior closely matches with kinematic hardening.



a) Isotropic Hardeing & Experimental

b) Kinematic Hardeing & Experimental



c) Isotropic Hardeing & Kinematic Hardeing

Figure 27: Comparison of hysteresis diagram for specimen KD-3

There is also a difference in the buckling shape and position in the specimens. The following figures shows the buckling comparison between the used hardening rule. Figure 28 shows the buckling shape and position in the specimen No.6 for isotropic hardening while Figure 29 shows for kinematic hardening. In kinematic hardening, elephant foot shape bulging

occurs where in the case of isotropic hardening a different shape of buckling occurs. There is also a difference in the position of buckling. Buckling occurs more close to the base in the case of kinematic hardening.

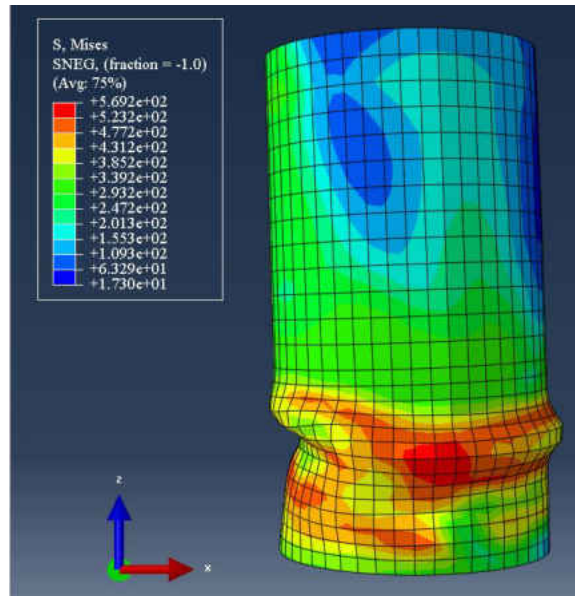


Figure 28: Buckling behavior of No.6 specimen at  $10 \delta y$  using Isotropic Hardening

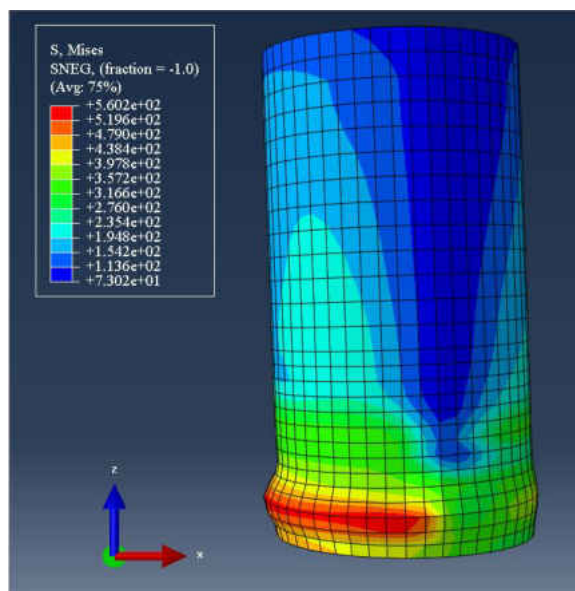


Figure 29: Buckling behavior of No.6 specimen at  $10 \delta y$  using Kinematic Hardening



Figure 30 and 31 shows the buckling shape of the specimen No.8. For kinematic hardening buckling shape is elephant foot bulging and occurs at the bottom of the specimen while for isotropic hardening buckling shape is different and location of the buckling moves upward.

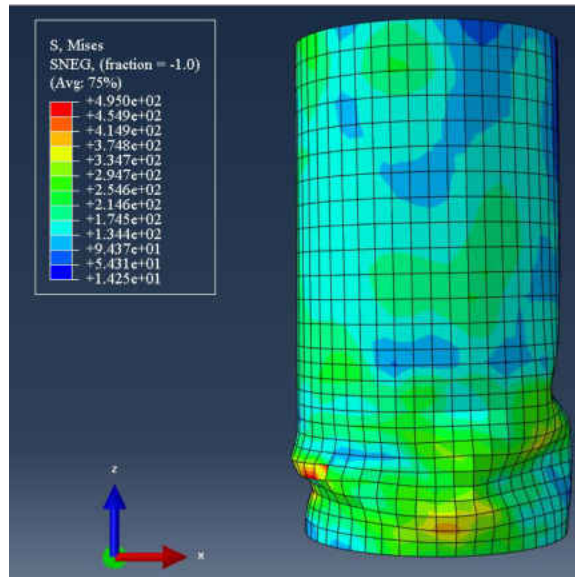


Figure 30: Buckling behavior of No.8 specimen at  $9 \delta_y$  using Isotropic Hardening rule

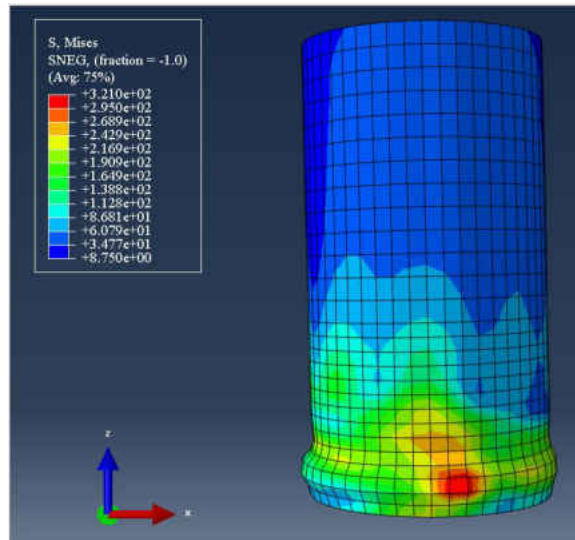


Figure 31: Buckling behavior of No.8 specimen at  $9 \delta_y$  using Kinematic Hardening

For the specimen KC-1, Figure 32 and 33, buckling shape and location is same regardless of the hardening rule. In both cases, a outward buckling occurs at the bottom of column, close to the base.

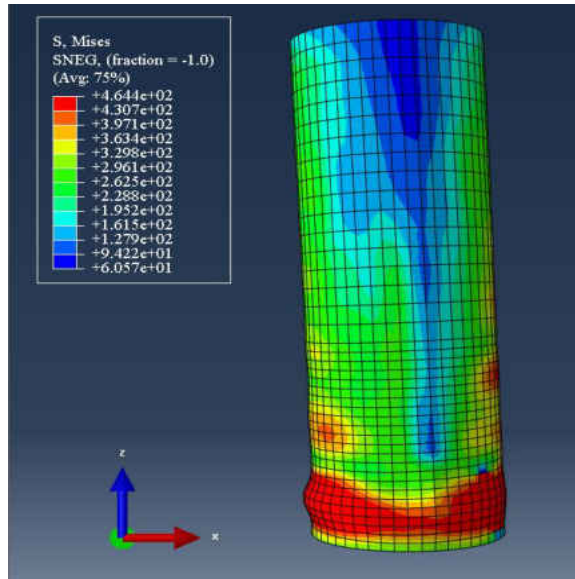


Figure 32: Buckling behavior of KC-1 specimen at  $9 \delta y$  using Isotropic Hardening

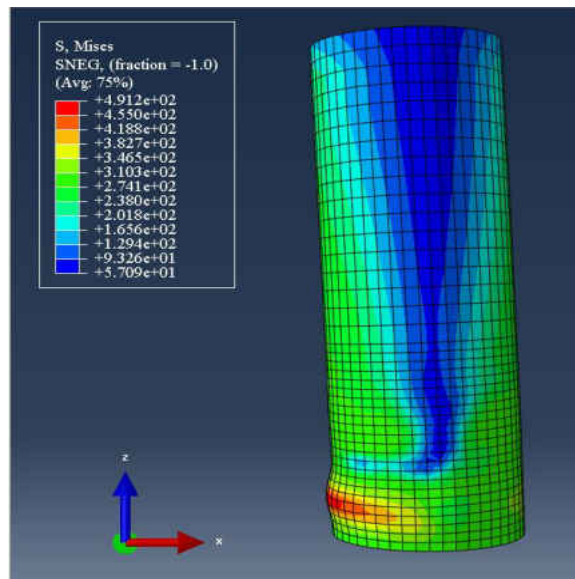


Figure 33: Buckling behavior of KC-1 specimen at  $9 \delta y$  using Kinematic Hardening

Figure 34 and 35 shows a comparison between buckling shape for the specimen No.2. In both cases buckling shape is same: outward buckling in web and inward buckling in the compression flange.

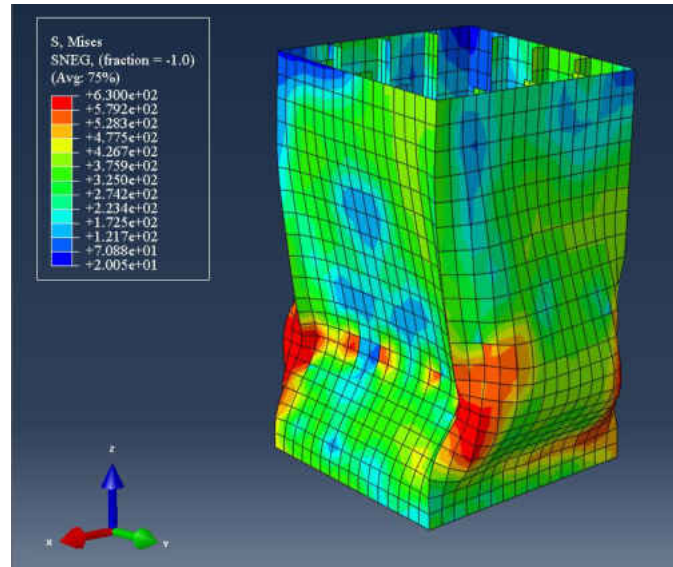


Figure 34: Buckling behavior of No.2 specemen at  $7 \delta y$  using Isotropic Hardening

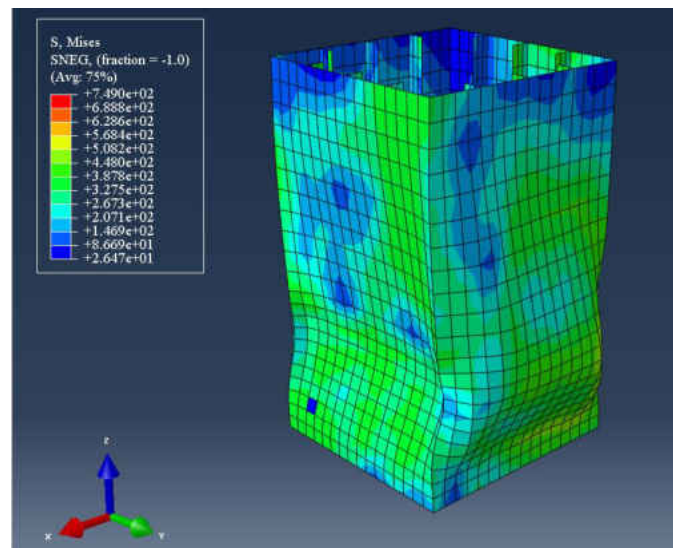


Figure 35: Buckling behavior of No.2 specemen at  $7 \delta y$  Kinematic Hardening

Figure 36 and 37 shows a comparison between buckling shape for the specimen KD-3. In both cases buckling shape and location is almost same: outward buckling in web and inward buckling in the compression flange.

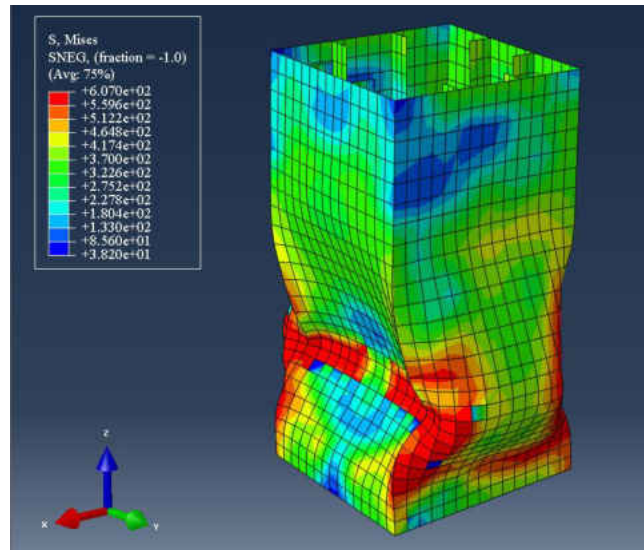


Figure 36: Buckling behavior of KD-3 specemen at 11  $\delta y$  using Isotropic Hardening

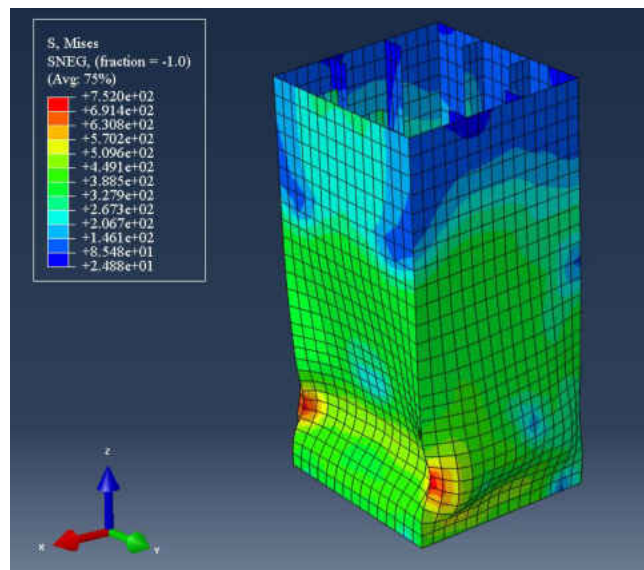


Figure 37: Buckling behavior of KD-3 specemen at 11  $\delta y$  Kinematic Hardening rule

The following Figure 38, shows a comparison of isotropic hardening and kinematic hardening result with its experimental counterpart. From the diagrams it is apparent that even though the initial stiffness of the structure is same for isotropic hardening, kinematic hardening and experimental one but the envelop curve changes after couple of cycles. Isotropic hardening overestimate the normalized hysteresis peak values but underestimate the deterioration of specimen.

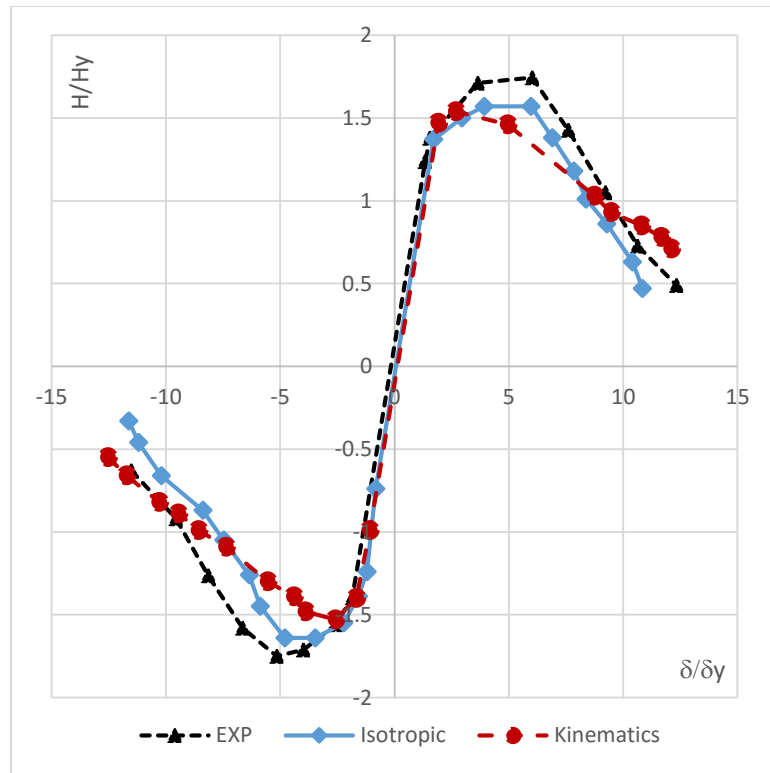


Figure 38: Comparison between envelop curve for specimen No.6

Figure 39 shows the comparison of different used hardening rule for specimen No.8. The initial stiffness is same but it changes after 2 cyclic load. Experimental values are lower than the analytical values. Higher magnitude of analytical normalized horizontal force indicates the underestimate of buckling in case analytical simulation. The reason could be due to the residual stress. In case of experiment, the specimens were fabricated by welding

cold-formed steel thin plates. This welding process left residual stress in specimen which is not considered in analytical simulation.

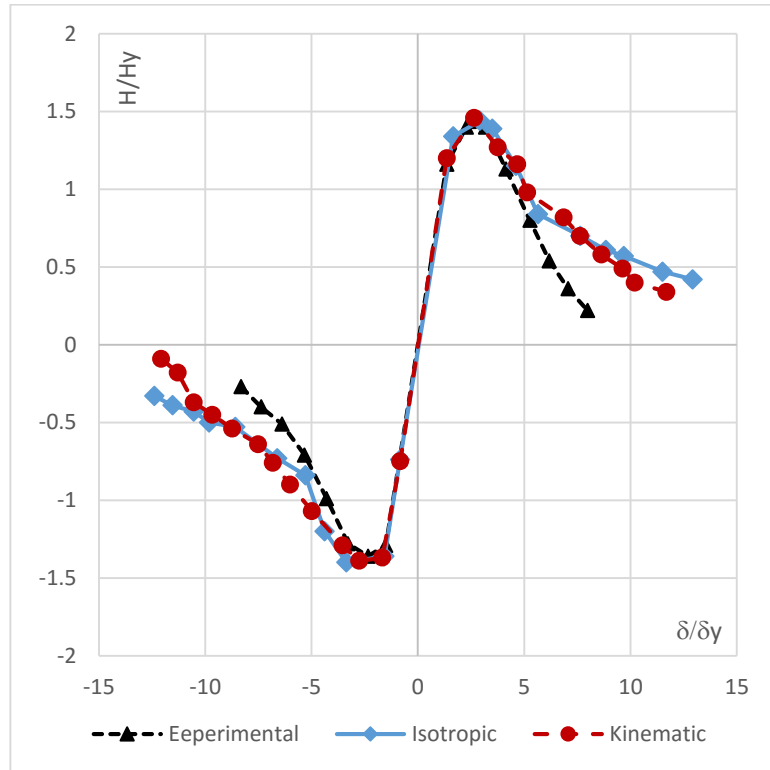


Figure 39: Comparison between envelop curve for specimen No.8

The following Figure 40 shows the comparison of different used hardening rule for specimen KC-1. Initial stiffness is same for isotropic hardening, kinematic hardening and experimental one but it changes after 2 cyclic load. Even though for isotropic hardening shows higher normalized horizontal force than kinematic hardening but it drops rapidly with the increase of cycles, indicates more severe buckling compare to kinematic hardening.

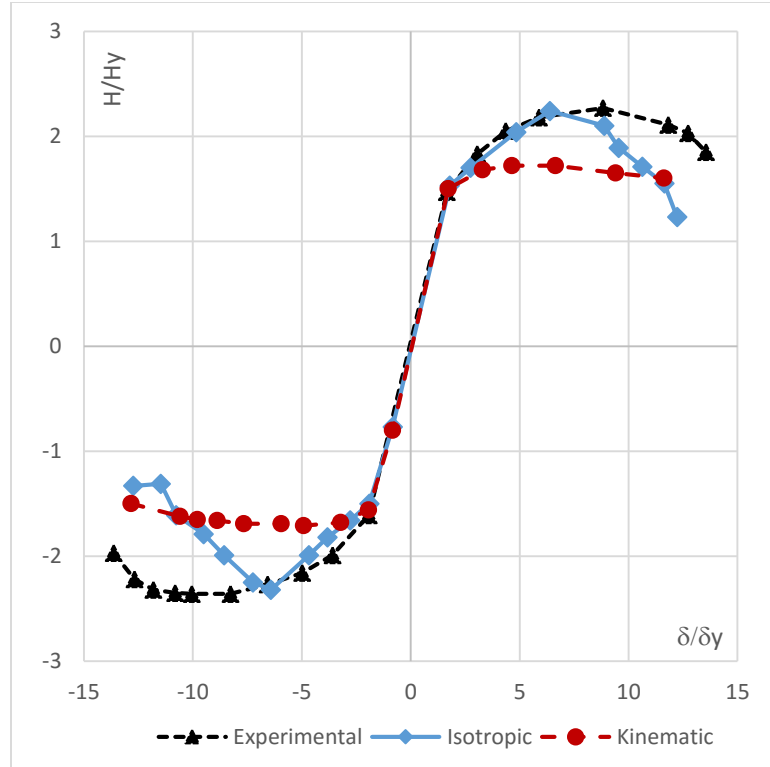


Figure 40: Comparison between envelop curve for specimen KC-1

The following Figure 41 shows the comparison of different used hardening rule for specimen No.2. The initial stiffness is same but it starts to change after couple of cycles. Even though at the initial cycles the experimental values are lower than the analytical values but eventually experimental values supersede the analytical values. In the initial cycles, specimen behavior was same for both isotropic and kinematic hardening but more severe buckling takes form for the isotropic hardening at higher cycles.

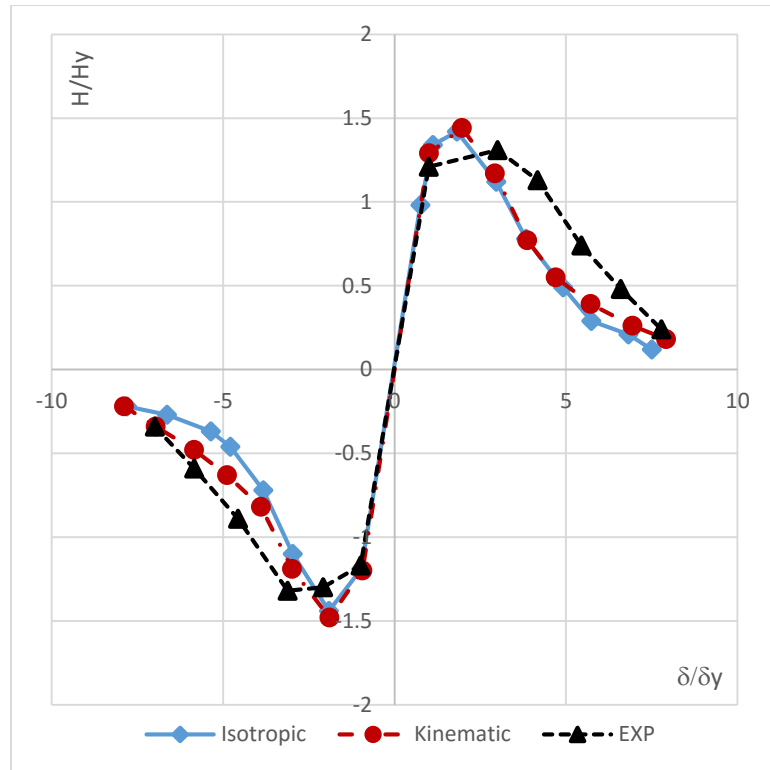


Figure 41: Comparison between envelop curve for specimen No.2

Figure 42 shows the comparison between different hardening rules for specimen KD-3. The initial stiffness is same for isotropic hardening, kinematic hardening and experiments but it changes after 3 cycles and experimental values become higher than the analytical values. In the initial cycles, specimen behavior was same for both isotropic and kinematic hardening but at the higher cycles more severe buckling appears for the isotropic hardening than kinematic hardening.



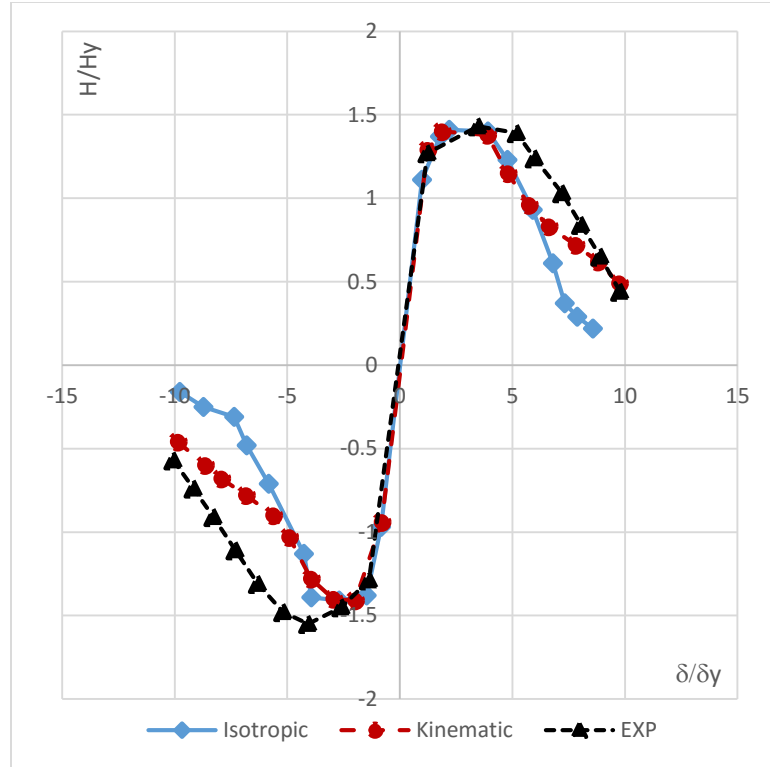


Figure 42: Comparison between envelop curve for specimen KD-3

### 3.6 Conclusion

In this study, the analytical results are obtained using ABAQUS 6.13. Then the results are compared with the experimental data to observe the validity of available material modeling. As it is apparent that, behavior of specimen is dependent on the used material modeling. The initial slope of the envelop curve which represent the stiffness of the structure is same regardless used material modeling but the value changes after couple of cycles. The reason is that, after some cycles structures enter into plastic zone, behavior of structure in plastic zone totally depends on the used hardening rule. In isotropic hardening material strength increases in both tension and compression side, moreover it allows the increment of yield surface with every cycles. Though the radius of yield surface increases so the material

become stronger and gives a higher normalized horizontal force. On the other hand, kinematic hardening rule allows to translate the yield surface without increasing the size. That's why when material become stronger in one direction, it become weak in another direction. These differences are apparent in normalized hysteresis behavior. There is also some differences in the pattern and location of buckling. For kinematic hardening rule, buckling occurs at the base of the column and buckling shape is either elephant foot bulging or outward bulging. While in the case of isotropic hardening location of buckling moves upward and shape of buckling is different from that of kinematic hardening.

In essence, by comparing the finite element analysis results to the experimental results the following observations can be made:

- There is a considerable deference in the cyclic seismic behavior of pier between two used material model, namely isotropic hardening model and kinematic hardening model.
- For kinematic hardening model either elephant foot bulging or outward buckling takes form at near to the base while for isotropic hardening model a different buckling shape occurs and the location of buckling moves upward from the buckling positon for kinematic hardening.
- The isotropic hardening model slightly overestimate the load carrying capacity and also overestimate the deterioration of envelop in the normalized hysteresis diagram than kinematic hardening model
- The difference between analytical results and experimental results can be explained by several factors, such as presence of residual stress and initial crookedness in the column, which are not considered in numerical analysis.

- Between two material models, kinematic hardening model predict the behavior more accurately than isotropic hardening model as kinematic hardening consider Bauschinger effect.

## CHAPTER IV

### CONCRETE FILLED STEEL COLUMN

#### 4.1 Introduction

After a lesson obtained from Kobe earthquake (1995), the use of concrete filled tube is increased for highway bridge piers. Researchers show that the strength and ductility of the thin-walled members are augmented considerably by the use of concrete, filling the hollowed steel section with concrete (Ge and Usami, 1996). In the recent era, the uses of concrete filled tube for elevated bridge in urban areas is increasing because of its high seismic resistance. These CFT are advantageous over concrete column even thin-walled steel member because of ductility enhancement without increasing or affecting other parameters.

Some experiments were carried out by Goto *et al.* (2010) to show the enhancement in ductility and strength due to concrete filling. In this chapter, FEM is used for numerical simulation to show this experimental fact.

One of the most important factor, while analyzing concrete filled tube discrete crack model is used to define the concrete property. Inserting a crack in the position of maximum stress is important because in plastic damage model, because of the isotropic property, strength in concrete increases in both side which affects the late formation of tension crack. To solve this problem, a crack is inserted and representative frictional behavior defined at the place

of maximum stress. It represent the pinching behavior, showing in the Figure 43, of concrete filled tubular steel column.

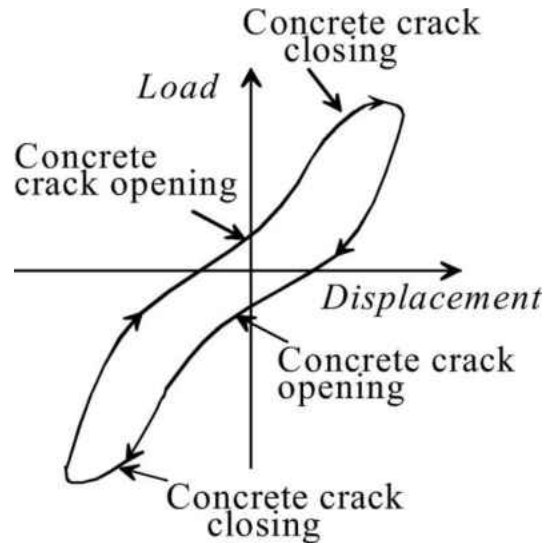


Figure 43: Pinching behavior of Concrete Filled Tube

## 4.2 Specimen

In this thesis, numerical studies on concrete filled tube are carried out by commercially available software ABAQUS (v 6.13). Using this software, two test specimen were analyzed, named: No. 16 and No. 30. Both of the specimen possess same geometrical properties e.g. height, thickness, diameter of column, thickness of diaphragm and height of the concrete, only normalized axial load and concrete strength are varied. Another two hollow specimen identical to No. 30 and No. 16, except no infill concrete, is analyzed to show the improvement in the seismic behavior due to concrete. Figure 44 shows the schematic diagram of the specimen. Geometrical and material properties of the specimens that were used by Goto *et al.* (2010) are mentioned in Table 4.

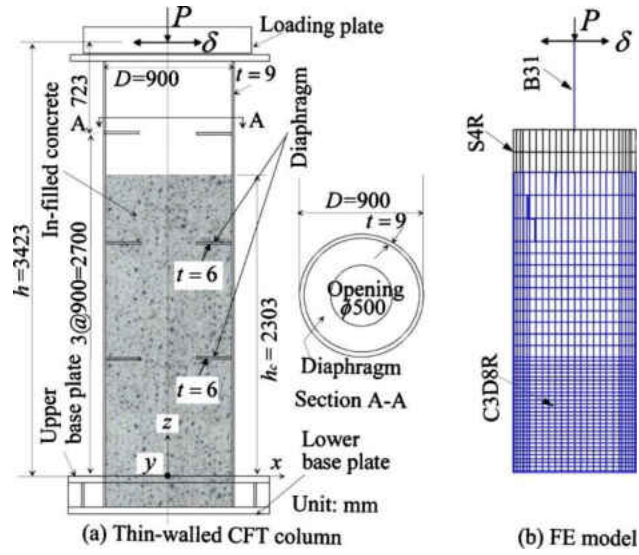
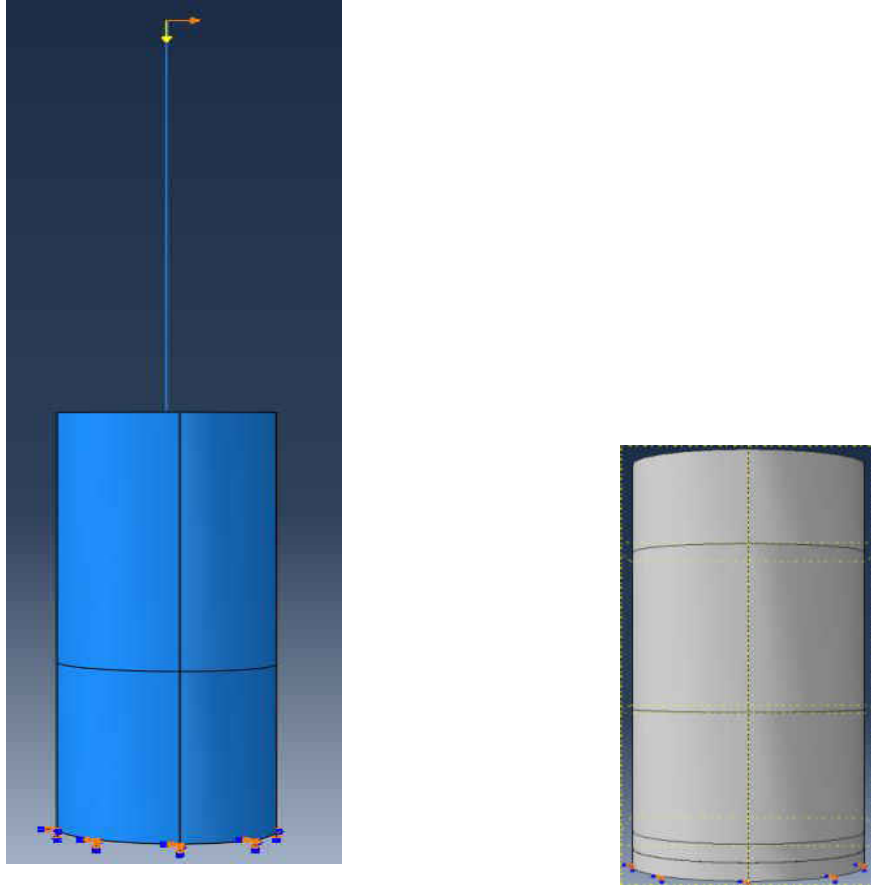


Figure 44: Dimension detailing of the Specimen

Table 4: Geometric and Material Properties of Specimens Goto *et al.* (2010)

Specimen	No.16 (CFT)	No.30 (CFT)	No.16 (Hollow)	No.30 (Hollow)
Material	SS400	SS400	SS400	SS400
h (mm)	3423	3423	3423	3423
t (mm)	9.0	9.0	9.0	9.0
D (mm)	900	900	900	900
$\bar{\lambda}$	0.268	0.268	0.268	0.268
$R_t$	0.123	0.123	0.123	0.123
$H_0$ (kN)	443.94	400.82	443.94	400.82
$\delta_0$ (mm)	11.53	10.5	11.53	10.5
$P/\sigma_y A_s$	0.114	0.199	0.114	0.199
$f'_c$	27.93	21.46	27.93	—



a) Boundary conditions for Steel column      b) Boundary conditions for Concrete

Figure 45: Boundary and loading condition of the specimen

Figure 45 shows the used boundary conditions for the simulation of the columns. For parametric studies, concrete height of the column is varied which is shown in Table 5.

Table 5: Height of concrete in Concrete Filled Tube

<b>h/h<sub>c</sub></b>	<b>30%</b>	<b>50%</b>	<b>53%</b>	<b>67%</b>
<b>No.16</b>	1030	1712	1815	2303
<b>No.30</b>	1030	1712	1815	2303

Here,  $R_t$  = radius-to-thickness ratio, and,  $\lambda$  = the slenderness ratio parameter, are two important parameters for concrete filled tube which are considered for design and ductility evaluation. These parameters are expressed by the following equations (Mamaghani and Packer, 2002):

$$R_t = \frac{r}{t} \sqrt{3(1 - \nu^2)} \frac{\sigma_y}{E} \quad (52)$$

$$\lambda = \frac{2h}{\pi} \sqrt{\frac{I}{A}} \sqrt{\frac{\sigma_y}{E}} \quad (53)$$

Where,  $t$  = plate thickness;  $\sigma_y$  = yield stress;  $E$  = Young's modulus;  $\nu$  = Poison's ratio;  $r$  = radius of the circular section;  $h$  = column height;  $I$  = Moment of inertia of the steel, and  $A$  = area of the cross section of steel.

Other two parameter,  $H_0$  = yield strength of the steel column and,  $\delta_0$  = yield deformation of the steel section is defined by the given equations.

$$H_0 = (\sigma_y - P/A) \frac{z}{h} \quad (54)$$

$$\delta_0 = \frac{H_0 h^3}{3EI} \quad (55)$$

Where,  $I$  = moment of inertia of the steel cross section,  $P$  = axial load,  $A$  = the steel cross-sectional area,  $h$  = the column height,  $EI$  = the bending rigidity of steel section, and  $z$  = the second modulus of steel section.

### 4.3 Material Modeling

#### 4.3.1 Steel Modeling

In the experiment steel SS400, which is comparable to A36, is used for fabricating the specimen. The detailed steel property is given in Table 6 and stress-stain curve is in shown



in Figure 46 and 47. As kinematic hardening predicts seismic behavior more accurately, for numerical simulation kinematic multilinear hardening is used for steel in this simulation.

Table 6: Parameters for steel Goto *et al.* (2010)

Property	No.16 (Hollow & CFT)	No.30 (Hollow & CFT)
$E_s$	205.8 GPa	205.8 GPa
$\sigma_y$	308 Mpa	308 Mpa
$\sigma_u$	559.5 Mpa	534 Mpa
$\nu_s$	0.3	0.3

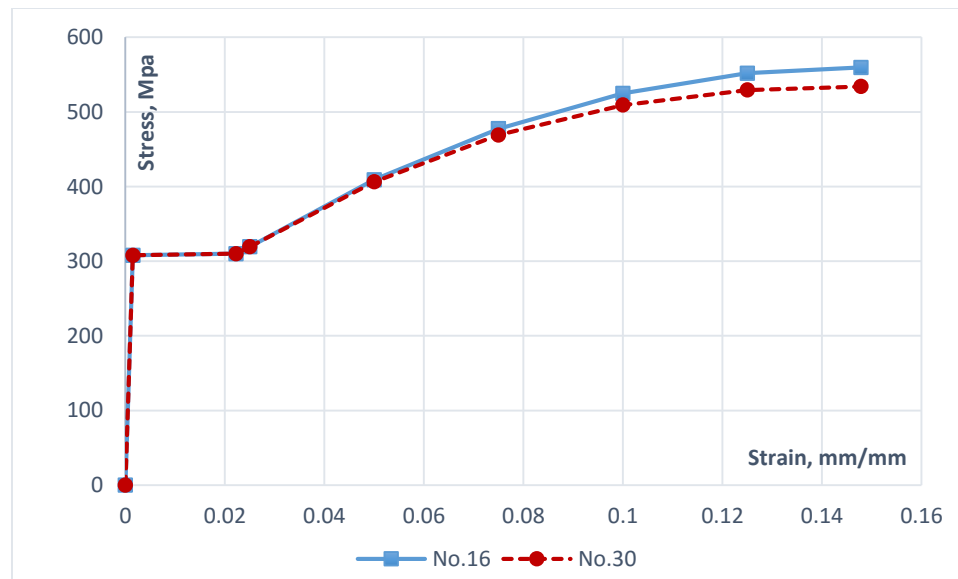


Figure 46: Stress-Strain diagram of steel SS400 Goto *et al.* (2010)

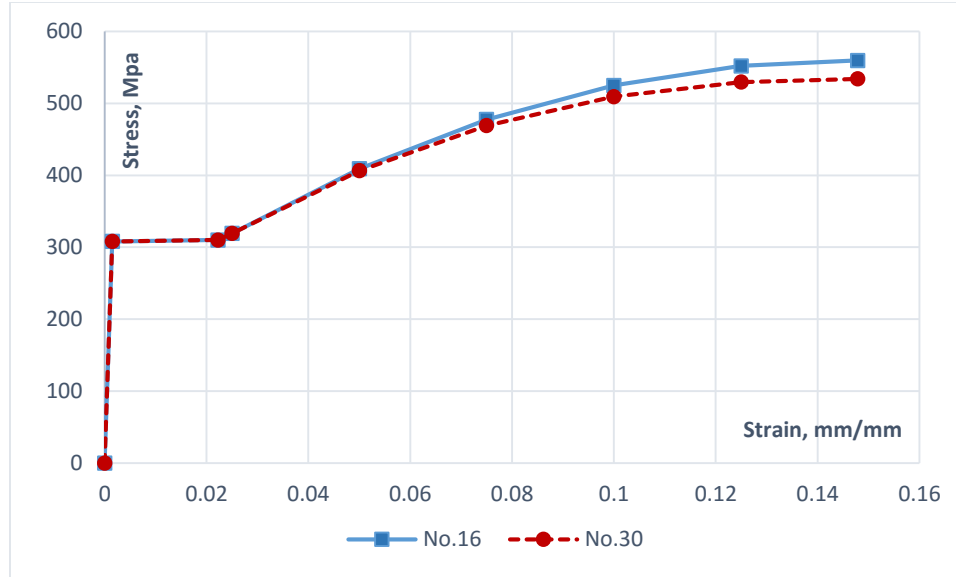


Figure 47: Stress-Plastic Strain of Steel SS400 Goto *et al.* (2010)

### 4.3.2 Concrete Modeling

For concrete modeling damage plasticity model is used. For the concrete under cyclic load damage plasticity model predicts better than smeared crack modeling in ABAQUS as it can express crack formation more accurately than other existing model. Axial compression and tension data is obtained from the test results while input damage data is calculated from the given equations:

Compressive damage parameter,  $d_c$ :

$$d_c = \frac{k_{ci}\varepsilon_c}{\left[1 + \left(\frac{\varepsilon_c}{\varepsilon_o}\right)^n\right]^n}; \varepsilon_c \leq 0.0184 \quad (56)$$

$$d_c = 0.3485; \varepsilon_c > 0.0184$$

Here,  $k_{ci} = 155$ ,  $\varepsilon_o = 0.0035$ ,  $n = 1.08$

Tension damage parameter,  $d_t$ :

$$d_t = \frac{1.24k_t}{\sigma_{to}} u^{cr} \quad (57)$$

Here,  $k_t, \sigma_{to}, u^{cr}$  depends on the concrete material property.

To define the post peak hardening for damage plasticity model ABAQUS use Drucker-Prager hardening rule. The hyperbolic Drucker-Prager flow potential function  $G$  is shown below.

$$G = \sqrt{(e\sigma_{to} \tan \psi)^2 + q^2} - p \tan \psi \quad (58)$$

Here,  $\sigma_{to}$ = tensile strength,  $\psi$ = dilation angle,  $e$ = flow potential eccentricity,  $q$  = Mises equivalent effective stress defined in terms of  $\sigma$  ,  $p$  = effective hydrostatic pressure.

Figure 48 shows the compressive behavior of concrete and Figure 49 shows plastic strain-stress for the concrete while Figure 50 shows the compressive damage of concrete.

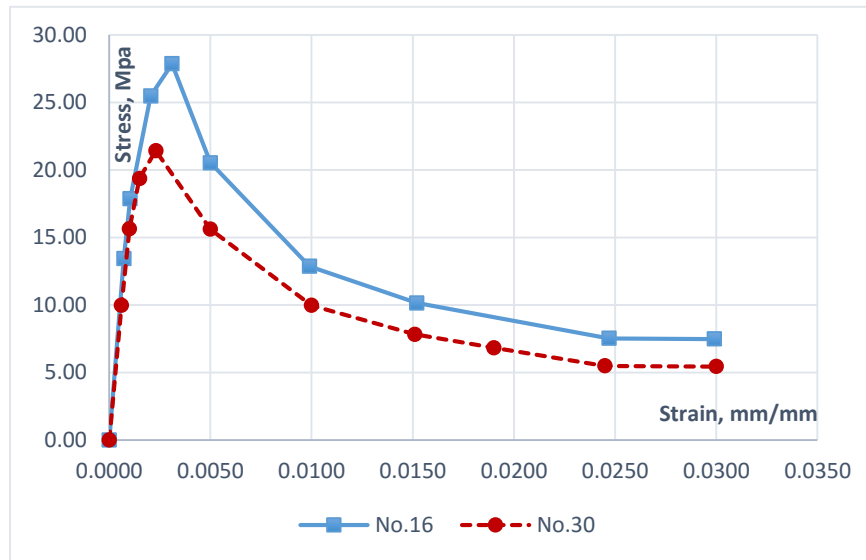


Figure 48: Compressive Stress-Strain of Concrete Goto *et al.* (2010)

Figure 51 shows the tensile behavior of concrete while the tensile damage of concrete is described in Figure 52.

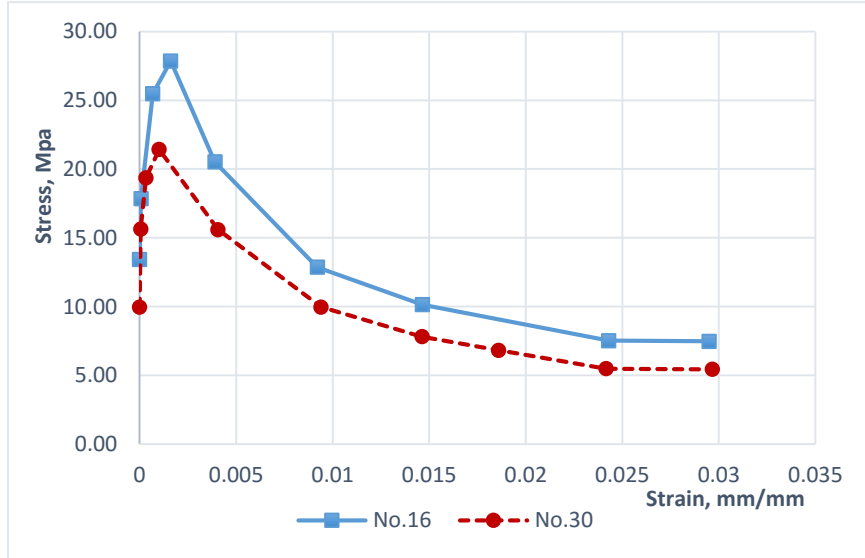


Figure 49: Compressive Plastic Stress-Strain curve of Concrete Goto *et al.* (2010)

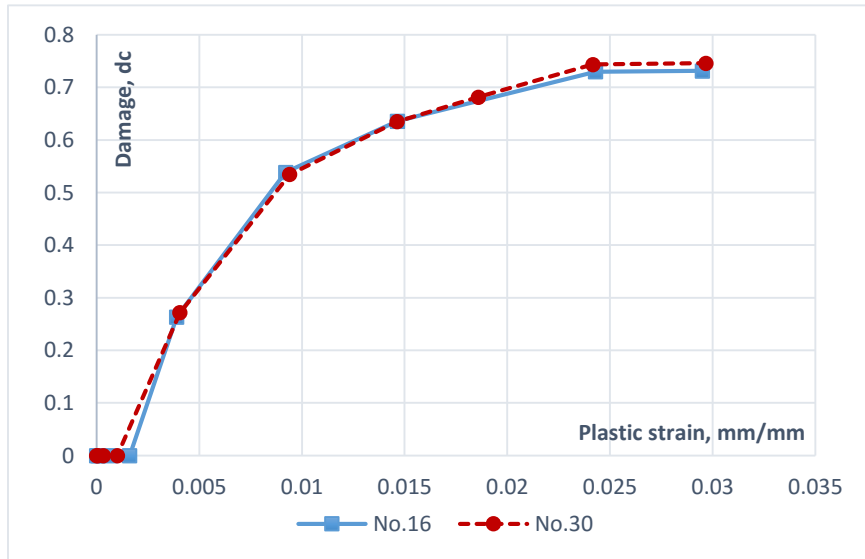


Figure 50: Compressive damage of Concrete Goto *et al.* (2010)

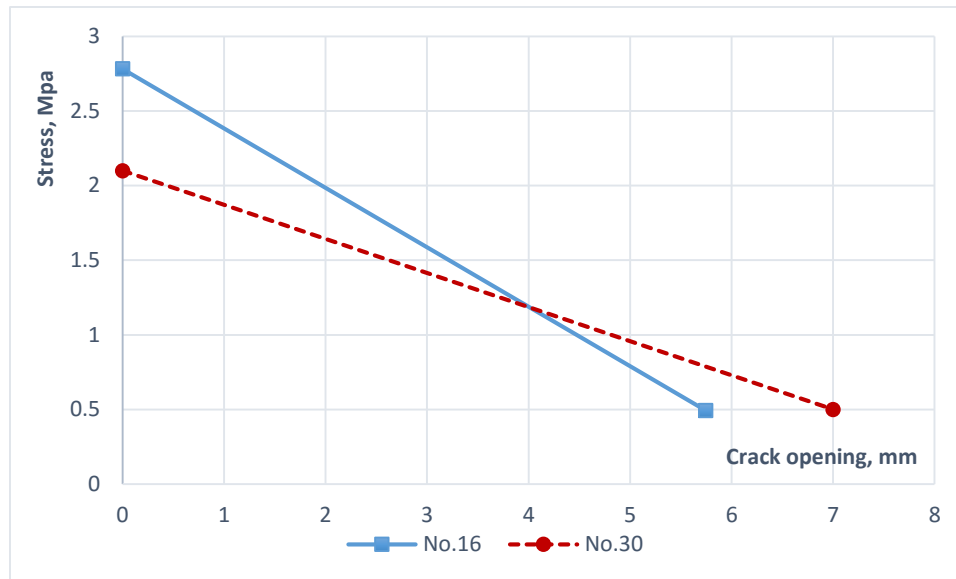


Figure 51: Tensile stress- crack opening of Concrete Goto *et al.* (2010)

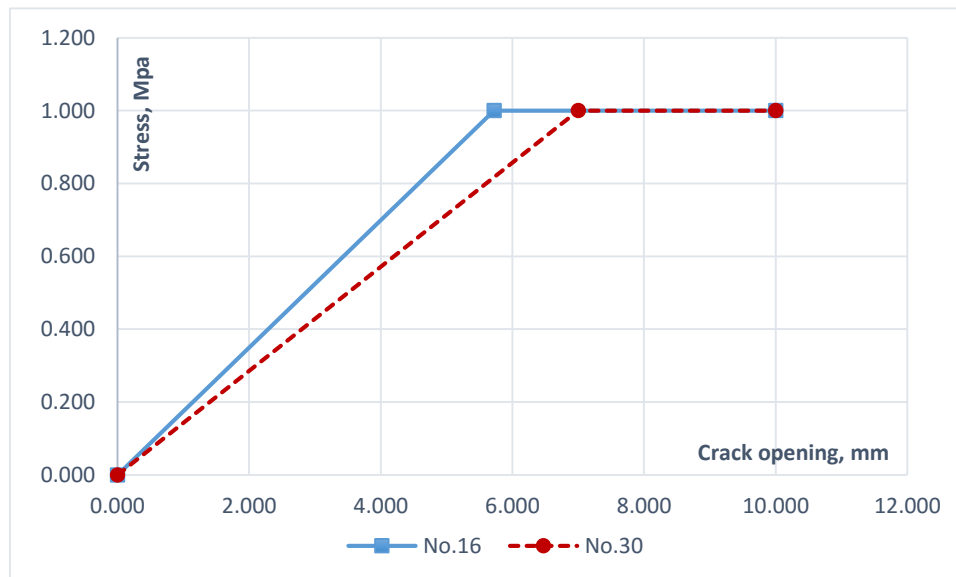


Figure 52: Tension Damage of Concrete Goto *et al.* (2010)

Other input parameter in ABAQUS for damage plasticity model is described in the given Table 7. To facilitate converging to solve the contact equations, it is recommended to input very little value in viscosity parameter instead of zero.

Table 7: ABAQUS material parameter for Concrete

Parameter	No. 16	No. 30
E	18670	16620
$\nu$	0.2	0.2
$\psi$	38	38
e	0.2	0.2
K <sub>c</sub>	0.7	0.7
$f_{bo}/f_c$	1.1	1.1
$\omega$	0.001	0.001

Here, E= modulus of elasticity of concrete,  $\nu$ = poison ratio,  $\psi$ = dilation angle, e= flow potential eccentricity, K<sub>c</sub>= compressive meridian,  $f_{bo}/f_c$ = ratio of the compressive strength under biaxial loading to uniaxial compressive strength,  $\omega$ = viscosity parameter.

#### 4.4 Finite element modeling

##### 4.4.1 Mesh and element

In order to reduce the analysis time these models are simplified to combination of beam, shell and solid element. Infilled concrete is modeled using 8 node solid element C3D8, and steel column is modeled as a combination of shell and beam element to reduce the number of unknowns. Bottom part, almost  $3h/4$ , is modeled with shell element S4R (4 node shell element) while top  $h/4$  is modeled using beam element B31 (2 node beam element). More the element the more accurately the result is but it also increases the simulation time greatly. To select the optimum element size without effecting the precision of result, sensitivity test was performed. For the case of infilled concrete, bottom  $D/5$  is finely meshed in order to facilitate interaction between the discrete crack and mesh size is  $D/15$ . The rest of the part is relatively coarsely meshed and mesh size is approximately  $D/10$ . For the steel column in bottom part of the shell the mesh size was  $D/15$ , rest of the

part up to infilled concrete height mesh size was approximately  $D/10$  while the rest of the mesh size was  $D/8$ . In case of the beam element the mesh size is selected as  $D/5$ . Figure 53 shows the meshing of the specimen.

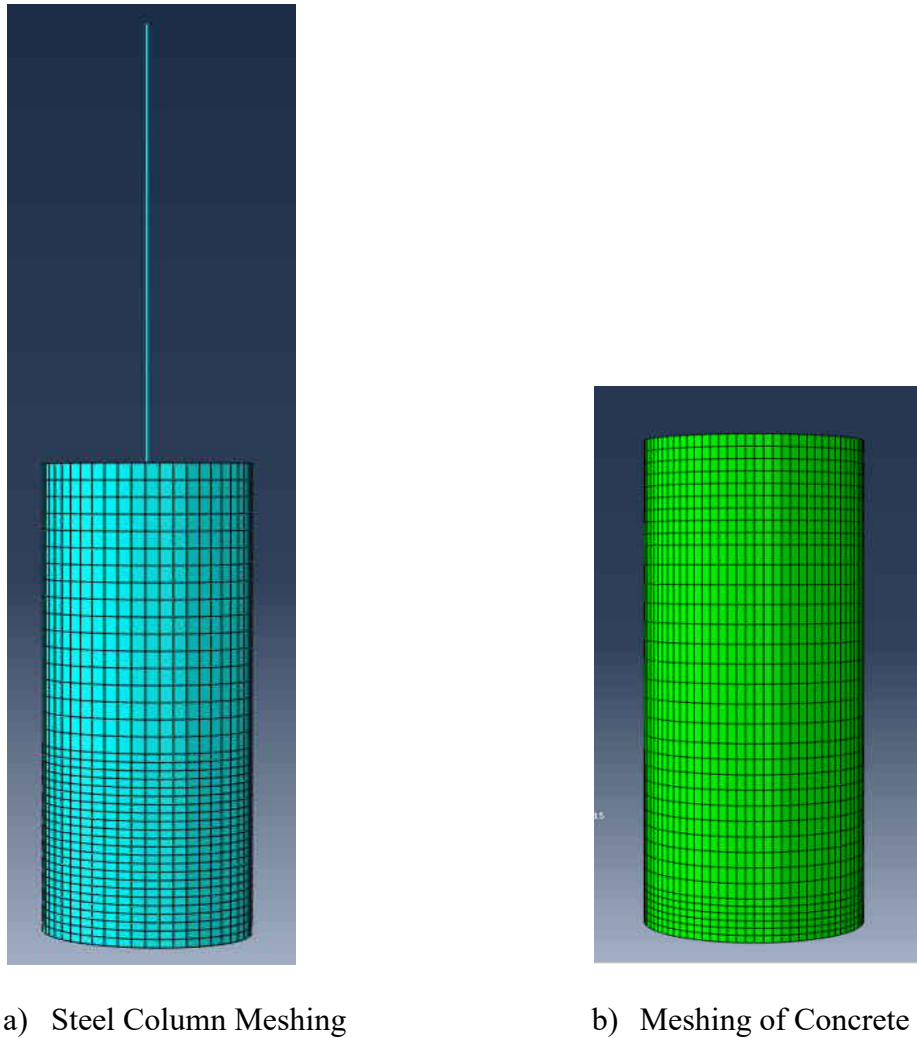


Figure 53: Meshing of the specimen

#### 4.4.2 Interface

Though damage plasticity model assume isotropic plasticity in tension zone similar to compression zone so it approximates in terms of tension behavior. So it can't express the crack opening and closing accurately when structure is under cyclic load. To define

crack behavior properly, a discrete crack is introduced in the concrete at the place where maximum tensile stress occurred during loading. The effect of crack is shown in Figure 54. To state the interaction between two separate part tangential behavior and normal was defined. For tangential interaction, frictional penalty surface is defined where friction coefficient is 0.5 for steel-concrete interface and 1.0 is for concrete-concrete interface. ABAQUS uses Mohr-Coulomb friction model to define the frictional interaction and default Lagrangian for contact formulation. For defining normal behavior hard contact surface model is used which allows separation after contact but no penetration. For defining the surface, steel surface is considered as master surface where concrete surface is defined as slave surface. For concrete-concrete interface bottom part of the top concrete portion is defined as master surface while bottom surface is selected as slave surface.

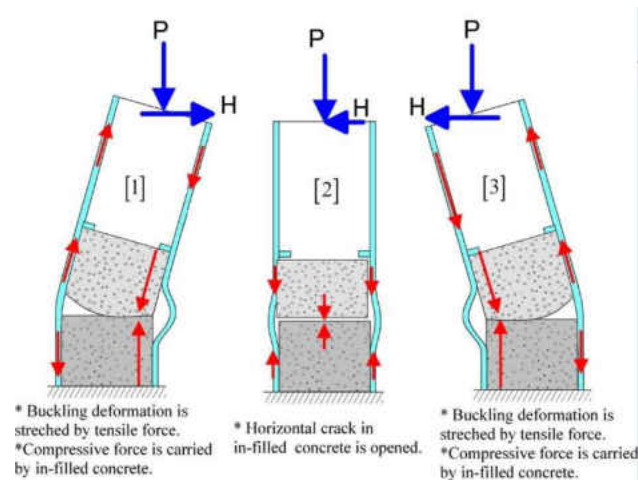


Figure 54: Crack behavior of the CFT

#### 4.4.3 Loading

All the specimen were subjected to vertical axial load and horizontal displacement. Unidirectional displacement was applied along X direction. The amplitude of the load is



an integer multiplication of yield displacement  $\delta_y$ . An axial load  $P$  is applied at the top of the column.  $\delta_y$  is calculated from the given equation.

$$\delta_y = \frac{H_y h^3}{3EI} \quad (59)$$

Here,  $H_y = (\sigma_y - P/A)z/h$  and represents the horizontal force,  $A$  = the cross-sectional area,  $h$  = the column height,  $EI$  = the bending rigidity, and  $z$  = the plastic modulus of section. Load was applied in two step. First vertical load was applied to established contact between the steel and concrete surface. Then in the second step horizontal displacement was applied. Figure 55 shows the applied horizontal displacement for the specimen.

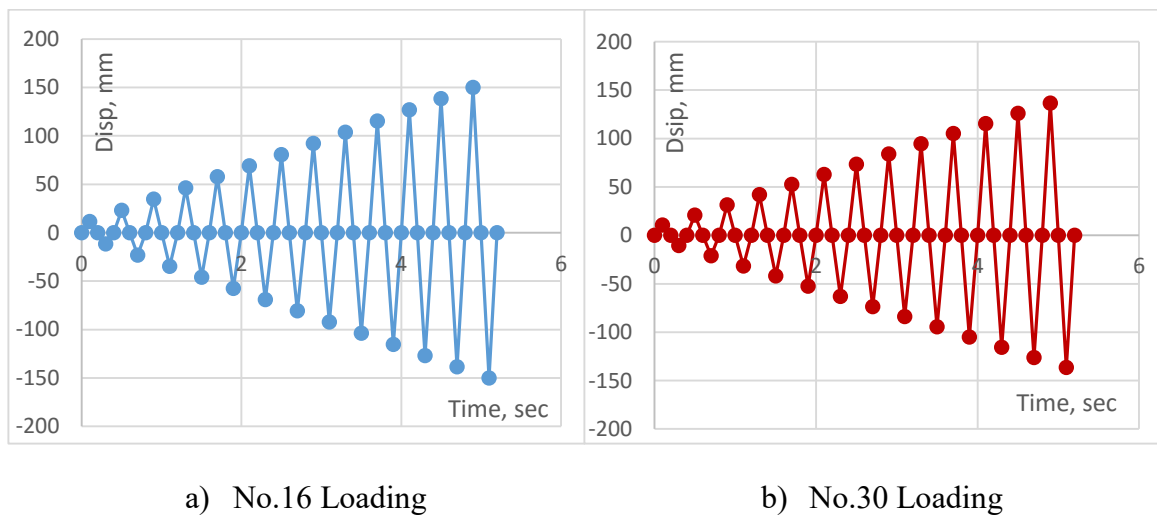


Figure 55: Loading condition of specimen

#### 4.5 Result

Specimen No.16 and No.30 models are analyzed by commercially available software ABAQUS both for hollow section and concrete filled section. Then these modeled are analyzed by varying height of concrete fill to observe the effect of concrete fill in buckling behavior. Another important observation is gotten from the analysis that is the

effect of diaphragm on the behavior of CFT. Introducing diaphragm on top of the concrete increases the ductility and strength at a great deal. The normalized hysteresis curve, buckling pattern and envelop curve is used to compare the data. For describing the steel behavior kinematic hardening rule is used. The effect of hardening rule is illustrated in chapter 3.

#### 4.5.1 Behavior of Specimen:

##### Behavior of No.16

After analyzing concrete filled tubular steel column specimen No. 16, the horizontal force,  $H$  and horizontal displacement,  $\delta$  were normalized by yield horizontal force  $H_y$  and yield displacement  $\delta_y$ . Then this normalized value was compared with the experimental result to show the accuracy and acceptability of the model.

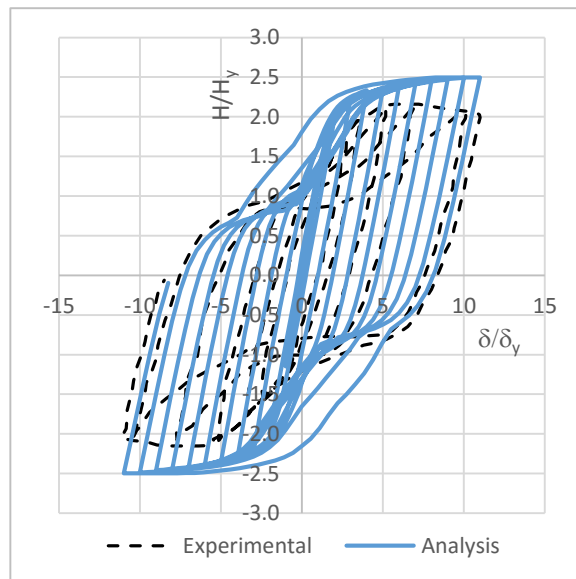


Figure 56: Comparison between Experimental and Analytical data

There is a small discrepancy between experimental result and the result got from numerical simulation. The reason could be attributed to some factors, such as presence of residual stress, initial crookedness etc. which are not considered in analytical modeling. The specimen was fabricated by welding cold-formed steel thin plates together and this procedure left residual stress in the specimen, causes buckling at lesser load. Initial crookedness creates additional moment in the specimen which is also responsible for buckling taking place at lower horizontal force.

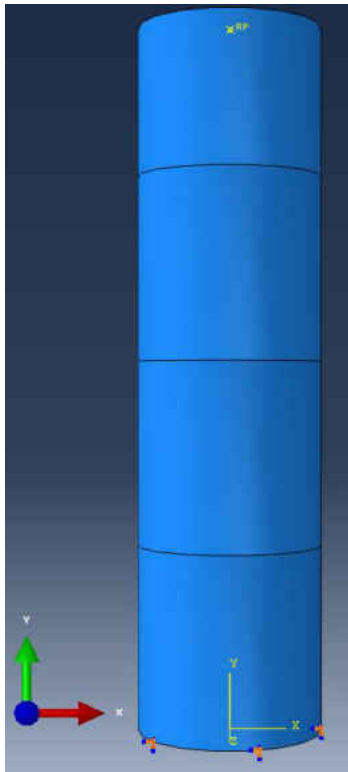
Figure 57- Figure 61 show the buckling shape and buckling location of the specimen No.16 for different height of concrete fill.

Figure 57 shows the geometry, meshing and buckling of specimen No.16 without any infill concrete. Finer mesh was created at the bottom part of column as buckling will take place here. A severe buckling takes place at the bottom of column.

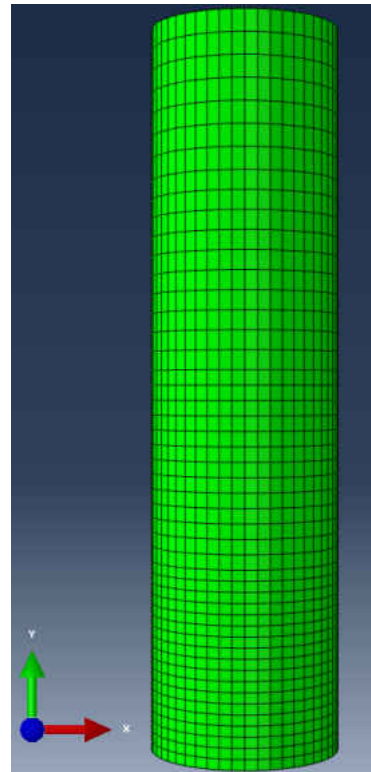
Figure 58 shows geometry, meshing and buckling of No.16 specimen, which has infill concrete upto 30% of column height. Finer mesh was created at the bottom part of column and above the top of the infill concrete, assuming buckling will take place at either of these two section. Analyse shows a severe buckling is taking place at the top of the concrete infill.

Figure 59 shows geometry, meshing and buckling of No.16 specimen, which has infill concrete upto 50% of column height. Finer mesh was created at the bottom part of column and above the top of the infill concrete, assuming buckling will take place at either of these two section. Analyse shows a outward buckling is taking place at the location of second

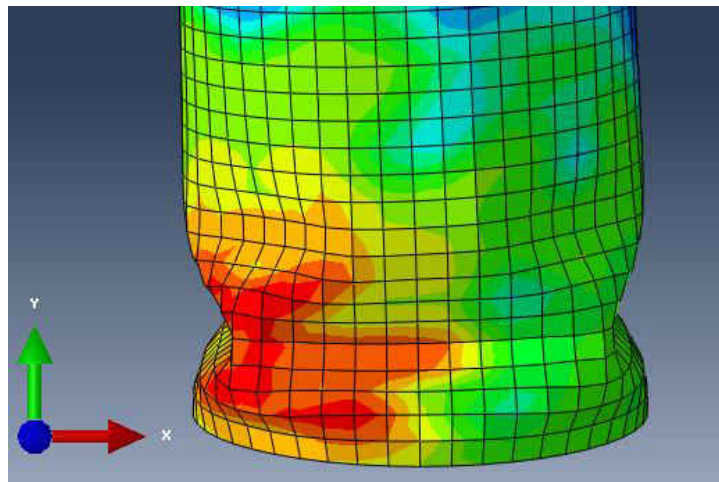
diagram. The reason is stress concentration is taking place at the location of second diaphragm as the area of concrete is less than that section.



a) Geometry and BC



b) Meshing

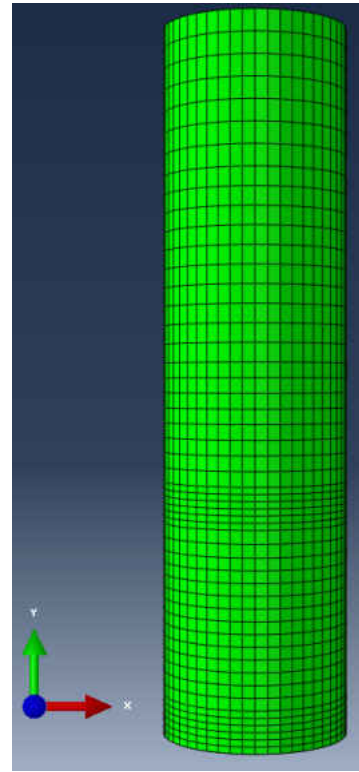


c) Buckling at  $11 \delta_y$

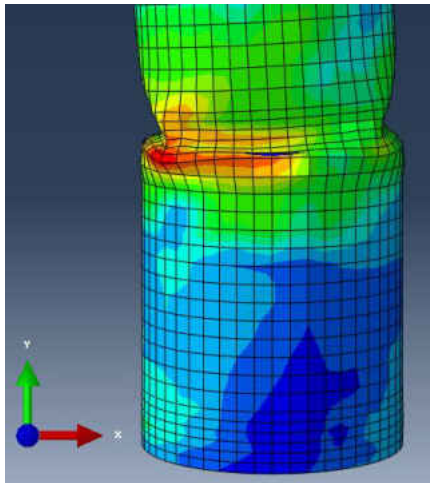
Figure 57: Details of No.16 hollow specimen



a) Geometry and BC



b) Meshing

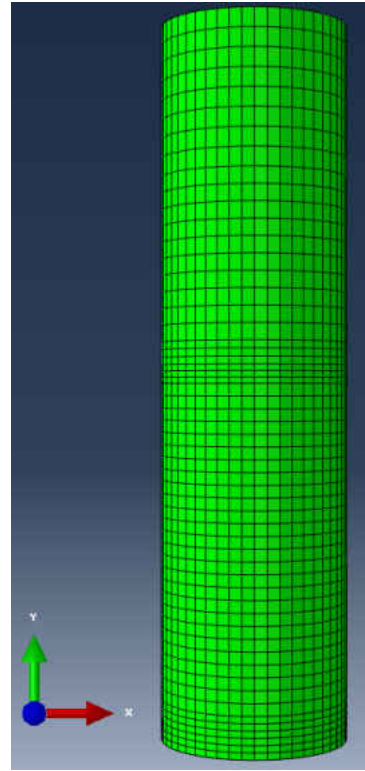


c) Buckling at  $11 \delta_y$

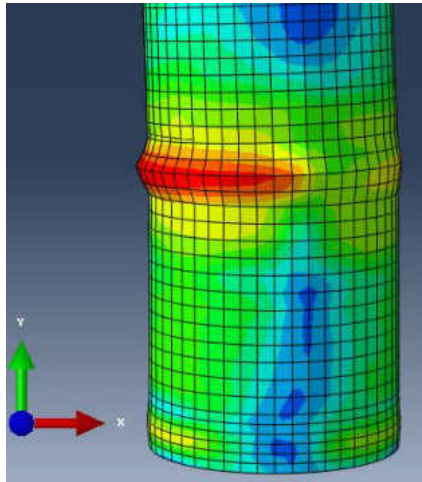
Figure 58: Details of No.16 specimen with 30% concrete fill



a) Geometry and BC



b) Meshing



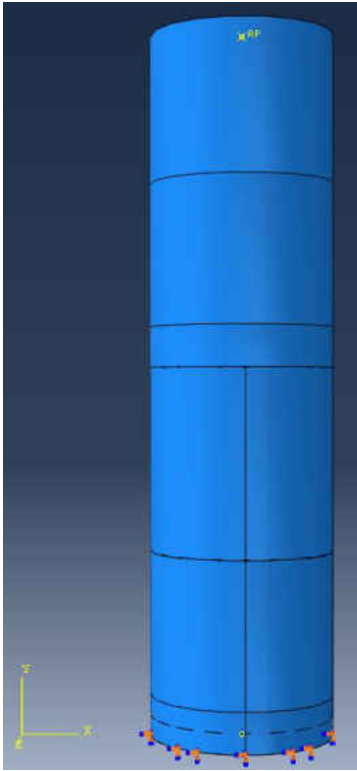
c) Buckling at  $11 \delta_y$

Figure 59: Details of No.16 specimen with 50% concrete fill

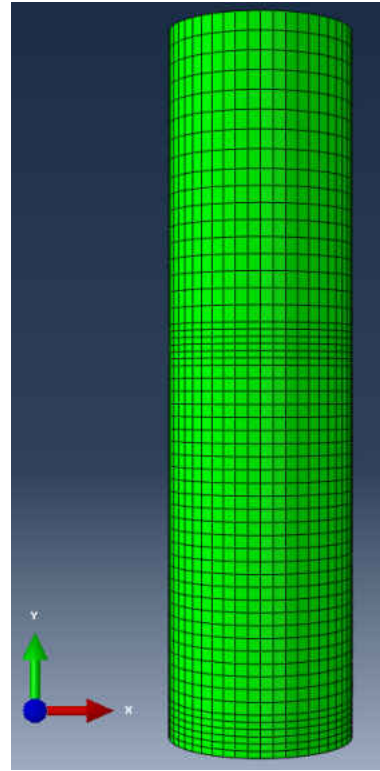
Figure 60 shows geometry, meshing and buckling of No.16 specimen, which has infill concrete upto 53% of height, just touching the diaphragm. Finer mesh was created at the bottom part of column and above the top of the infill concrete, assuming buckling can take place at either of these two section. Analyse shows a small outward buckling is taking place at the lower section of column even at  $11 \delta_y$ .

Figure 61 is showing geometry, meshing and buckling of No.16 specimen, which has infill concrete upto 67% of height. Finer mesh was created at the bottom part of column, assuming buckling will take place at this section. Analyse shows a small outward buckling is taking place at the lower section of column even at  $11 \delta_y$ .

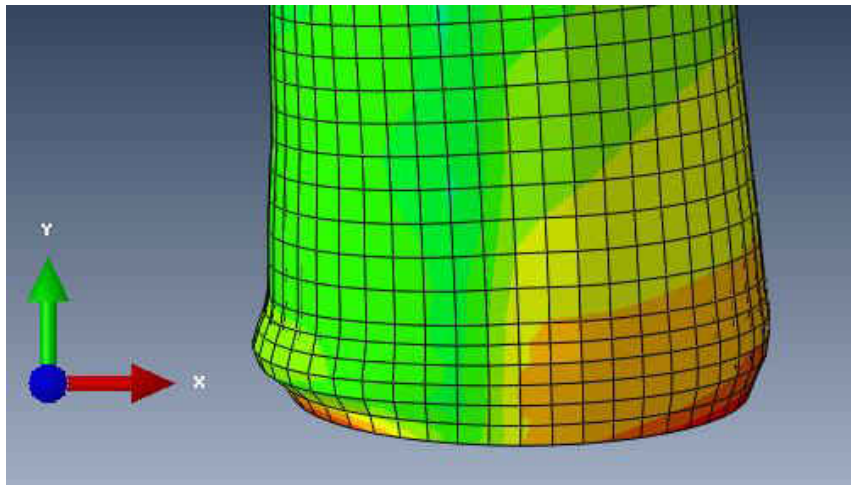
Figure 62 shows the varying buckling position with height of concrete fill. For hollow steel section, 67% concrete and 53% concrete buckling occurred at the bottom of the column. Where for 50% concrete buckling occurs near the second diaphragm because of the lack of concrete support at the part. For 30% concrete buckling occurs at the top part of filled-concrete.



a) Geometry and BC



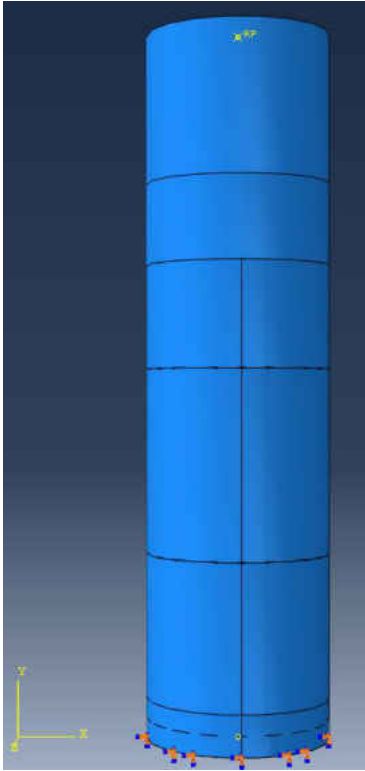
b) Meshing



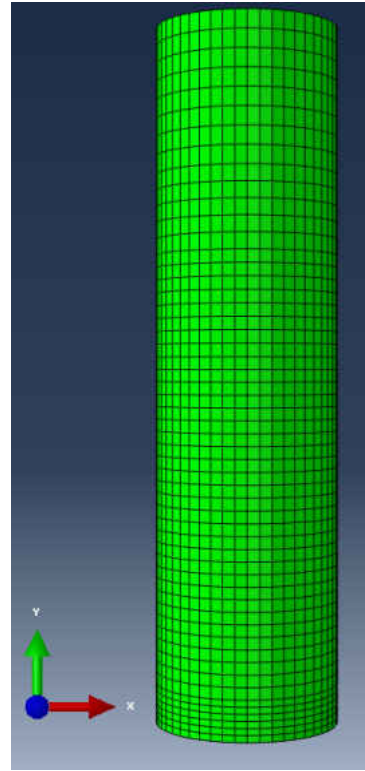
c) Buckling at  $11 \delta_y$

Figure 60: Details of No.16 specimen with 53% concrete fill

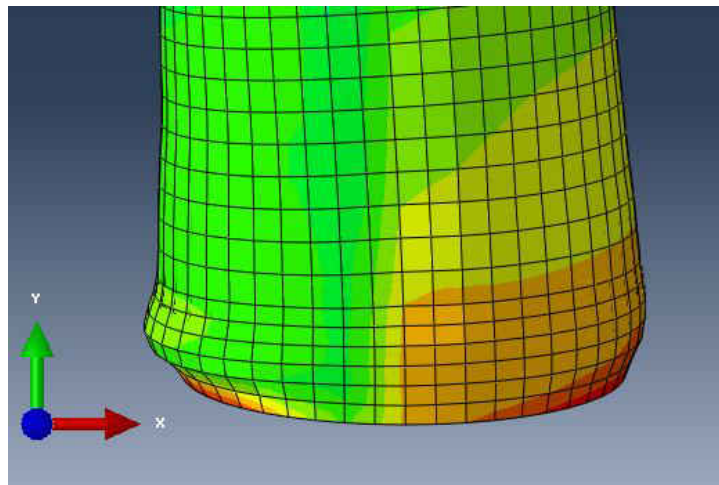




a) Geometry and BC



b) Meshing



c) Buckling at  $11 \delta_y$

Figure 61: Details of No.16 specimen with 67% concrete fill

The following figure, Figure 63, shows the improvement in CFST due to concrete fill. This improvement can be describe in two ways: firstly restraining buckling which provides greater stability and secondly higher energy absorption which provides greater ductility. For hollow steel column buckling at  $4 \delta_y$  is comparable with buckling at  $11 \delta_y$  for CFST, to be more specific 53% and above height of concrete. Even though a increased ductility is observed for 30% and 50% height of concrete but severe buckling is occurred at heigher cyclic displacement.

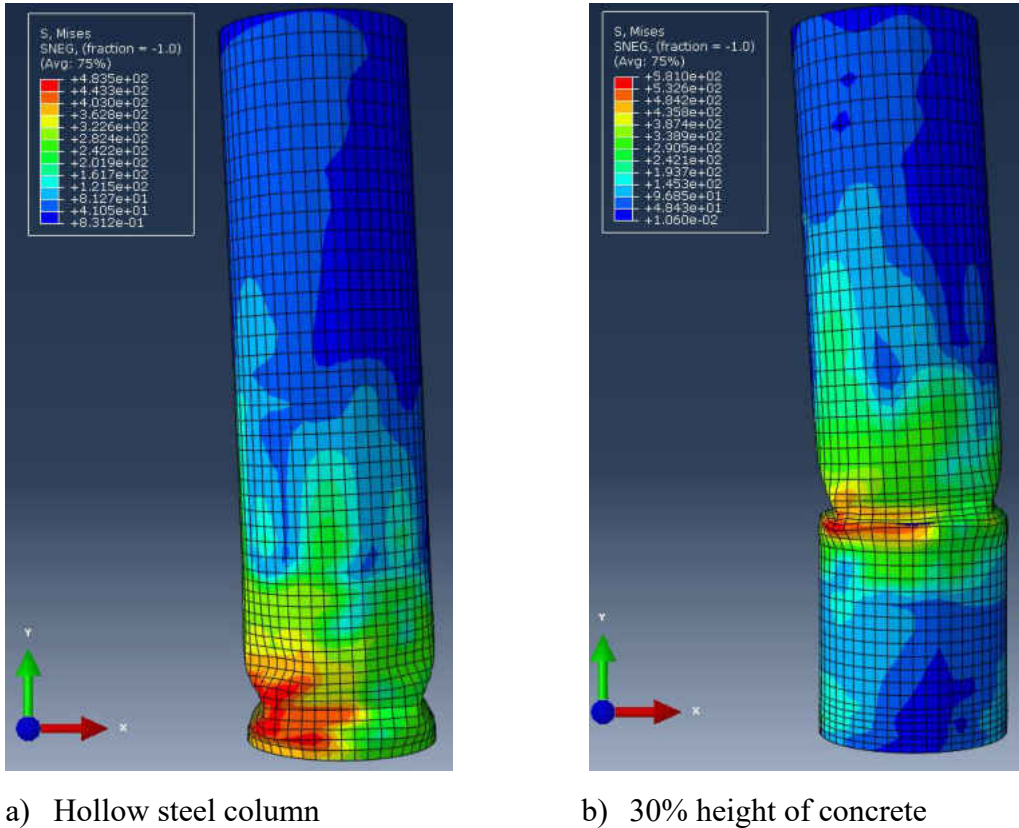
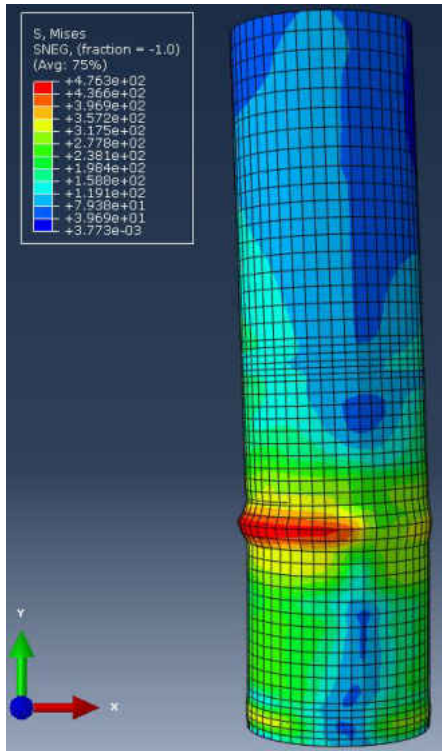
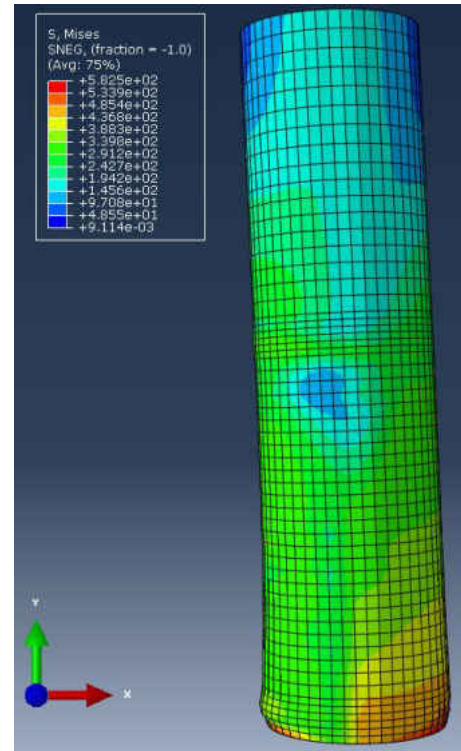


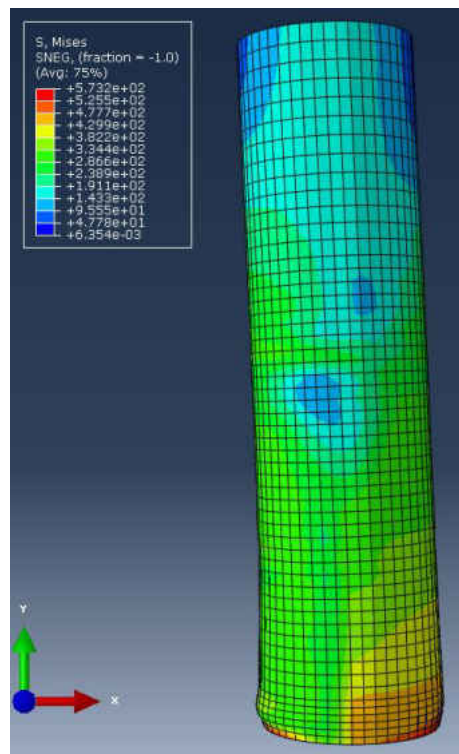
Figure 62: Buckling height for different concrete fill height (continued)



c) 50% height of concrete

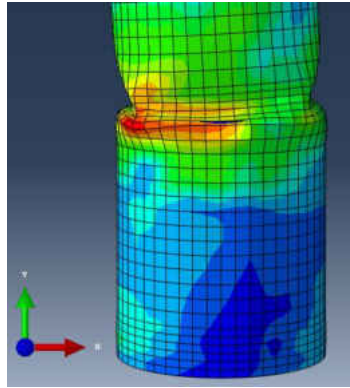


d) 53% height of concrete

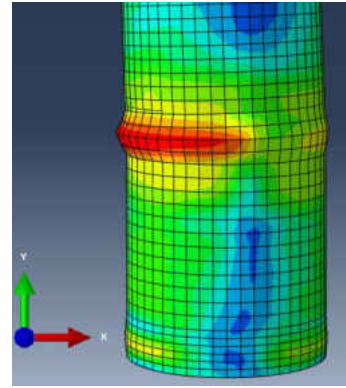


e) 67% height of concrete

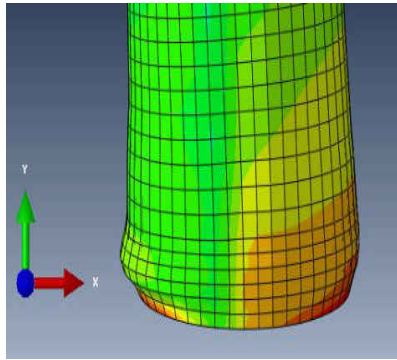
Figure 62: Buckling height for different concrete fill height



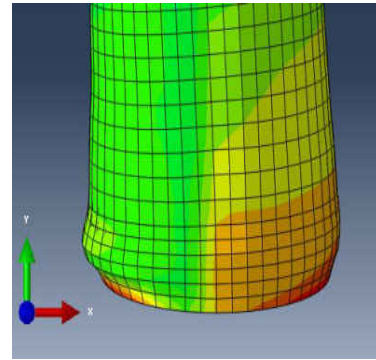
a) 30% concrete height,  $11 \delta_y$



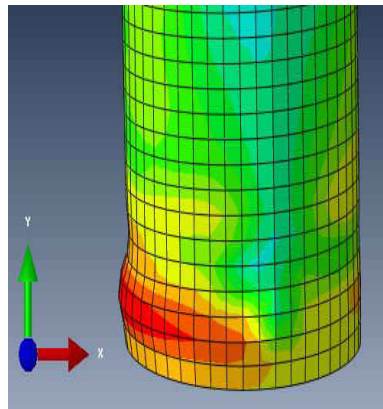
b) 50% concrete height,  $11 \delta_y$



c) 53% concrete height,  $11 \delta_y$



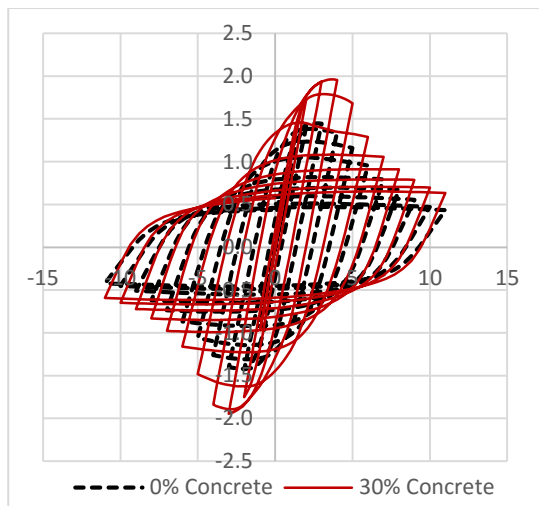
d) 63% concrete height,  $11 \delta_y$



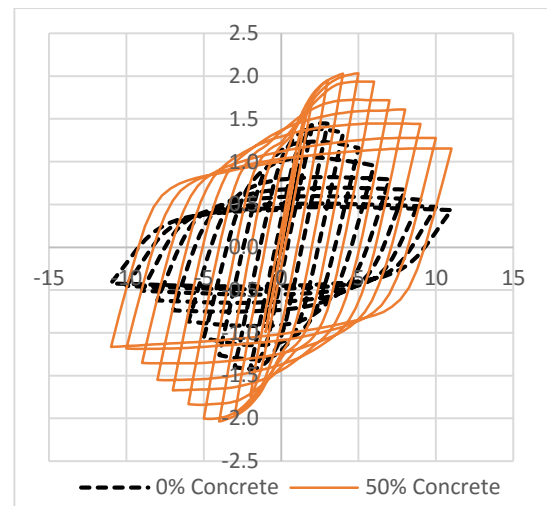
e) Hollow steel column,  $4 \delta_y$

Figure 63: Improvement in buckling pattern for different concrete height

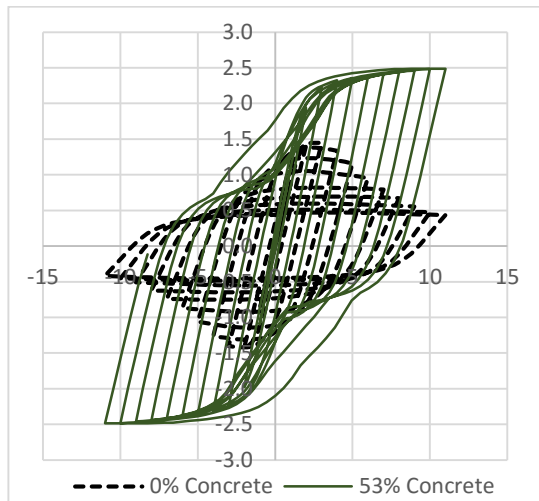
Figure 64 shows the improvement in normalized hysteresis diagram for infill concrete. It shows column is gaining ductility for concrete infill. Although for 30% and 50% column is gaining ductility but severe buckling is taking place at higher cycles. But for 53% and above column is performing at its best, no severe buckling is taking place even at higher cycles. This figure also shows, there is no significance improvement in ductility by adding more concrete after 53% height of infill concrete.



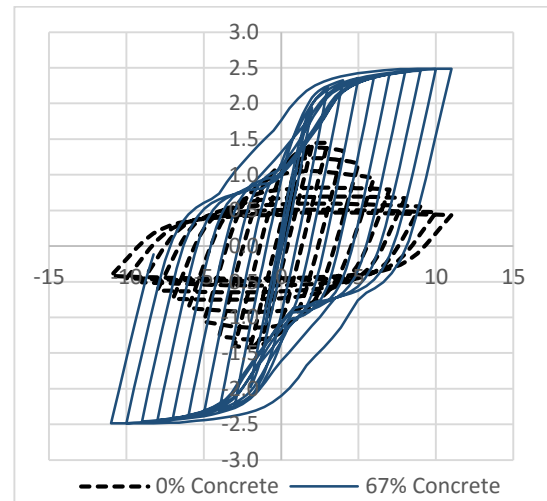
a) 30% height of concrete fill



b) 50% height of concrete fill



c) 53% height of concrete fill



d) 67% height of concrete fill

Figure 64: Improvement in hysteresis diagram for different height of concrete

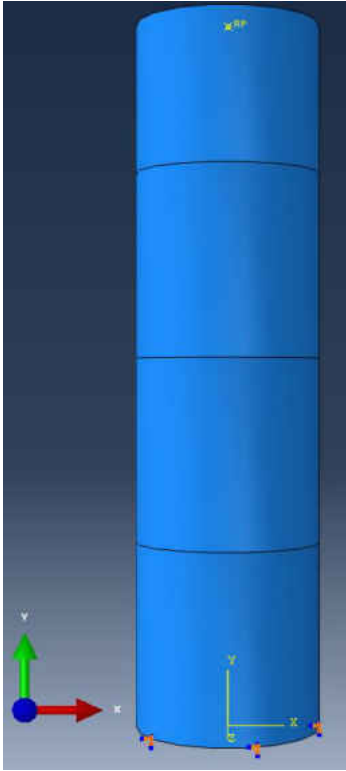
### **Behavior of No.30**

The following sets of figures shows the behavior of CFST column No.30 varying height of concrete fill. Figure 65 shows the detailing of hollow No.30 specimen: boundary condition, meshing and buckling shape. Finer mesh was created at the bottom part of column, assuming buckling will take place at this section. Analyse shows a severe elephant foot bulge shape buckling is taking place at the bottom.

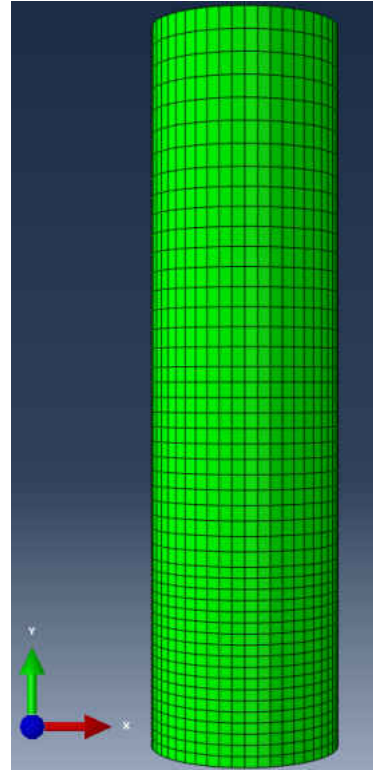
Figure 66 shows the detailing of No.30 specimen: boundary condition, meshing and buckling shape, having 30% height of infill concrete. Finer mesh was created at the bottom part of column and top the infill concrete, assuming buckling will take place at either of these two section. Analyse shows a severe buckling is taking place at the the top of the concrete section.

Figure 67 shows the detailing of No.30 specimen: boundary condition, meshing and buckling shape, having 50% height of infill concrete. Finer mesh was created at the bottom part of column and top the infill concrete, assuming buckling will take place at either of these two section. Analyse shows a severe buckling is taking place at the location of first diaphragm. Lack of concrete support at the top of concrete in fill causes the formation of buckling at the location of least concrete section.

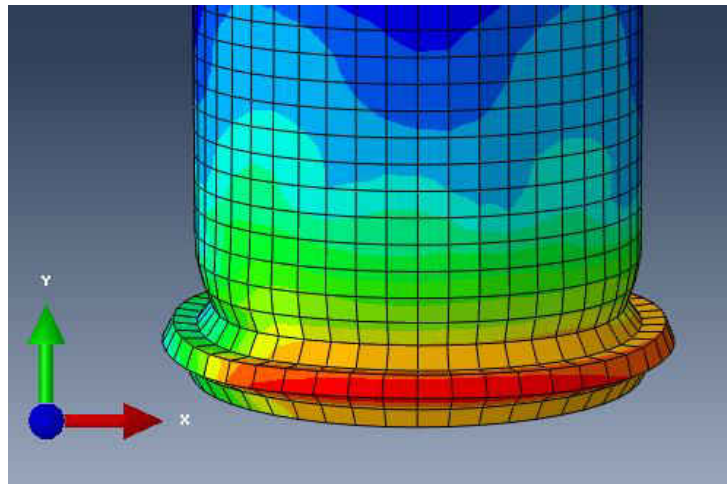




a) Geometry and BC



b) Meshing

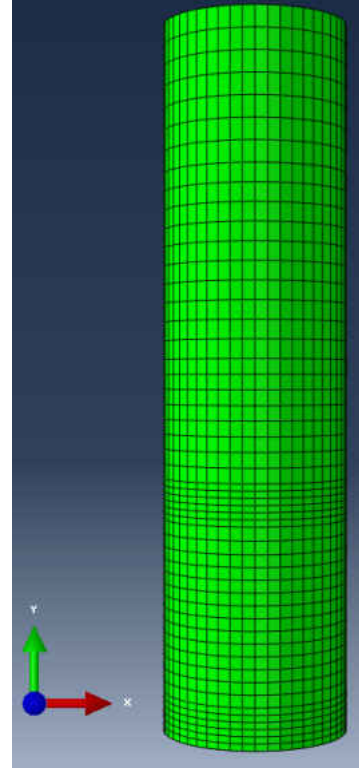


c) Buckling at  $10 \delta_y$

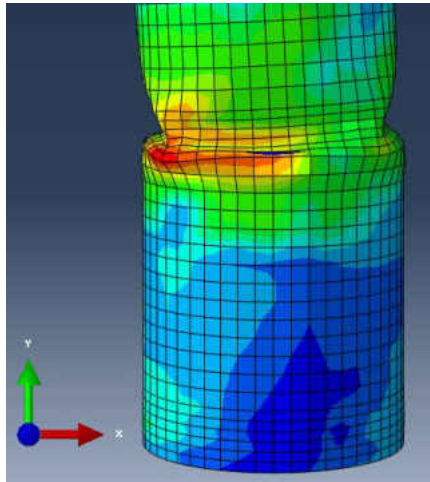
Figure 65: Details of No.30 hollow specimen



a) Geometry and BC



b) Meshing



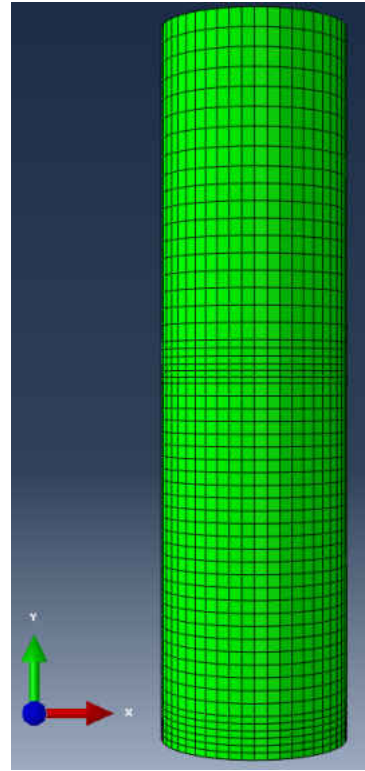
c) Buckling at  $10 \delta_y$

Figure 66: Details of No.30 specimen with 30% concrete fill

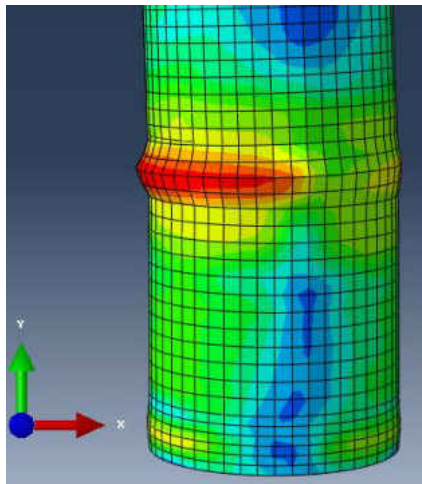




a) Geometry and BC



b) Meshing



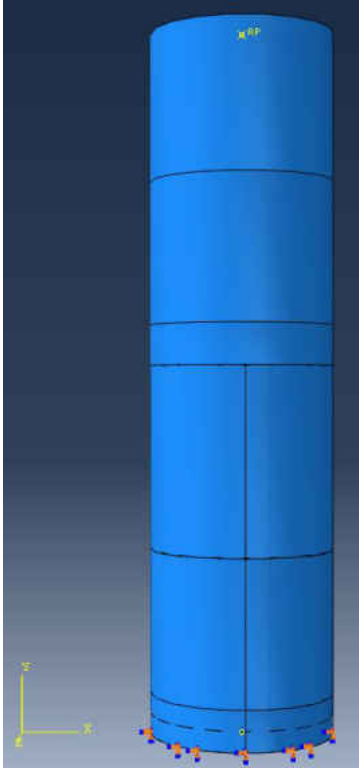
c) Buckling at  $8 \delta_y$

Figure 67: Details of No.30 specimen with 50% concrete fill

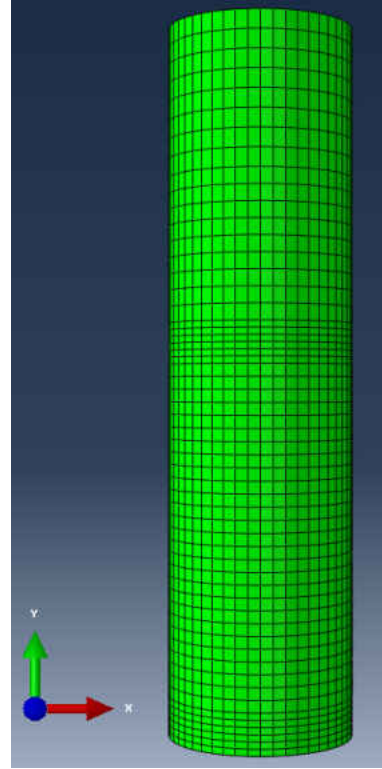
Figure 68 shows the detailing of No.30 specimen: boundary condition, meshing and buckling shape, having 53% height of infill concrete. The reason for making 53% is, so that the top of the infill concrete touches the diaphragm. Finer mesh was created at the bottom part of column and top the infill concrete, assuming buckling will take place at either of these two section. Analyse shows a severe outward buckling is taking place at bottom at initial cycles but the reason for failure of the column is formation of severe elephant foot bulging at the top of concrete infill.

Figure 69 is showing geometry, meshing and buckling of No.30 specimen, which has infill concrete upto 67% of height. Finer mesh was created at the bottom part of column, assuming buckling will take place at this section. Analyse shows even at  $10 \delta_y$  a small outward buckling is taking place at the lower section of column.

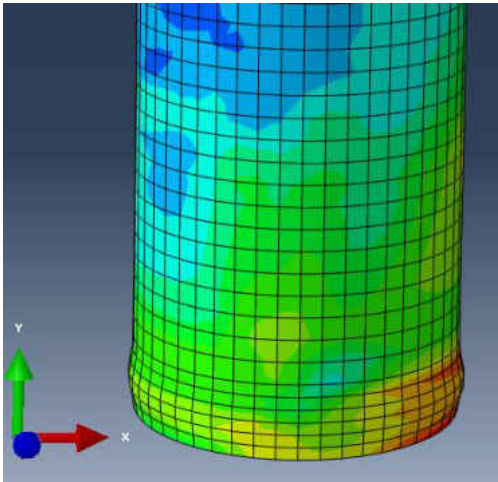
Figure 70 shows the varying buckling position with height of concrete fill. For hollow steel section and 67% concrete buckling occurred at the bottom of the column. Where for 50% concrete buckling occurs near the second diaphragm because of the lack of concrete support at the part. For 30% concrete buckling occurs at the top part of filled-concrete. In the case of 53% concrete, at lower cycles buckling takes place near the base. But the reason for failure the column is losing structural stability due to severe buckling at the height of top of the concrete.



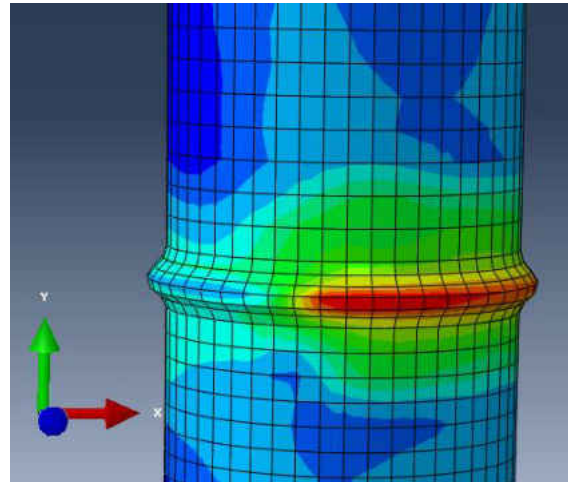
a) Geometry and BC



b) Meshing

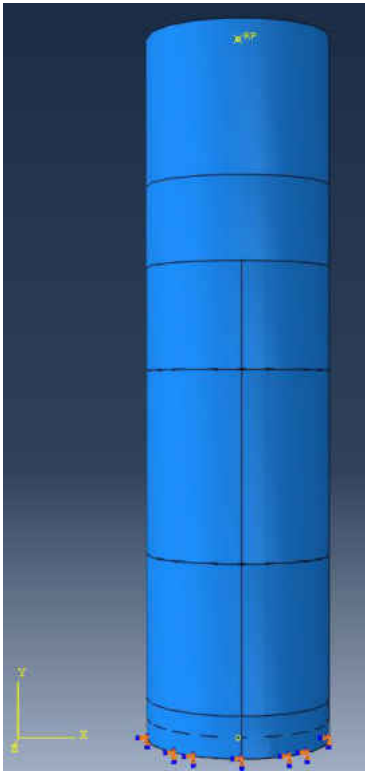


c) Buckling at  $8 \delta_y$

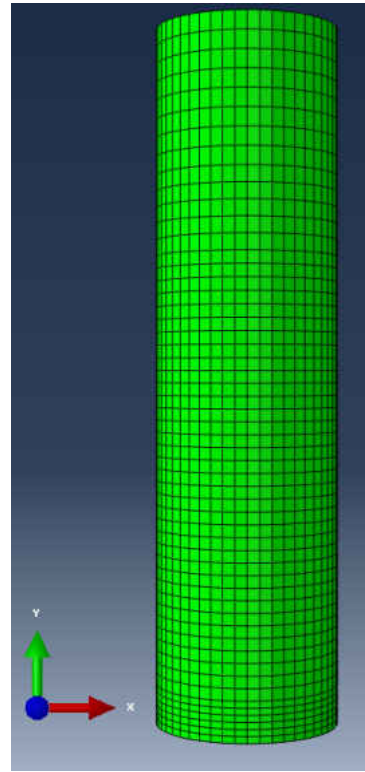


d) Buckling at  $10 \delta_y$

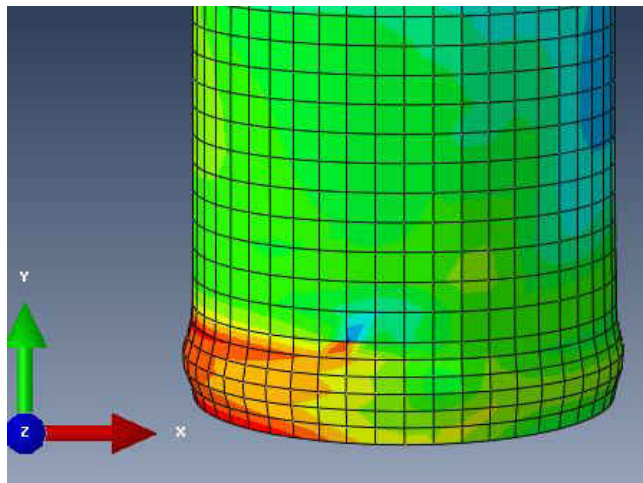
Figure 68: Details of No.30 specimen with 53% concrete fill



a) Geometry and BC

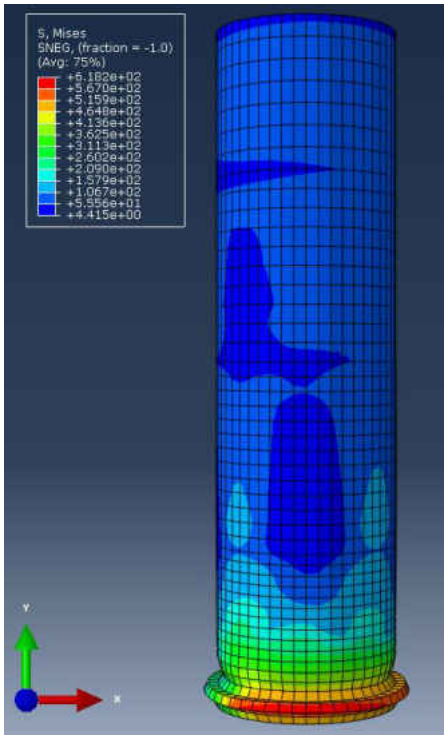


b) Meshing

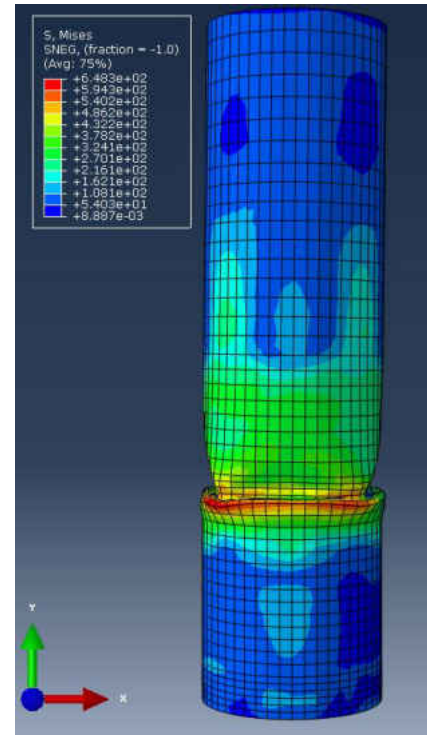


c) Buckling at  $11 \delta_y$

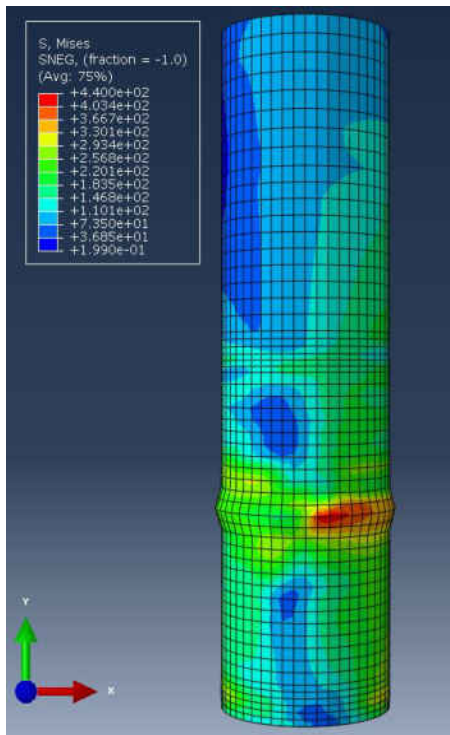
Figure 69: Details of No.30 specimen with 67% concrete fill



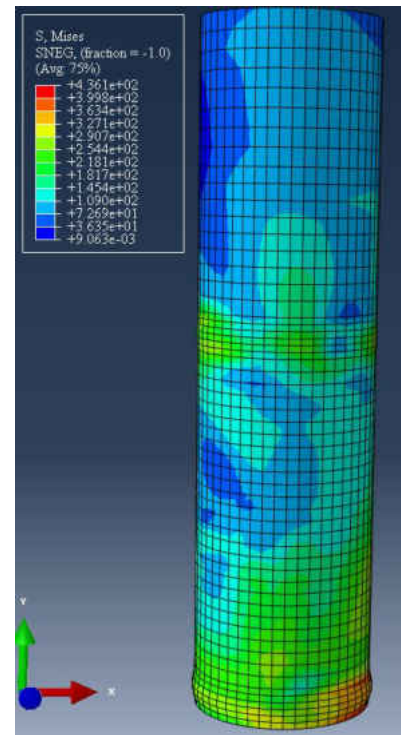
a) Hollow steel column



b) 30% height of concrete

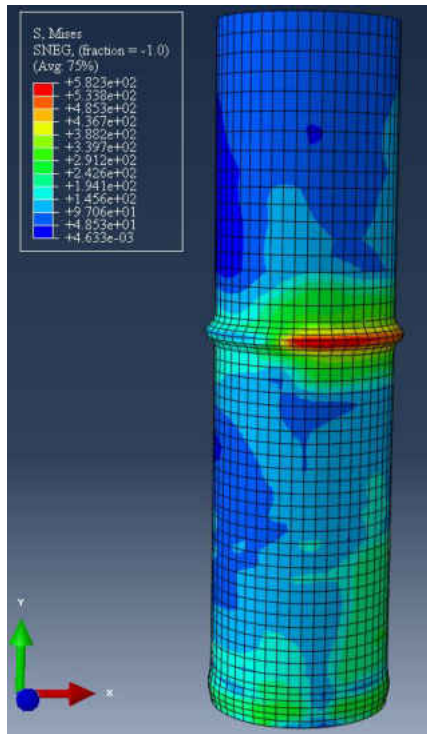


c) 50% height of concrete

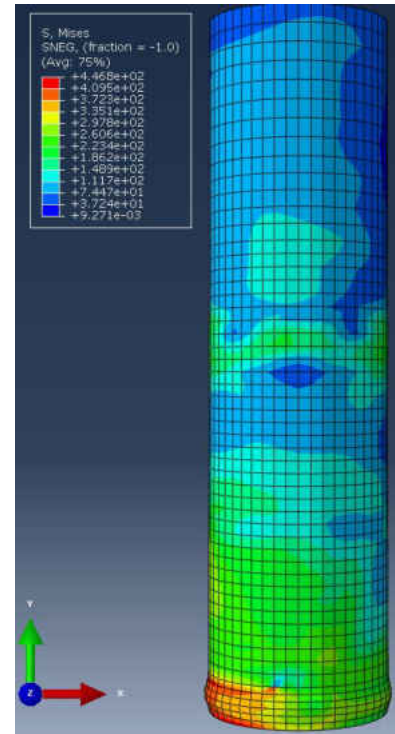


d) 53% height of concrete,  $8\delta_y$

Figure 70: Buckling position in column, specimen No.30 (continued)



e) 53% height of concrete,  $10 \delta_y$

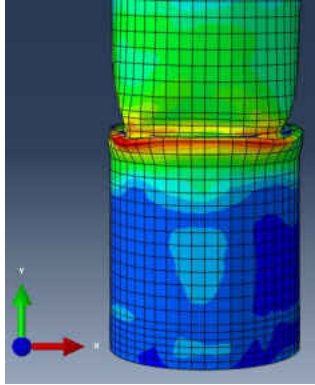


f) 67% height of concrete,  $8\delta_y$

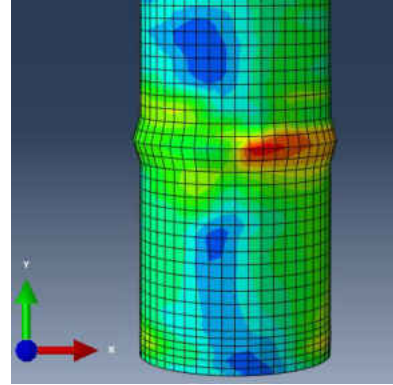
Figure 70: Buckling position in column, specimen No.30

The following figure, Figure 71, shows the improvement in CFST due to concrete fill. This improvement can be describe in two ways: firstly restraining buckling which provides greater stability and secondly higher energy absorption which provides greater ductility. For hollow steel column buckling at  $8 \delta_y$  severe elephant foot bulging is taking place. But in the column having 53% height of concrete infill less severe outward buckling is taking place, indicating increased ductility. Column having 50% concrete infill also shows less severe outward buckling. Eventhough column having only 30% concrete infill shows severe buckling, but yet it shows higher energy absorption capability from hysteresis diagram.

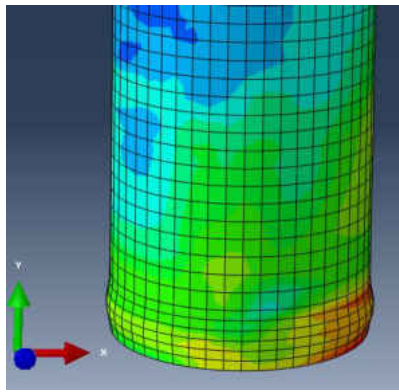




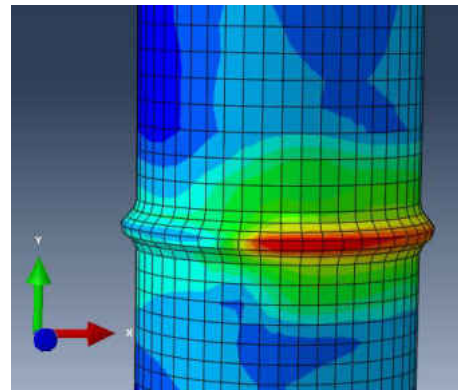
a) 30% concrete height,  $8 \delta_y$



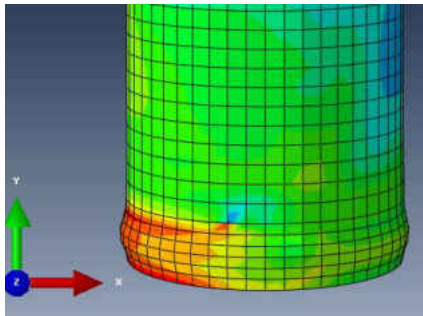
b) 50% concrete height,  $8 \delta_y$



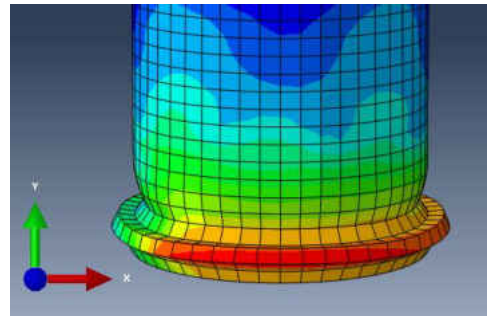
c) 53% concrete height,  $8 \delta_y$



d) 53% concrete height,  $10 \delta_y$



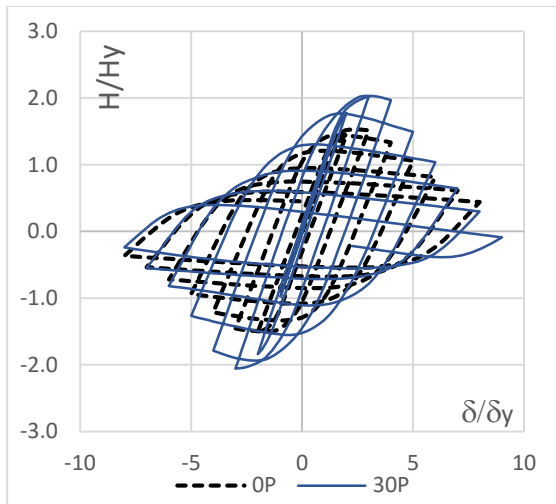
e) 67% concrete height,  $8 \delta_y$



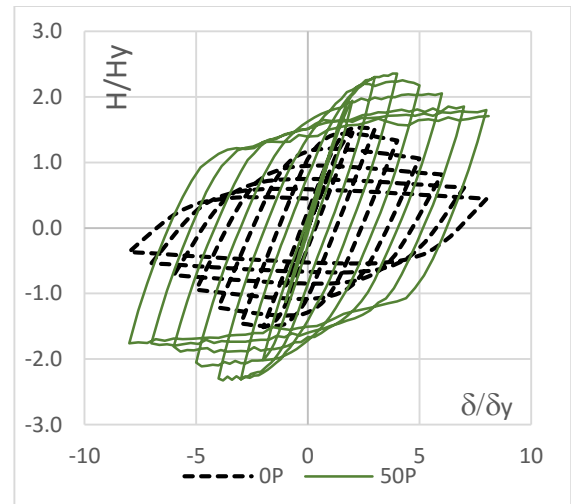
f) Hollow steel column,  $8 \delta_y$

Figure 71: Improvement in buckling pattern for different concrete height

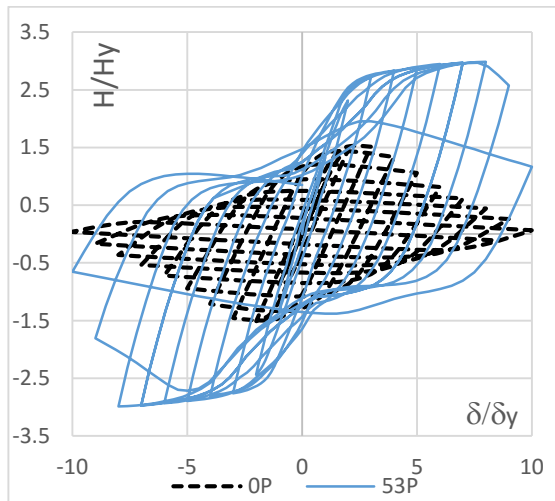
Figure 72 shows the improvement in normalized hysteresis diagram for infill concrete. It shows column is gaining ductility for concrete infill. Although for 30% and 50% column is gaining ductility but severe buckling is taking place at higher cycles. But for 53% and above column is performing at its best, no severe buckling is taking place. This figure also shows, there is no significance improvement in ductility by adding more concrete after 53% height of infill concrete.



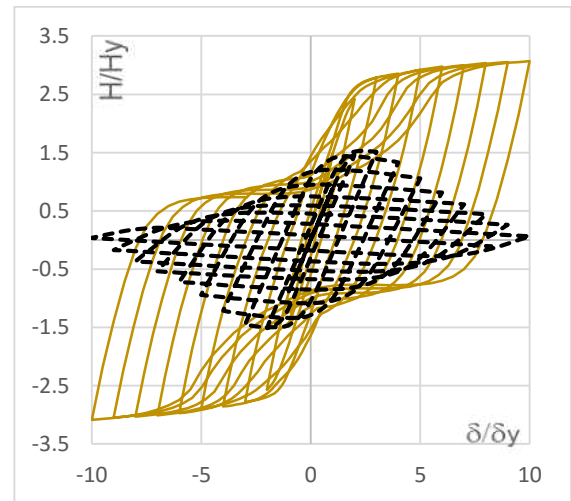
a) 30% height of concrete fill



b) 50% height of concrete fill



c) 53% height of concrete fill



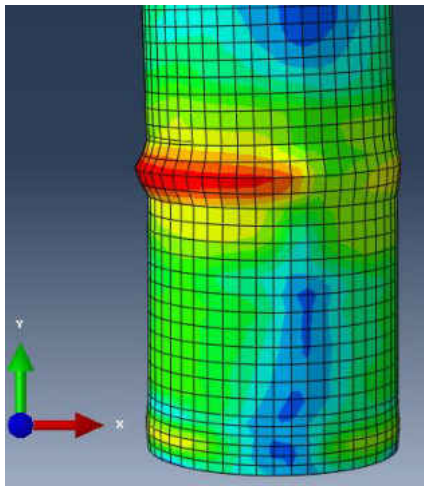
d) 67% height of concrete fill

Figure 72: Improvement in hysteresis diagram for different height of concrete

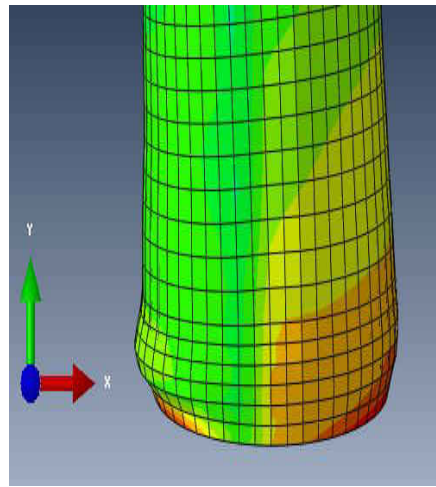


#### 4.5.2 Effect of diaphragm

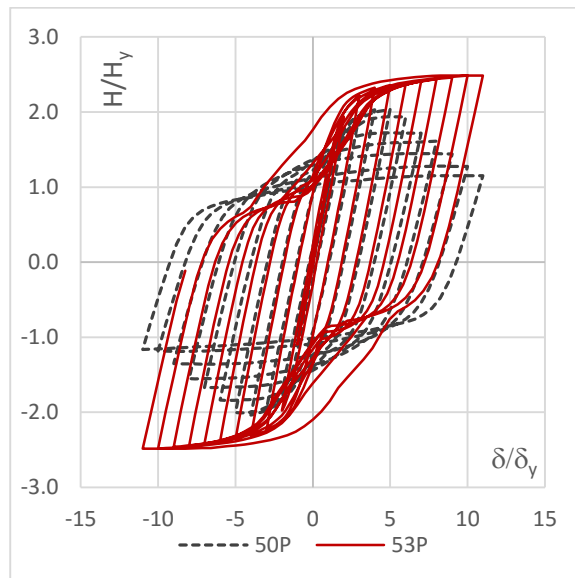
Eventhough there is no significant difference between 50% and 53% height of filled-concrete in terms of concrete amount but the analysis result shows a great difference in the cyclic behavior. The presence of diaphragm effects the behavior of CFT at a great deal. Figure 73 shows the effect of diaphragm.



a) Buckling, 50% concrete



b) Buckling, 53% concrete



c) Hysteresis diagram

Figure 73: Effect of diaphragm in concrete filled tubular structure, No.16

Eventhough there is no significant difference between 50% and 53% height of filled-concrete in terms of concrete amount but the analysis result shows a great difference in the cyclic behavior. The presence of diaphragm affects the behavior of CFST at a great deal. For 53% concrete infill CFST still shows ductility as no severe buckling is taking place but in case of 50% concrete infill outward buckling is taking place. Moreover, energy absoroption capacity is more in the case of 53% concrete than 50% concrete infill. Figure 74 shows the effect of diaphragm for No.30 specimen.

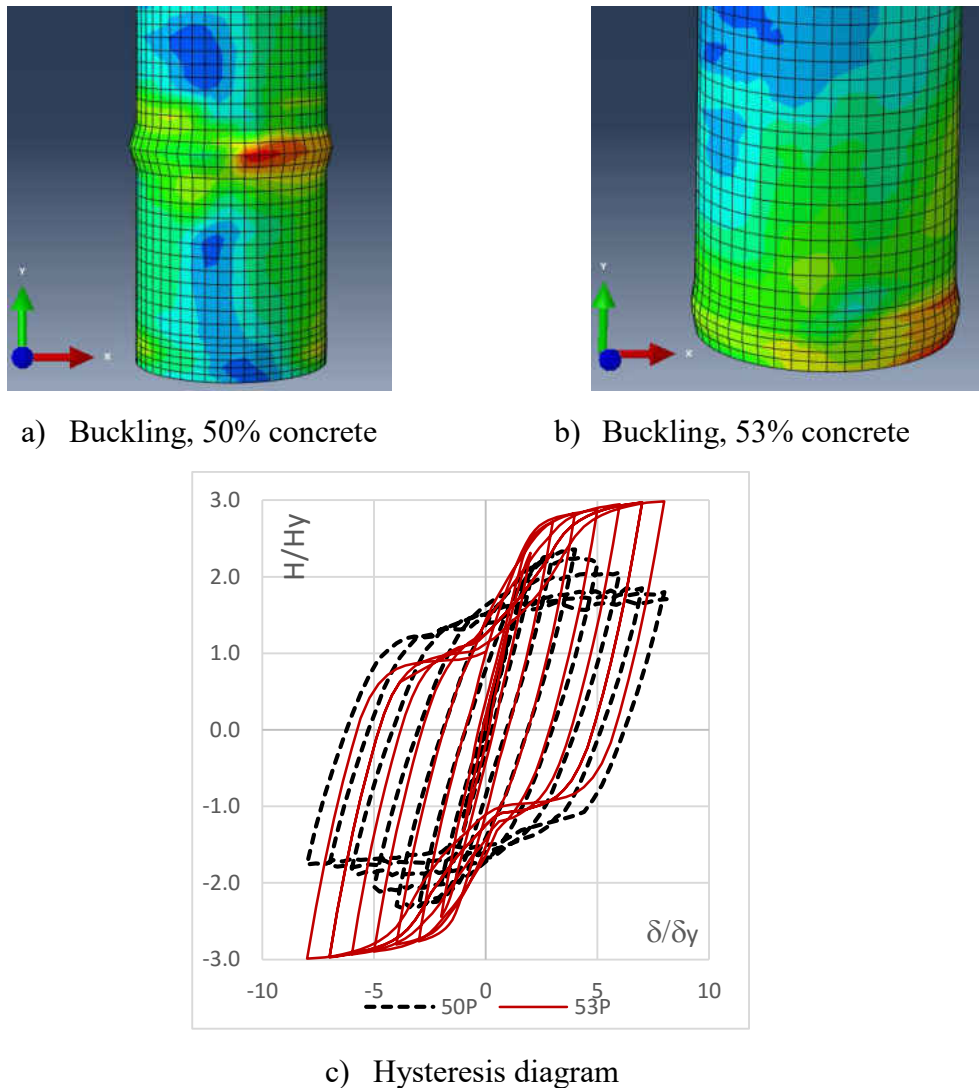


Figure 74: Effect of diaphragm in concrete filled tubular structure, No.30

### 4.5.3 Comparison

The following Figure 75 and Figure 76 shows a comparison between different axial load. For the hollow steel column, the hysteresis diagram shows, even though normalized axial reaction is almost same in initial stages but, due to severe buckling, behavior changes after couple of load cycles, in this case after 3 cycles. At the end of 10<sup>th</sup> loading cycles severe buckling occurred in case of No.30 hollow steel column and it loses its stability. Compare to No.30 hollow column, No.16 specimen shows more stability at the higher cycles.

In case of CFST columns, cyclic behavior is considerably different from hollow steel column. For 50% and 53% concrete height, in case of No.30, the peak normalized reaction is higher than No.16 specimen despite of lower strength concrete used in No.30 specimen. This could be explained by late formation of crack. In the case of No.30 specimen, higher axial load causes more compressive stress on inner concrete core and delays the formation of crack which gives high axially loaded CFST columns more ductility compare to low axially loaded CFST columns at the initial stages. Although No.30 specimen shows higher energy absorption capacity but it loses its stability faster than No.16 specimen. Because once buckling takes place in No.30, higher axially loaded specimen, the severity of buckling become faster due to the presence of high axial load.

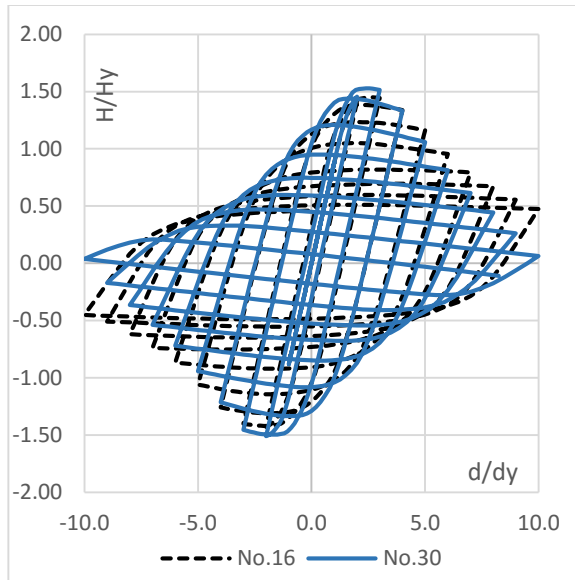
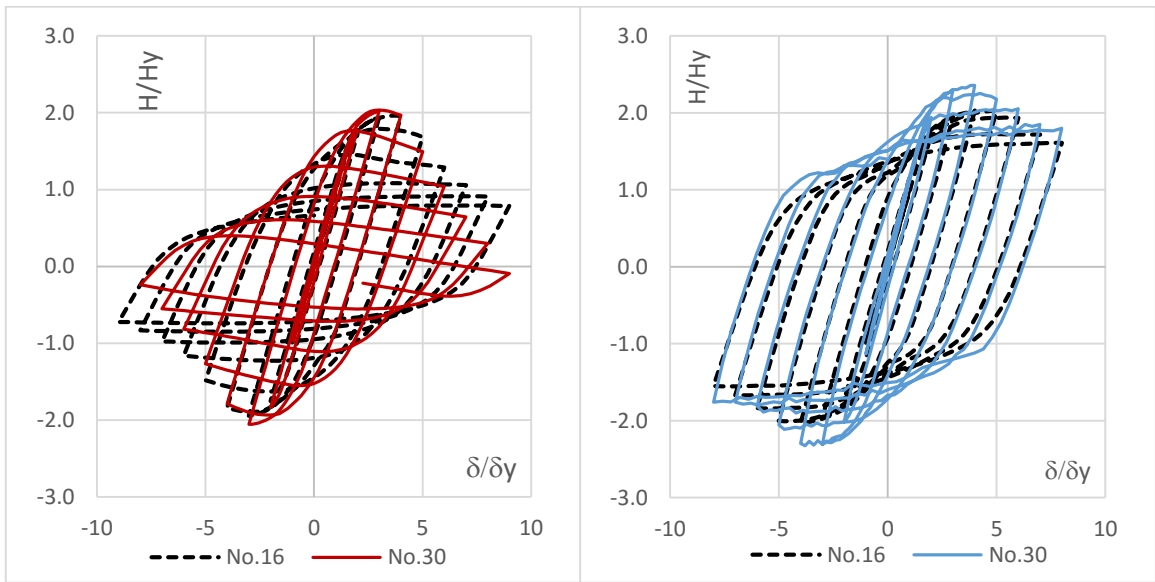


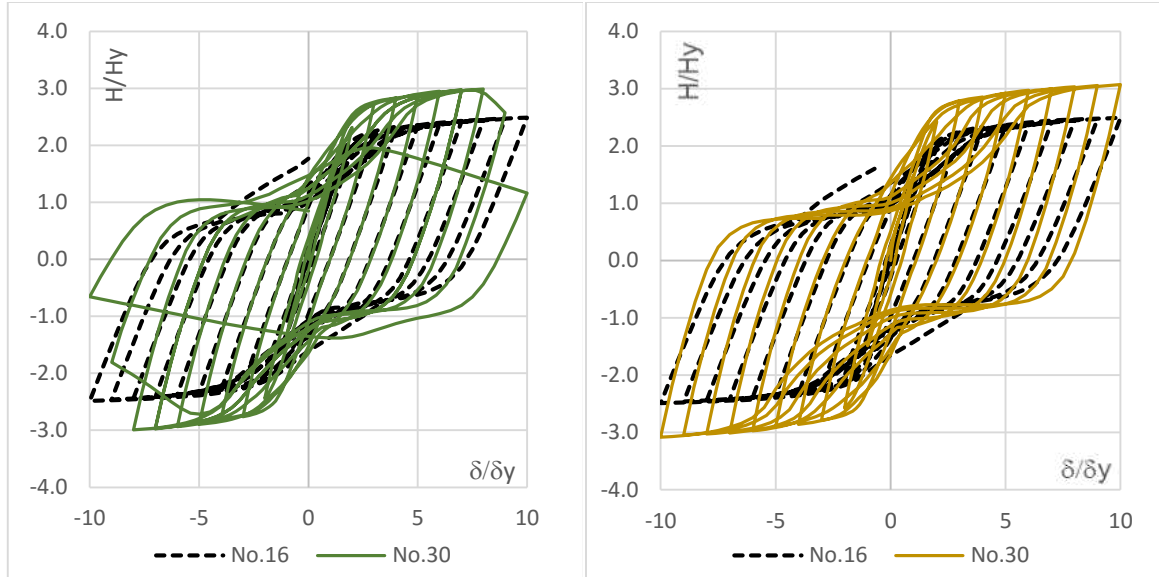
Figure 75: Comparison between hysteresis diagram of hollow steel columns



a) 30% concrete

b) 50% concrete

Figure 76: Comparison of hysteresis diagram for different axial load (continued)



c) 53% concrete

d) 67% concrete

Figure 76: Comparison of hysteresis diagram for different axial load

#### 4.6 Conclusion

In this study, the analytical results are obtained using ABAQUS 6.13. Then these results are compared with the experimental data to observe the accuracy of model. Even though there is small discrepancy, due to some factors such as presence of residual stress, initial crookedness etc., between experimental result and numerical result, this model is accurate enough to predict the behavior of concrete filled column. Analytical simulation of both specimen shows the improvement due to infill concrete even though the degree of improvement depends on the several factors, such as, height of the infill concrete, presence of the diaphragm etc. For 30% height of the infill concrete usually severe buckling takes place at the top of the concrete. Although by increasing the height of the infill concrete up to half of the column, an increase in strength and ductility could be achieved, but introducing a diaphragm on the top of the concrete affects the stability significantly.

Introducing a diaphragm on the top of the concrete keeps the infill concrete in triaxial compression state, which prevent the crack formation or, if any, resist crack opening. This attributes in the column stability at a great deal. Usually, increasing the height of the infill concrete more than 50% height of column has an inconsequential effect on column strength.

## CHAPTER V

### CONCLUSION

The use of thin-walled steel tubular columns in highway bridge systems as bridge piers is increasing in Japan and other countries with severe constructional restrictions such as areas with high population, soft ground, bay areas or reclaimed area that cannot sustain heavy structures. Light in weight, greater ductility and high earthquake resistance can be attributed to the continuing popularity of thin-walled tubular steel column over the other conventional practices such as reinforced concrete bridge piers.

New ways to improve design procedures constantly are a major concern of the structural engineers. Specially, the necessity to accurately predict the ultimate behavior of thin-walled steel bridge piers during severe earthquakes is one of the major areas of great concern. In this thesis, behavior of tubular steel column under cyclic load is analyzed using different material model available in ABAQUS and compared with the experimental result obtained from cyclic loading test at the Public Work Research Institute of Japan (Nishikawa *et al.*, 1996) in order to get the material model which could comparatively describe the column behavior more accurately. This material model is used to analyze the steel column in CFST.

From the analysis in Chapter 3, it is apparent that, behavior of specimen is dependent on the used material modeling. The initial slope of the envelop curve which represent the stiffness of the structure is same regardless used material modeling but the

value changes after couple of cycles. The reason is that, after some cycles structures enter into plastic zone, behavior of structure in plastic zone totally depends on the used hardening rule. In isotropic hardening material strength increases in both tension and compression side, moreover it allows the increment of yield surface with every cycles. Though the radius of yield surface increases, the material become stronger and gives a higher normalized horizontal force. On the other hand, kinematic hardening rule allows to translate the yield surface without increasing the size. That's why when material become stronger in one direction, it become weak in another direction. These differences are apparent in normalized hysteresis behavior. There are also some differences in the pattern and location of buckling. For kinematic hardening rule, buckling occurs at the base of the column and buckling shape is either elephant foot bulging or outward bulging. While in the case of isotropic hardening location of buckling moves upward and shape of buckling is different from that of kinematic hardening. In summarizing the Chapter 3, behavior of tubular steel column depends on the material model that is used to describe the evolution of yield surface in elastic zone. Between two available material models, namely: Isotropic hardening model and Kinematic hardening model, kinematic hardening rule best predict the behavior of column as it consider Bauschinger effect. On the other hand, even though at the initial loading cycles, isotropic hardening shows the same behavior but it significantly changes when the material enters into plastic zone.

Recent advancement in structural material, member fabrication method, material modeling, and computer technology provides the tools to improve the design standards, increase the accuracy in predicting and even change the design procedure to a new one if necessary. Lessons from Kobe earthquake (Japan, 1995), especially the performance of the



hollow tubular column which were inadvertently partially filled with concrete, gave a new insight about column stability and ductility, hence create an opportunity to study and do research in this field.

In Chapter 4, numerical studies on concrete filled tube are carried out by commercially available software ABAQUS (v 6.13). Using this software, two test specimens, named: No. 16 and No. 30, experiment carried out by Goto *et al.* (2006), having same geometrical properties e.g. height, thickness, diameter of the column, thickness of the diaphragm and height of the concrete, only varies in normalized axial force and concrete strength. For describing the steel behavior multi-linear kinematic hardening rule is used. Another two hollow specimen No. 30 and No. 16 except the filled concrete, is analyzed to show the improvement in the seismic behavior due to concrete. The normalized hysteresis curve, buckling pattern and envelop curve is used to compare the data.

After analyzing CFST columns, the normalized values were compared with the experimental result to show the accuracy and acceptability of the model. There is a small discrepancy between experimental result and the result got from numerical simulation. The reason could be attributed to some factors, such as presence of residual stress, initial crookedness etc. which are not considered in analytical modeling. Those specimens were fabricated by welding cold-formed steel thin plates together and this procedure left residual stress in the specimen, causes buckling at lesser load. Initial crookedness creates additional moment in the specimen which is also responsible for buckling taking place at lower horizontal force.

Once the reasonability of model is confirmed, these models are analyzed by varying height of concrete infill to show the effect of infill concrete on the strength and stability of column.

From the analysis, it is obvious that infill concrete has a significant effect on the strength and ductility of the column. However, the degree of improvement depends on several other factors. Analysis shows that, improvement in the strength of column could be achieved just by introducing concrete in the hollow section. But from the analysis, 30% height of the infill concrete shows a premature buckling in column at the top of the concrete level, hence loses its stability rapidly. On the other hand adding concrete more than 50% height of column has inconsequential effect on strength and stability of the column.

Analysis also reveals an interesting fact about the effect of diaphragm. Presence of diaphragm affects the strength and stability of the column at a great deal. Introducing a diaphragm at the top of concrete increases the strength of the column as well as its ductility. Introducing a diaphragm on the top of the concrete keeps the infill concrete in triaxial compression state, which prevents the crack formation or, if any, resist crack opening. Thus by resisting crack progression, diaphragm prevents buckling and hence increases the strength and stability of column. To get the maximum benefit from concrete infill, it is recommended, on the basis of this analysis, to fill the hollow column up to 50% height and introduce a plate on the top of concrete.

This thesis finds another interesting fact about CFST that is; it works better for the higher axial load. While hollow steel column shows reduced strength and ductility for higher normalized axial load, CFST shows higher values in strength and ductility at the earlier stages of the loading. But at the higher loading stage, CFST under higher axial load loses stability rapidly compare to lower axial loaded one. The reason could be higher axial load create a better interaction between infill concrete and steel. The differences in position ratios of concrete and steel, may be, offset by the higher axial load. But once the crack is

created, at the higher loading stage, it loses stability rapidly. Further research could be done to evaluate this hypothesis: the effect of axial load on the improvement in the performances of CFST.

The concrete-filled steel tubular (CFST) columns have evolved an alternative to the conventional hollow steel and reinforced concrete (RC) columns in recent years. Its usage as a structural member in transferring load from super structure is increasing as the in-filled concrete increases the strength and ductility of columns without increasing the given amount of steel. Because of its high strength, stability, ductility and better seismic resistance, CFST is more advantageous than ordinary RC columns, and is even more advantageous than the hollow steel column. The main reason for its high-strength and ductility lies in the composite in-filled concrete-steel interaction. The concrete is confined by outer steel which acts like longitudinal and transverse reinforcement. Moreover due to the confinement, the inner concrete core experiences tri-axial compression which restrained the formation of tension crack in concrete. Conversely, the outer steel shell is strengthened by the inner core which delays the inward local buckling and causes the outward buckling of steel member. Therefore the outer thin-walled steel can reach to the yield stress before local buckling occurs. Hence strength and stability of the CFST column is increased by 50% just because of introducing concrete. In addition, strength deterioration in CFST is not severe compared to hollow steel columns because the spalling of concrete is restrained by outer steel. On the other hand, CFST has higher fire resistance compared to hollow steel column, especially when the concrete core is designed to sustain the dead and live load (Kodur, 1997), as concrete has a larger thermal resistance than air which is

entrapped in hollow columns. Besides, due to the steel confinement the use of formwork can be discarded.

In this thesis, thickness of column and diaphragm is kept constant. Using this model further studies could be done to observe the effect of thickness of diaphragm and column on the improvement in strength and ductility of column. Also, research could be done to increase the material economy by varying the arrangement of diaphragm.

In summary, by comparing the finite element analysis results to the experimental results and from parametric study, the following conclusion can be made:

- A reasonably good agreement between the experiment and the analysis confirms the validity of the finite element modeling adopted in this study
- The optimum ductility capacity of thin-walled steel tubular columns can be achieved by arranging the column parameters such as  $R_f$ ,  $\lambda$ ,  $h_c/h$ , and axial load.
- Ductility of the column is improved for the height of concrete fill between 30 to 50 percent of the column height.
- Ductility of the column is improved as a diaphragm is placed on top of in-fill concrete

## REFERENCE

- Bažant, Z. P., and Becq-Giraudon, E. (2002). Statistical prediction of fracture parameters of concrete and implications for choice of testing standard. *Cement and concrete research*, 32(4), 529-556.
- Chen, W.-F., and Chen, C. (1973). Analysis of concrete-filled steel tubular beam-columns. *Publication*, 33, 37-52.
- Ellobody, E., Young, B., and Lam, D. (2006). Behaviour of normal and high strength concrete-filled compact steel tube circular stub columns. *Journal of Constructional Steel Research*, 62(7), 706-715.
- Fam, A., Qie, F. S., and Rizkalla, S. (2004). Concrete-filled steel tubes subjected to axial compression and lateral cyclic loads. *Journal of structural engineering*, 130(4), 631-640.
- Furlong, R. W. (1967). Strength of steel-encased concrete beam columns. *Journal of the Structural Division, American Society of Civil Engineers*, 93, 113.
- Gardner, N. J., and Jacobson, E. R. (1967). *Structural behavior of concrete filled steel tubes*. Paper presented at the ACI Journal Proceedings.
- Ge, H., and Usami, T. (1996). Cyclic tests of concrete-filled steel box columns. *Journal of structural engineering*, 122(10), 1169-1177.
- Gho, W.-M., and Liu, D. (2004). Flexural behaviour of high-strength rectangular concrete-filled steel hollow sections. *Journal of Constructional Steel Research*, 60(11), 1681-1696.
- Goto, Y., Jiang, K., and Obata, M. (2006). Stability and ductility of thin-walled circular steel columns under cyclic bidirectional loading. *Journal of structural engineering*, 132(10), 1621-1631.
- Ghosh, R. S. (1977). Strengthening of slender hollow steel columns by filling with concrete. *Canadian Journal of Civil Engineering*, 4(2), 127-133.
- Giakoumelis, G., and Lam, D. (2004). Axial capacity of circular concrete-filled tube columns. *Journal of Constructional Steel Research*, 60(7), 1049-1068.

- Goto, Y., Kumar, G. P., and Kawanishi, N. (2010). Nonlinear finite-element analysis for hysteretic behavior of thin-walled circular steel columns with in-filled concrete. *Journal of structural engineering*, 136(11), 1413-1422.
- Ghosh, R. S. (1977). Strengthening of slender hollow steel columns by filling with concrete. *Canadian Journal of Civil Engineering*, 4(2), 127-133.
- Goto, Y., Wang, Q., and Obata, M. (1998). FEM analysis for hysteretic behavior of thin-walled columns. *Journal of structural engineering*, 124(11), 1290-1301.
- Gourley, B. C., Tort, C., Denavit, M. D., Schiller, P. H., and Hajjar, J. F. (2008). A synopsis of studies of the monotonic and cyclic behavior of concrete-filled steel tube members, connections, and frames: Newmark Structural Engineering Laboratory. University of Illinois at Urbana-Champaign.
- Guo, L., Zhang, S., Kim, W.-J., and Ranzi, G. (2007). Behavior of square hollow steel tubes and steel tubes filled with concrete. *Thin-Walled Structures*, 45(12), 961-973.
- Han, L.-H., Yao, G.-H., and Tao, Z. (2007). Performance of concrete-filled thin-walled steel tubes under pure torsion. *Thin-Walled Structures*, 45(1), 24-36.
- Hillerborg, A., Modéer, M., and Petersson, P.-E. (1976). Analysis of crack formation and crack growth in concrete by means of fracture mechanics and finite elements. *Cement and concrete research*, 6(6), 773-781.
- Hu, H.-T., Huang, C.-S., and Chen, Z.-L. (2005). Finite element analysis of CFT columns subjected to an axial compressive force and bending moment in combination. *Journal of Constructional Steel Research*, 61(12), 1692-1712.
- Hu, H.-T., Huang, C.-S., Wu, M.-H., and Wu, Y.-M. (2003). Nonlinear analysis of axially loaded concrete-filled tube columns with confinement effect. *Journal of structural engineering*, 129(10), 1322-1329.
- Huang, C., Yeh, Y.-K., Liu, G.-Y., Hu, H.-T., Tsai, K., Weng, Y., . . . Wu, M.-H. (2002). Axial load behavior of stiffened concrete-filled steel columns. *Journal of structural engineering*, 128(9), 1222-1230.
- Jankowiak, T., and Lodygowski, T. (2005). Identification of parameters of concrete damage plasticity constitutive model. *Foundations of civil and environmental engineering*, 6, 53-69.
- Knowles, R. B., and Park, R. (1969). Strength of concrete filled steel columns. *Journal of the structural division*.
- Kodur, V. K. R. (1997). *Fire Resistance of Concrete-Filled Steel Columns*: Institute for Research in Construction, National Research Council of Canada.

- Liew, J., Xiong, D., and Zhang, M. (2011). *Experimental studies on concrete filled tubes with ultra-high strength materials*. Paper presented at the Proceedings of the 6th International Symposium on Steel Structures. Seoul:[sn].
- Lu, Y. Q., and Kennedy, D. L. (1994). The flexural behaviour of concrete-filled hollow structural sections. *Canadian Journal of Civil Engineering*, 21(1), 111-130.
- Mamaghani, I. H. P. (2005). Development of Uniaxial Stress-Strain Relationship for Concrete Confined by Steel Tubes Under Cyclic Loading. *33rd Annual General Conference of the Canadian Society for Civil Engineering*.
- Mamaghani, I. H. P., Montazeri, S., and Nemati, N. (2010). Stability Evaluation of Thin-Walled Steel Tubular Columns under Cyclic Multidirectional Loading. *Structural Stability Research Council*, 43-61.
- Mamaghani, I. H. P., and Packer, J. A. (2002). Inelastic Behavior of Partially Concrete-Filled Steel Hollow Section. *4th Structural Speciality Conference*.
- Mamaghani, I.H.P., Ahmad, F., Dorose, B. (2014a). *Cyclic Large Displacement Analysis of Steel Tubular Bridge Piers under Combined Axial and Bidirectional Lateral Loading*, International Journal of Applied Science and Technology (IJAST), Vol. 4, No. 6, November, PP. 38-47.
- Mamaghani, I.H.P., Ahmad, F., Dorose, B. (2014b). *Cyclic Elastoplastic Analysis and Ductility Evaluation of Thin-walled Steel Box Columns*, 4th International Structural Specialty Conference, Halifax-Canada, May 28-31, Paper ID: CST-165.
- Mamaghani, I.H.P., Ahmad, F., Dorose, B. (2015a). *Stability Evaluation of Thin-Walled steel Tubular Bridge Piers under Cyclic Multidirectional Loading*, Transportation Research Board, TRB 94th Annual Meeting, January 11-15, 2015, Washington, D.C., Paper ID: 15-4359.
- Mamaghani, I.H.P., Dorose, B., Ahmad, F. (2015b). *Cyclic Inelastic Finite Element Analysis and Ductility Evaluation of Steel Braced Frames*, ASCE, 2015 Structures Congress, Portland, OR., April 23-25, 2015, Paper ID: 250.
- Mamaghani, I.H.P., Ahmad, F., and Dorose, B., (2015c), "Strength and Ductility Evaluation of Thin-Walled Steel Tubular Columns under Cyclic Multidirectional Loading", Transportation Research Board (TRB).
- Mamaghani, I.H.P., Ahmad, F., and Dorose, B., (2015d), "Enhanced Seismic and Local Buckling Restraining Behavior of Concrete-filled Steel Tubular (CFST) Columns", ATC-SEI 2nd Conference on Improving the Seismic Performance of Existing Buildings and Other Structures, December 10-12, 2015.

- Mander, J. B., Priestley, M. J., and Park, R. (1988). Theoretical stress-strain model for confined concrete. *Journal of structural engineering*, 114(8), 1804-1826.
- Nie, J.-g., Wang, Y.-h., and Fan, J.-s. (2012). Experimental study on seismic behavior of concrete filled steel tube columns under pure torsion and compression–torsion cyclic load. *Journal of Constructional Steel Research*, 79, 115-126.
- Nie, J.-g., Wang, Y.-h., and Fan, J.-s. (2013). Experimental research on concrete filled steel tube columns under combined compression-bending-torsion cyclic load. *Thin-Walled Structures*, 67, 1-14.
- Nishikawa, K., Yamamoto, S., Natori, T., Terao, O., Yasunami, H., and Terada, M. (1996). An experimental study on improvement of seismic performance of existing steel bridge piers. *Journal of Structural Engineering, JSCE*, 42, 975-986.
- Papanikolaou, V. K., and Kappos, A. J. (2007). Confinement-sensitive plasticity constitutive model for concrete in triaxial compression. *International Journal of Solids and Structures*, 44(21), 7021-7048.
- Patil, V. P. (2012). Finet Element Approach To Study The Elastic Instability Of Concrete Filled Steel Tubular Column Under Axial Loads.
- Patton, M. L., and Singh, K. D. (2014). Finite element modelling of concrete-filled lean duplex stainless steel tubular stub columns. *International Journal of Steel Structures*, 14(3), 619-632.
- Richart, F. E., Brandtzaeg, A., and Brown, R. L. (1928). A study of the failure of concrete under combined compressive stresses.
- Sakino, K., Nakahara, H., Morino, S., and Nishiyama, I. (2004). Behavior of centrally loaded concrete-filled steel-tube short columns. *Journal of structural engineering*, 130(2), 180-188.
- Sakino, K., and Sun, Y. (1994). Stress-strain curve of concrete confined by rectilinear hoop. *Journal of Structural Construction Engineering*, 461, 95-104.
- Schneider, S. P. (1998). Axially loaded concrete-filled steel tubes. *Journal of structural engineering*, 124(10), 1125-1138.
- Susantha, K., Ge, H., and Usami, T. (2001). Uniaxial stress–strain relationship of concrete confined by various shaped steel tubes. *Engineering Structures*, 23(10), 1331-1347.
- Susantha, K., Ge, H., and Usami, T. (2002). Cyclic analysis and capacity prediction of concrete-filled steel box columns. *Earthquake engineering & structural dynamics*, 31(2), 195-216.



- Tao, Z., Uy, B., Han, L.-H., and Wang, Z.-B. (2009). Analysis and design of concrete-filled stiffened thin-walled steel tubular columns under axial compression. *Thin-Walled Structures*, 47(12), 1544-1556.
- Tao, Z., Uy, B., Liao, F.-Y., and Han, L.-H. (2011). Nonlinear analysis of concrete-filled square stainless steel stub columns under axial compression. *Journal of Constructional Steel Research*, 67(11), 1719-1732.
- Tao, Z., Wang, Z.-B., and Yu, Q. (2013). Finite element modelling of concrete-filled steel stub columns under axial compression. *Journal of Constructional Steel Research*, 89, 121-131.
- Thai, H.-T., Uy, B., Khan, M., Tao, Z., and Mashiri, F. (2014). Numerical modelling of concrete-filled steel box columns incorporating high strength materials. *Journal of Constructional Steel Research*, 102, 256-265.
- Tomii, M., Yoshimura, K., and Morishita, Y. (1977). *Experimental studies on concrete-filled steel tubular stub columns under concentric loading*. Paper presented at the Stability of Structures Under Static and Dynamic Loads.
- Usami, T., and Ge, H. (1994). Ductility of concrete-filled steel box columns under cyclic loading. *Journal of structural engineering*, 120(7), 2021-2040.
- Uy, B. (2001). Strength of short concrete filled high strength steel box columns. *Journal of Constructional Steel Research*, 57(2), 113-134.
- Uy, B., Tao, Z., and Han, L.-H. (2011). Behaviour of short and slender concrete-filled stainless steel tubular columns. *Journal of Constructional Steel Research*, 67(3), 360-378.
- Uy, B., Tao, Z., Han, L.-H., and He, S.-H. (2008). Design of concrete-filled steel tubular members according to the Australian Standard AS 5100 model and calibration. *Australian Journal of Structural Engineering*, 8(3), 197.
- Yu, T., Teng, J., Wong, Y., and Dong, S. (2010a). Finite element modeling of confined concrete-I: Drucker-Prager type plasticity model. *Engineering Structures*, 32(3), 665-679.
- Yu, T., Teng, J., Wong, Y., and Dong, S. (2010b). Finite element modeling of confined concrete-II: Plastic-damage model. *Engineering Structures*, 32(3), 680-691.
- Zhong, S. (1988). *The development of concrete filled tubular structures in China*. Paper presented at the Proceedings of the int. conf. on concrete filled steel tubular structures, China.